NORTHWESTERN UNIVERSITY

An Investigation of the Musculoskeletal Changes in the Hand After Chronic Hemiparetic Stroke and Their Impact on Hand Opening: Using Integrated Experimental and Computer Simulation Methods

A DISSERTATION

SUBMITTED TO THE GRADUATE SCHOOL
IN PARTIAL FULFILLMENT OF THE REQUIREMENTS

for the degree

DOCTOR OF PHILOSOPHY

Field of Biomedical Engineering

By

Benjamin I. Binder-Markey

EVANSTON, ILLINOIS

MARCH 2018

ABSTRACT

An Investigation of the Musculoskeletal Changes in the Hand After Chronic Hemiparetic Stroke and Their Impact on Hand Opening Using Integrated Experimental and Computer Simulation Methods

Benjamin I. Binder-Markey

Up to two thirds of individuals with chronic hemiparetic stroke suffer life-long residual impairments to their paretic hands, affecting their independence and quality of life. These impairments stem initially from losses of direct corticospinal projections that result in an increased reliance on indirect bulbospinal pathways. This reliance on the indirect pathways causes motor control deficits including weakness, loss of independent joint control (LIJC), and muscle hyperactivity. In addition to these neurologic impairments secondary musculoskeletal adaptations may occur that produce biomechanical changes increasing the passive joint torques in the paretic limb as compared to the non-paretic limb. Such biomechanical alterations within the hand would further contribute to hand impairments post stroke in addition to the neurological motor control deficits, yet quantitative data of these adaptations within the hand is lacking.

To gain a greater understanding of how altered passive joint biomechanics affects hand impairments post-stroke separate from the neurological impairments, both experimental and computer simulation methods were utilized. First, a dynamic computational musculoskeletal model of the finger was developed using a novel technique to incorporate the complex passive properties of the hand muscles. Next, to quantify how the passive torques adapt post-stroke within the hand, the passive torques about the wrist and four metacarpophalangeal joints were collected in 35 individuals with chronic hemiparetic stroke. Finally, to differentiate how the altered joint

mechanics versus neurological deficits impair hand function, computational simulations were developed incorporating both the experimentally collected impaired biomechanics and neurological deficits.

In individuals with chronic hemiparetic stroke there were not substantial differences in torques between the paretic and non-paretic hands, unless the individual had received Botulinum Neurotoxin (BoNT) in their wrist and finger muscles at any point following their stroke. Currently BoNT is the preferred treatment for muscle hyperactivity however this work has found that BoNT may have residual long-term effects that substantially increase the stiffness of muscles that were injected with it. The computational simulations demonstrated these increases in muscles stiffness due to BoNT limits the ability to extend the fingers in individuals with severe and moderate hand impairments. However, the simulations also demonstrated that the flexion synergy and resulting increased involuntary flexor muscle drive is the primary driver of hand impairments following chronic hemiparetic stroke and overshadows the increases due to the biomechanical changes. The findings from this work indicates the use of BoNT for treatment of muscle hyperactivity following a stroke should be further evaluated and that future rehabilitation and pharmaceutical interventions developed for these individuals should focus on reducing the impact of the neural deficits following stroke to maximize hand function.

ACKNOWLEDGEMENTS

A PhD is not the accomplishment of one person but the result of the knowledge, guidance, and support of the community around them. I want to first and foremost sincerely thank my advisors Dr. Wendy M Murray and Dr. Julius PA Dewald for the insight, patience, and guidance throughout this journey. Wendy, thank you for your focus and eye for detail that has guided me through these 8 years when I tried to do too many things at once. Jules, thank you for your advice and guidance to come up from the details and look at the big pictures.

I would also like to thank my dissertation committee; Dr. Kirsten Moisio, Dr. Derek Kamper, and Dr. Thomas Sandercock; who all stuck with me over this journey. Your fresh eyes, inquisitive questions, and thought insights have helped mold my project and development as a scientist.

To all the present and past members of the Applied Research in Musculoskeletal Simulations (ARMS) lab; especially Amy Adkins, Katherine Rodzak, Sarah Wohlman, Jennifer Nichols, James Buffi, Carrie Peterson, Xiao Hu, Jeremy Mogk, and Craig Geohler; thank you for your brainstorming and problem solving when simulations didn't run and eye rolling when the 80's playlists comes on for group therapy in the SRALab.

To all the past and present members of the Dewald Lab; especially Natalia Sanchez, Sam Perlmutter, Meriel Owen, Kevin Wilkins, Netta Gurira, Carolina Carmona, Ana Maria Acosta, Justin Drogos, and Mike Ellis. Thank you for your help with the laborious yet fulling task of subject recruitment and conversations on ranging from our work to world events that always left me better informed.

To all the other crazy dual degreers who started before, with, and after me. Thank you Lindsay Garmirian for taking this journey with me. To Rosalind Heckman, Christa Nelson, Rachel Hawe, Laura Miller/McPherson, Theresa Sukal Moulton, Stephen Antos, Emma Baillargeon, Joseph Kopke, Nayo (Anita) Hill, and Andrew Dragunas, thank you all for your support and camaraderie during this journey.

To Arno Stenien, Paul Kruguer, and Vikram Darbhe thank you very much for assistance in device development. Arno, thank you all your valuable input from the initial conception through the multiple design modifications and final device design. Paul, thank you for your friendship and assistance in manufacturing all the device modifications. Vikram, thank you for assistance in the calibration of the device and your assistance with the experimental set up and data collection, and then sneaking in and out of the lab during the experiments as if there was a sleeping baby in there.

To all the faculty in both the BME and PTHMS departments. To the BME faculty thank you for your guidance in the my early classroom years as well as towards the end of my PhD with your career advice and guidance. To the PTHMS faculty thank you for your unwaiving support and encouragement through both PT school and following my DPT. I would especially like to thank Dr. Marjorie Hillard for all her guidance and mentorship in teaching with the DPT curriculum.

To all my friends that I've made along this wonderful journey. Thank you for being an outlet when I needed to get my mind off school. Thank you for being supportive when I needed it. Thank you for being the people I could turn to.

To the most important people in my life, my family. To my wife, Caitlin, thank you so much for being patient with me in this journey and all your moral support during the highs and lows. I

love you, you are my rock. To my mother and father, Catriona and Stuart, thank you for everything. You are where it all started, seeing that the apple doesn't fall far from the tree, coming from an OT, PT, and Academic, I didn't stray too far from the family work. Truly without your support, (insider knowledge- Dad), guidance, and love I would not be where I am today. To my sister, Rina, thank you for all your support and sense of humor. To my in-laws, Jack and Kathleen, thank you for being understanding of this path and all your support throughout this journey. And final to my new siblings, Alyssa and Ian, thank you taking me at who I am and again for all your support and love. And most importantly my sons, Deacon and Finn, I hope you are inspired and awed by the world as I have been and that you seek to understand it, even if it's just a little, with your own discoveries.

Last but not least, this work would not be possible without funding. I have been very fortunate throughout my early career and I would like to thank all my funding sources for their support. The American Heart Association for the Pre-Doctoral Fellowship (16PRE30970010), The Foundation for Physical Therapy for the PODS II Award, NIH-NIBIB dual degree training program (T32EB009406), NIH for research funding relating to my work (R01HD084009), The Feinberg School of Medicine for the Dean's Dual Degree Scholar Award supporting my DPT education, and Searle Fund of the Chicago Community Trust.

LIST OF ABBREVIATIONS

BoNT	Botulinum neurotoxin
CMSA-HS	Chedoke McMaster stroke assessment – hand score
CP	Cerebral palsy
DIP	Distal interphalangeal
DOF	Degree of freedom
ECM	Extracellular matrix
ECR	Extensor carpi radialis
EDC	Extensor digitorium communis
EDCI	Extensor digitorium communis indicis
EDCL	Extensor digitorium communis little
EDCM	Extensor digitorium communis middle
EDCR	Extensor digitorium communis ring
EDM	Extensor digitorium minimi
EIP	Extensor indicis proprius
EMG	Electromyography
FCU	Flexor carpi ulnaris
FDPI	Flexor digitorium profundus indicis
FDPL	Flexor digitorium profundus little
FDPM	Flexor digitorium profundus middle

FDPR	Flexor digitorium profundus ring
FDS	Flexor digitorium superficialis
FDSI	Flexor digitorium superficialis indicis
FDSL	Flexor digitorium superficialis little
FDSM	Flexor digitorium superficialis middle
FDSR	Flexor digitorium superficialis ring
LIJC	Loss of independent joint control
FES	Functional electrical stimulation
MAS	Modified Ashworth Acale
MCP	Metacarpophalangeal
PIP	Proximal interphalangeal
ROM	Range of motion

TABLE OF CONTENTS

Abstract 2

Acknowledgements 4

List of Abbreviations 7

List of Figures 11

List of Tables 14

1 Introduction 16
1.1 Focus of Dissertation 18
1.2 Significance 20
1.3 Overview 21
1.4 List of key contributors by chapter 22

2 Background 23
2.1 Etiology of Stroke 23
2.2 Upper extremity impairments post stroke 24
2.3 Changes in joint and muscle structure post stroke 25
2.4 Biomechanical design of the hand and fingers 27
2.5 Computational musculoskeletal modeling 31

3 Incorporating the Length-Dependent Passive-Force Generating Muscle Properties of the Extrinsic Finger Muscles Into a Wrist and Finger Biomechanical Musculoskeletal Model 34
3.1 Introduction 35
3.2 Methods 36
3.3 Results and Discussion 44
3.4 Conclusion 46

4 The Biomechanical Basis of the Claw Finger Deformity: A Computational Simulation Study 47
4.1 Introduction 48
4.2 Methods 51
4.3 Results 61
4.4 Discussion 66
4.5 Conclusion 70

5 Passive Elastic Torques Within the Hand Change Minimally in Individuals with Chronic Hemiparetic Stroke 71
5.1 Introduction 72
5.2 Materials and Methods 74
5.3 Results 81

5.4 Discussion 88
5.5 Conclusion 91

6 Chronic Stroke Individuals who received Botulinum Toxin Injections Have Long Term Increases of Muscle Stiffness 92
6.1 Introduction 93
6.2 Materials and Methods 95
6.3 Results 102
6.4 Discussion 110
6.5 Conclusion 115

7 Increased Flexion Torques Lead to Hand Impairments in Chronic Hemiparetic Stroke: A Simulation Study 117
7.1 Introduction 118
7.2 Methods 121
7.3 Results 131
7.4 Discussion 135
7.5 Conclusion 139

8 Conclusion 140
8.1 Contributions 142
8.2 Future Directions 143

References 145

Appendices 156

A Appendix A. Muscle Model Validation 156

B Appendix B: Four finger model development 162
B.1 Development of the four finger dynamic musculoskeletal models of the hand. 162
B.2 Experimentally collected passive torque about each finger 162
B.3 Separation of the structures contributing to the total torque: 164
B.4 Incorporation of the passive single joint torques. 164
B.5 Incorporation of the passive extrinsic finger muscle torques. 167

LIST OF FIGURES

Figure 2.1: Cartoon depicting the descending pathways from the cortex that are involved following a stroke 24
Figure 2.2. Overview of the fingers defining the joints, bones, ligaments and joint capsule at about joint 28
Figure 2.3. Overview of the extrinsic finger muscles of the fingers..... 29
Figure 2.4. Overview of the intrinsic finger muscles and extensor mechanism of the finger 30
Figure 2.5. Schematic of the Hill-Type muscle model and the normalized tendon force-length curve, muscle fiber active and passive force-length curves, and muscle fibers force-velocity curve..... 33
Figure 3.1. Figure depicting the nominal and updated wrist and hand model..... 37
Figure 3.2. Moment arm data about the metacarpophalangeal (MCP), proximal interphalangeal (PIP), and distal interphalangeal (DIP) joints of the current model and expiremental data . 38
Figure 3.3. Wrist and index finger joint postures as a function of time during the simulations... 45
Figure 4.1: Flow chart demonstrating the process of the forward dynamic simulations..... 53
Figure 4.2: The nominal and altered elastic torques produced by intrinsic muscles and joint structures about the MCP, PIP, and DIP joints within the model..... 55
Figure 4.3: Moment arm plots about the PIP joint for the extrinsic extensors with the nominal and altered wrapping surfaces 56
Figure 4.4: The sum of the FDSI and FDPI passive flexion torques throughout the MCP joint range of motion with muscle-tendon unit at the nominal and altered resting lengths..... 58
Figure 4.5: Final equilibrium position for extension of the forward simulations with increased laxity, stretched extensor mechanism, and shortened flexor muscles 62
Figure 4.6: Final equilibrium position for extension of the forward simulations with an extended and flexed wrist of the models combining the small, medium, and large changes..... 63
Figure 4.7 Joint angle plots of the non-impaired model of the metacarpophalangeal, proximal interphalangeal, and distal interphalangeal joints throughout the forward dynamic simulations. 64

Figure 4.8: The operational range of the Extensor Indicis Profundus and Extensor Digitorium Communis Indicis throughout the full finger and wrist range of motion within the biomechanical musculoskeletal model 68

Figure 5.1: Picture of the experimental set-up with the subject seated upright with their hand attached to the WFTS device and a schematic of the data points collected as the MCP joint was ranged through its range of motion..... 76

Figure 5.2: Wrist torque data over the wrist's range of motion of individuals with severe, moderate, and mild hand impairments..... 82

Figure 5.3: MCP torque data over the MCP joints' range of motion of the paretic and non-paretic of individuals with severe, moderate, and mild hand impairments 83

Figure 5.4: Wrist torque of the wrist muscles and other joint structures about the wrist over the wrist's range of motion of the paretic and non-paretic of individuals with severe, moderate, and mild hand impairments..... 85

Figure 5.5: MCP torque of the intrinsic hand muscles and other joint structures about the MCP joints over the MCP range of motion of the paretic and non-paretic of individuals with severe, moderate, and mild hand impairments..... 85

Figure 5.6: MCP torque of the extrinsic finger muscles about the MCP joints over the MCP range of motion of the paretic and non-paretic with severe, moderate, and mild hand impairments 86

Figure 6.1: Picture of the experimental set-up with the subject seated upright with their hand attached to the Wrist Finger Torque Sensor. 97

Figure 6.2: Mean end of MCP passive range of motion in extension and flexion throughout the wrist's ROM for the paretic and non-paretic of the no-BoNT severe group and BoNT group within in the experimental device 103

Figure 6.3: Wrist torque data versus over the wrist's range of motion the paretic and non-paretic the no-BoNT and BoNT groups..... 104

Figure 6.4: MCP torque data versus over the MCP joints' range of motion with the fingers locked in -60, 0, and 60 degrees of the paretic and non-paretic the no-BoNT and BoNT groups . 105

Figure 6.5: MCP torque of the extrinsic finger muscles about the MCP joints versus over the MCP range of motion of the paretic and non-paretic of the no-BoNT and BoNT groups..... 108
Figure 6.6: Wrist torque of the wrist muscles and other joint structures about the wrist joint's range of motion of the paretic and non-paretic of the no-BoNT and BoNT groups..... 109
Figure 6.7: The MCP torque of the intrinsic hand muscles and other joint structures about the MCP joint's range of motion of the paretic and non-paretic of the no-BoNT and BoNT groups 110
Figure 7.1: Normalized force length curves for the active force, nominal passive force, and Botulinum Neurotoxin optimized passive force curve 128
Figure 7.2: Plots of the excitation inputs for the forward dynamic simulations..... 129
Figure 7.3: Representation of the equilibrium posture at the end of the extension phase of the forward dynamic simulations of the non-impaired and impaired models 132
Figure 8.1: Muscle-tendon unit lengths over time of the triceps long head, triceps lateral head, biceps long head, and biceps short head during the passive forward simulation 158
Figure 8.2: The muscle-tendon unit, tendon, and muscle fiber lengths of the biceps long head and short head over time..... 160
Figure 8.3: Plot of elbow angle over time for a gravity driven simulation within the SIMM and Dynamics Pipline platform and the OpenSim platform..... 161

LIST OF TABLES

Table 3.1. Interial Parameters For Bone Segments..... 39
Table 3.2. Optimized Tendon Slack Lengths And Precent Changes..... 43
Table 4.1: Optimal Fiber, Tendon Slack, and Muscle-Tendon Resting lengths of the FDSI and FDPI at nominal lengths and shortened to 98%, 95%, and 90% of nominal length..... 58
Table 4.2: Summary counting the simulations run during the sensitivity analysis. Set one consists of the simulations with an extended wrist posture within the nominal model, the 'one-at-a-time' analysis, and the combined models. Set two of the simulations run with a flexed wrist posture mimicking the Andre-Thomas sign was run with the combined models only..... 60
Table 4.2: Final equilibrium postures of the MCP, PIP, and DIP joints at the end of extension for the simulations with the single parameter changes and combined changes. 65
Table 5.1: Table of Inclusion Criteria for Subjects..... 75
Table 5.2: Subject Demographics..... 75
Table 5.3: Median Parameters for the fit analytical models of paretic and non-paretic at the MCP and wrist at each impairment level 87
Table 6.1: Subject Demographics..... 98
Table 6.2: Median Parameters for the fit analytical models of paretic and non-paretic at the MCP and wrist at each impairment level 106
Table 7.1: Median parameters of the analytical fit of the total passive torques about the MCP joints of the index, middle, ring, and little fingers of the non-paretic hands and paretic hands the receive Botulinum Neurontoxin..... 125
Table 7.2: Optimized Tendon Slack Lengths for the Non-paretic Model and Percent Change for all the fingers included in the model..... 126
Table 7.3: Summary of the Simulations with the model and level of involuntary activation . .. 131
Table 7.4: Summary of extension equilibrium positions of the forward dynamic simulations.. 134
Table 8.1: Parameters of the matched torques..... 166
Table 8.2: Optimized Tendon Slack Lengths for the Non-paretic Model and Percent Change for all the fingers included in the model..... 167

Table 8.3 Table of the unimpaired and BoNT parameters defining the passive force length curve within the Millardequlibrium2012 muscle model within the OpenSim platform..... 168

1 INTRODUCTION

Each year at least 795,000 individuals suffer a fatal or debilitating stroke in the United States. Approximately eighty percent of these individuals survive and across all survivors the combined direct costs (health care and rehabilitation) and indirect costs (loss of job, loss of independence, and future complications) exceed $33.6 billion each year (Mozaffarian D, 2015). Contributing to these costs are loss of function and independence associated with upper extremity impairments for two thirds of these survivors never regain normal use of their upper extremity, making upper extremity impairment the most common physical impairment post-stroke (Lawrence et al., 2001). In addition, more than half of these individuals have such severe impairments that they cannot open or control their paretic hand requiring them to rely on the other hand or caregivers to perform activities of daily living, thus decreasing their independence and quality of life (Broeks et al., 1999; Nakayama et al., 1994; Parker et al., 1986).

The hand is an extremely complex system consisting of over 17 joints and 22 degrees of freedom (DOF) that are controlled by at least 40 muscles. To control these multiple joints and DOF, healthy hand function is dependent on a complex set of interactions between both neural and biomechanical components. These interactions are aided by the mechanical design of the hand that balances the input forces from multiple sources including the muscles and passive structures (ligaments, joint capsule, etc.) of the hand. However, this complexity causes the hand to be highly susceptible to impairments if there is any imbalance of force due to an injury that impairs muscle control or damages any of the structures of the hand. A stroke is one such injury that affects both muscle control and the structures of the hand.

Within in the post-stroke populations hand and upper limb impairments stem initially from damage to the cerebral cortex that disrupts the direct corticospinal pathways causing an increased reliance on indirect corticofugal pathways (Baker, 2011; Dewald et al., 1995; Dewald et al., 2001; Riddle and Baker, 2010; Riddle et al., 2009). The increased reliance on the indirect pathways causes motor deficits manifesting as weakness (Kamper et al., 2006; Kamper et al., 2003), loss of independent joint control (Baker, 2011; Dewald et al., 1995; Dewald et al., 2001; Miller and Dewald, 2012), and muscle hyperactive (hypertonicty – constant muscle activity, and spasticity – hyperactive stretch reflexes) (Ellis et al., 2017; Hu et al., 2006; McPherson et al., 2008; McPherson et al., 2017) that impair the neural control of the muscles.

Secondary to the neurologic changes there are potential changes to the musculoskeletal system that develop and persist after the neural deficits have plateaued. These secondary changes to the muscles and structures are thought to be due to the neural impairments and prolonged disuse of the paretic arm (Eby et al., 2016; Gao et al., 2009; Gao and Zhang, 2008; Given et al., 1995; Lieber and Friden, 2002; Lieber et al., 2004; Malhotra et al., 2010; Mirbagheri et al., 2008; Smith et al., 2011) which result in increased passive torques about the elbow and ankle (Gao et al., 2009; Gao and Zhang, 2008; Li et al., 2007; Nelson et al., 2015). But increases in muscle stiffness may also be due to potential long-term consequences of botulinum neurotoxin (BoNT) injections, that are initially used to decrease stiffness by reducing muscle hyperactivity but may result in increased collagen and passive stiffness of the muscle (Minamoto et al., 2015; Thacker et al., 2012; Ward et al., 2017).

If the passive torques about the finger and wrist joints were to change, due to adaptations of the muscles or structures of the hand, the alterations would disrupt the delicate force balance within

the complex structure of the hand. This disruption could prevent many chronic stroke individuals from recovering the ability to use their hand, even as there is some recovery from the neurological deficits.

Research on the changes of the musculoskeletal system post stroke has largely been neglected, especially in the wrist and hand, with the majority of research focused on the neurologic deficits. There are only a handful of studies that have looked at musculoskeletal changes of the upper extremity post stroke. Two of which have investigated the biomechanical changes at the elbow post stroke (Given et al., 1995; Li et al., 2007) and other have studied the neural and biomechanical changes at the hand and wrist post stroke with a focus on the neural deficits (de Gooijer-van de Groep et al., 2016; Kamper et al., 2006; Kamper et al., 2003). The lack of evidence in this area limits our current understanding of how muscles and structures adapt in the upper extremity and hands post stroke, and limits our ability to most effectively rehabilitate and manage upper-extremity impairments post stroke.

1.1 Focus of Dissertation

The focus of this dissertation will be to gain a greater understanding of how hand function is impaired post-stroke, specifically concentrating on the effects of altered passive biomechanics. This research will give insights into how the musculoskeletal system adapts after a stroke by investigating how the muscles and structures of the hand alter passive joint torques within the hand. The work will substantially contribute to the understanding of how altered joint biomechanics as compared to neural deficits post stroke impair hand opening and function.

These insights will be realized by focusing on the following objectives. The first objective of this work is to understand how the passive biomechanical structures of the hand coordinate both passive and active movements within healthy hands. The second objective is to quantify the extent to which the passive torques about the fingers and wrist change in the paretic limb of individuals with chronic hemiparetic stroke while also investigating the long-term consequences of BoNT injections. The final objective is to elucidate, through the use of computational musculoskeletal modeling, how these passive biomechanical changes impair hand opening as compared to the neural control deficits. These objectives will be achieved through the following aims:

Aim 1: Demonstrate how the musculoskeletal structures of the hand coordinate motion of the fingers and wrist in a biomechanical hand model.

Aim 1a: *Demonstrate how the musculoskeletal structures of the hand coordinate passive coupling between the fingers and wrist in a non-impaired biomechanical hand model.*

Aim 1b: *Demonstrate how the musculoskeletal structures of the hand coordination active extension of the three finger joints using non-impaired and impaired biomechanical hand models.*

Aim 2: Determine the passive torques produced in the paretic and non-paretic limbs about the wrist and finger in individuals with chronic hemiparetic stroke.

Aim 2a: *Determine the passive torques of the paretic versus the non-paretic wrist and finger structures in individuals with chronic hemiparetic stroke across the spectrum of hand impairments.*

Aim 2b: *Determine the passive torques of the paretic versus the non-paretic wrist and finger structures in individuals with chronic hemiparetic stroke of have received BoNT injections.*

Aim 3: Using a computational musculoskeletal model, quantify how the biomechanical alterations versus neural mediated increases of finger flexion torques contribute to impairment in hand opening of the paretic hand in individuals with chronic hemiparetic stroke.

1.2 Significance

This work will significantly enhance the understanding of how musculoskeletal structures adapt post stroke leading to a substantial positive impact on stroke rehabilitation. Current upper extremity rehabilitation strategies for the upper extremity focus on the neurological effects of the injury through constraint-induced therapy (Corbetta et al., 2010; Sirtori et al., 2009), mental practice (Barclay-Goddard et al., 2011; Braun et al., 2013), mirror therapy (Thieme et al., 2013; Thieme et al., 2012), and high dose repetitive task practice (French et al., 2008; French et al., 2010; French et al., 2007) though with limited success (Pollock et al., 2014). BoNT injections are commonly used to reduce the resistance of the muscles originating from neural origins however the long-term consequences of these treatments on muscle properties post stroke is unknown. The knowledge of how the passive properties of musculoskeletal structures alter due to the natural course of the injury versus potential changes due to therapeutic treatments such as BoNT will assist in directing care for individuals with brain injury in the future.

Furthermore, the innovative quantitative methods used in this study will be the first to quantify how the separate musculoskeletal structures about the finger joints and wrist contribute to the total

passive joint torques in the chronic stroke population. Additionally, novel methods and techniques for the development and use of computational musculoskeletal hand models will be used to demonstrate how alterations to the musculoskeletal properties of the hand isolated from the neural deficits affect hand opening and function. This is an important step in identifying the most detrimental factors contributing to hand impairments post stroke and will guide future development of more targeted and effective therapeutic interventions, assistive device designs, and pharmaceutical interventions that targeting these factors following a stroke to improve the quality of life and independence of these individuals.

1.3 Overview

The remaining chapters of this dissertation will discuss in depth the musculoskeletal biomechanical modeling and experimental work aimed at answering the above objectives. Chapters 3 and 4 focus on the development of the musculoskeletal biomechanical model used in this dissertation. Chapter 3 details the methods used to incorporate the complex passive structures of the hand into the model. Chapter 4 examines how potential biomechanical alterations to the structures of the hand affect the ability to open and close the hand focusing specifically on the development of the claw finger deformity that is often present in many individuals with a stroke and other populations with intrinsic finger paralysis as they attempt to extend their fingers. Chapters 5 & 6 focus on the experimentally collected musculoskeletal changes of the hand and wrist post hemiparetic stroke. Chapter 5 explores how impairment levels affect passive biomechanical adaptations in individuals with chronic hemiparetic stroke. Chapter 6 explores the potential effects of BoNT injections on the passive biomechanical properties of the paretic

muscles. Chapter 7 develops and uses computational musculoskeletal models to explore how the passive musculoskeletal alterations and neural deficits affect the ability to open and close the hand post hemiparetic stroke.

1.4 List of key contributors by chapter

The main chapters of this dissertation are structured as independent journal articles. The additional contributors to these articles are listed below:

Chapter 3: Wendy Murray

Chapter 4: Julius Dewald and Wendy Murray

Chapter 5: Wendy Murray and Julius Dewald

Chapter 6: Wendy Murray and Julius Dewald

Chapter 7: Remi Shittu, Julius Dewald, and Wendy Murray

2 BACKGROUND

2.1 Etiology of Stroke

A stroke is a cerebrovascular accident that occurs when oxygen rich blood is blocked to a portion of the brain causing brain cells and neurons to die within minutes. There are two main types of a stroke, ischemic and hemorrhagic. An ischemic stroke occurs when an artery that supplies blood and oxygen to the brain becomes blocked, commonly by a blood clot that originated elsewhere in the body. Ischemic strokes account for 87% of all strokes thereby making them the most prevalent type of stroke (Benjamin et al., 2017). The remaining 13% of stokes are hemorrhagic. For these there is a breakage or rupture of an artery, commonly caused by high blood pressure or an aneurism, that results in uncontrolled bleeding leading to increased pressure and loss blood flow to the area resulting in cell death (Benjamin et al., 2017). After both types of stroke there is often significant damage to the brain that results in the death of approximately 21% individuals within a year (Benjamin et al., 2017). The remaining 600,000 or more survivors of a stroke each year are often left with lasting impairments which include difficulty speaking and understanding written or spoken language, cognitive deficits, and difficulty with controlled movements of their face, upper extremities, and lower extremities (Benjamin et al., 2017). Throughout this dissertation, I will focus on impairments to the upper extremity specifically of the hand which is the most common physical impairment post-stroke. Up to two-thirds of survivors never regain normal use of the hand and upper extremity after the stroke (Lawrence et al., 2001).

2.2 Upper extremity impairments post stroke

Impairments to the upper extremity stem initially from damage to portions of the cerebral cortex that affects the most direct connections between the cortex and the motoneurons of the spinal cord and brainstem, the corticospinal and corticobulbar pathways (also referred to a corticofugal pathways) (Figure 2.1). The loss of the corticofugal projections gives rise to an increased reliance on indirect brainstem pathways, such as the contralesional corticoreticulospinal pathways (Figure 2.1).

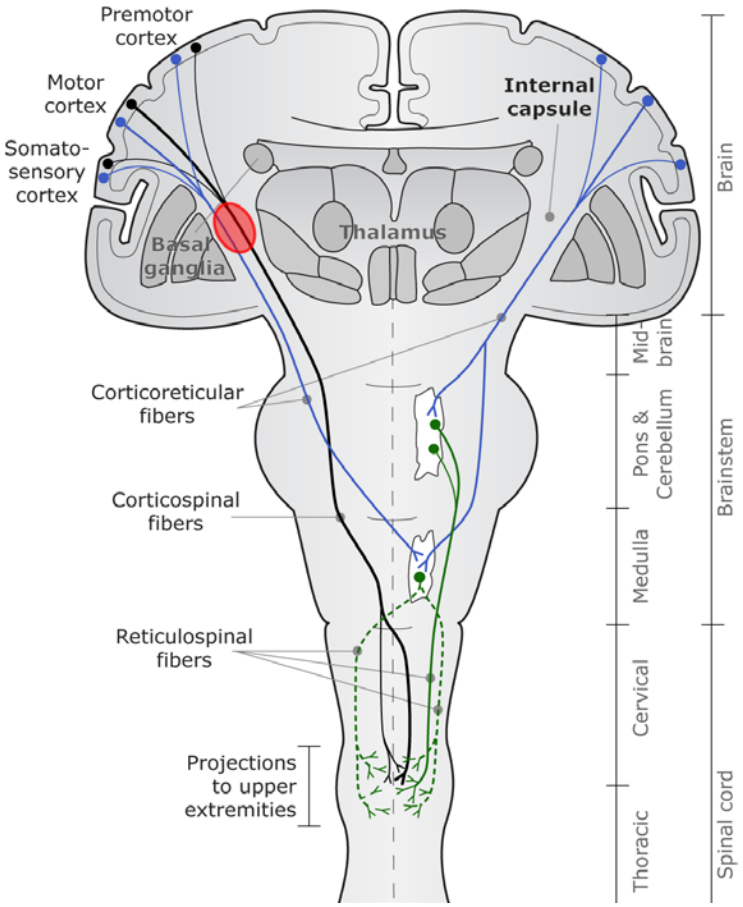

Figure 2.1: Cartoon depicting the descending pathways from the cortex that are involved following a stroke. Black lines trace the direct corticospinal pathways. Blue and green lines trace the indirect corticoreticulospinal pathways. The red oval depicts the damage side of the brain and disrupted corticofugal pathways following a stroke (Used with the permission of unpublished work by Stienen and Chen).

The increased reliance on the contralesional corticoreticulospinal pathways result in weakness, loss of independent joint control, and hypertonicity (constant muscle activity), spasticity (hyperactive stretch reflexes). The loss of direct corticospinal pathways results in individuals post-stroke who are not able to effectively activate their muscles (Kamper et al., 2006; Kamper et al., 2003; Klein et al., 2010; Knarr et al., 2013). These deficits are especially evident in the wrist and finger extensor muscles which exhibit significant weakness post-stroke (Kamper et al., 2006; Kamper et al., 2003). Loss of independent joint control is thought to be due to an increased reliance on indirect contralesional corticoreticulospinal pathways. This loss of independent joint control manifests as increased abnormal flexor muscle activity of the elbow, wrist, and finger flexor muscles as an individual attempts to lift their paretic upper extremity and is described as the flexion synergy (Dewald et al., 1995; Dewald et al., 2001; Hu et al., 2006; Miller and Dewald, 2012). Hypertonicity and spasticity are a result of upregulation of the reticulospinal pathways which causes an increase in monoaminergic signaling to the spinal cord which in turn increases the motoneuron excitability and the resulting muscle hyperactivity (Fedirchuk and Dai, 2004; Heckman et al., 2008; Johnson and Heckman, 2014; McPherson et al., 2008; McPherson et al., 2017; Owen et al., 2017).

2.3 Changes in joint and muscle structure post stroke

In addition to these neural driven impairments, associated potential secondary biomechanical changes may occur in the muscles and joints of individuals with chronic hemiparetic stroke. Previous studies in the upper and lower extremities have examined these secondary changes. However, the results of these studies do not consistently demonstrate changes in joint torques and stiffness at the ankle, elbow, or wrist (de Gooijer-van de Groep et al., 2016; Eby et al., 2016; Freire

et al., 2017; Gao et al., 2009; Gao and Zhang, 2008; Given et al., 1995; Kwah et al., 2012; Li et al., 2007; Nelson et al., 2015). At the ankle, a couple of studies have demonstrated joint torque and stiffness to increase (Gao et al., 2009; Given et al., 1995) while others have found that there is no difference (Freire et al., 2017; Kwah et al., 2012). In the upper extremity, increases of passive torque and stiffness at the wrist and elbow have been demonstrated (de Gooijer-van de Groep et al., 2016; Eby et al., 2016; Nelson et al., 2015) but others have not found substantial changes of the passive torques of the upper extremity (Given et al., 1995; Kamper et al., 2006). Even with these inconsistencies the prevailing belief, in both the research and clinical realms because of the majority of evidence indicating and clinical observations of increased joint stiffness, is that passive biomechanical changes occur within the muscles and joints that increase the joint's resistive torques.

Further validating this belief of increased passive torques about the joints post stroke are *in vivo* imaging studies that have demonstrated muscle fascicles about the ankle and elbow in individuals become shorter in chronic hemiparetic stroke individuals while the individual is in a relaxed state (Gao et al., 2009; Gao and Zhang, 2008; Kwah et al., 2012; Li et al., 2007; Nelson et al., 2015). This fascicle shortening would contribute to a shift in the force-length properties of the muscles and an increase in the passive torques and stiffness about those joints. Additional insight into muscle adaptation in the stroke population could potentially be realized from past research of spastic muscle in individuals with cerebral palsy. Spastic muscle of children with cerebral palsy (CP) has been demonstrated to become shorter and stiffer, contributing to shifts in the force-length properties of the muscles and increasing passive torques and stiffness about the joints in the lower extremity (Friden and Lieber, 2003; Lieber and Friden, 2002; Smith et al., 2011). However, these

secondary biomechanical changes of the musculoskeletal system that occur within the spastic muscles of children with CP likely will not translate directly into the adult stroke population. The reason is because there are fundamental differences in how the two musculoskeletal systems developed. In children with CP, the musculoskeletal system developed with an impaired nervous system whereas in adults with chronic hemiparetic stroke the musculoskeletal systems were fully developed when the brain injury occurred.

If there is increased muscle stiffness in the muscles that control the hand in the chronic stroke population it is likely these increases would prevent any potential recovery of the ability to use their hand. Currently only a limited number of studies have looked at the passive torque changes of the hand and wrist post stroke. These studies were focused on the neurally driven impairments and stiffness (de Gooijer-van de Groep et al., 2016; Kamper et al., 2006; Kamper et al., 2003). Knowing how the passive biomechanical structures change in the chronic stroke population is important as these passive properties play a very important role in the coordination of finger movements and function (Esteki and Mansour, 1997; Kamper et al., 2002). If they are disrupted they could have a significant impact on hand function and impairment.

2.4 Biomechanical design of the hand and fingers

In an effort to understand how potential musculoskeletal changes post stroke impact hand impairments, we must first begin to comprehend healthy hand biomechanics. The hand is a complex biomechanical structure that allows for the controlled movement of over 22 degrees of freedom (DOF) by at least 40 muscles; this complexity causes the hand to be highly susceptible to impairments. Specifically, each finger (digits two to five) is comprised of four bones, the metacarpal proximal, middle, and distal phalangeal bones that are connected by three joints; the

metacarpophalangeal (MCP), proximal interphalangeal (PIP), and distal interphalangeal (DIP) joints (Figure 2.2A). The MCP joint has two DOF, flexion/extension and abduction/adduction, and the PIP and DIP have a single DOF, flexion/extension.

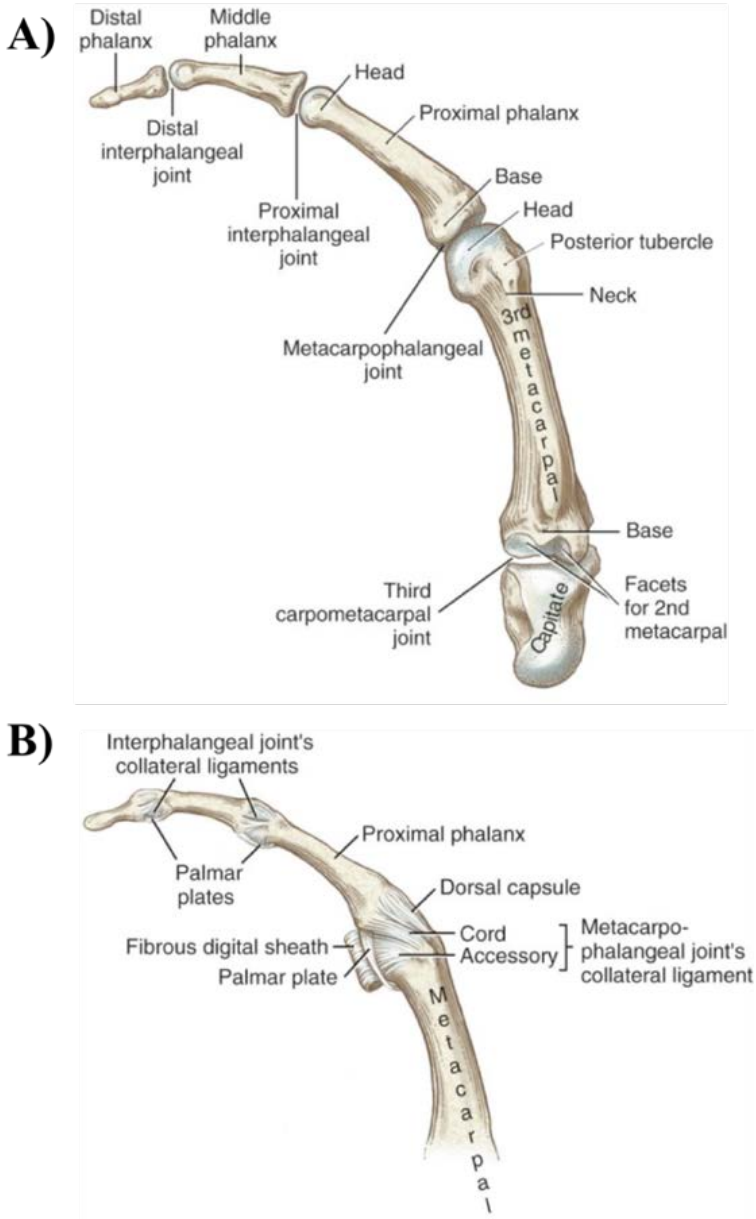

Figure 2.2. Overview of the fingers defining the A) joints and bones and B) the ligaments and joint capsule at about joint. (Neumann et al., 2017)

The primary movers that flex and extend the fingers are the extrinsic finger muscles that originate in the forearm, cross the wrist, and attach distally on the phalangeal bones of the fingers (Li et al., 2000). The extrinsic finger muscles are the flexor digitorium superficialis, flexor digitorium profundus, and extensor digitorium communis (Figure 2.3). The index finger and little finger each have one additional extensor, the extensor indicis proprius and the extensor digiti minimi respectively (Figure 2.3).

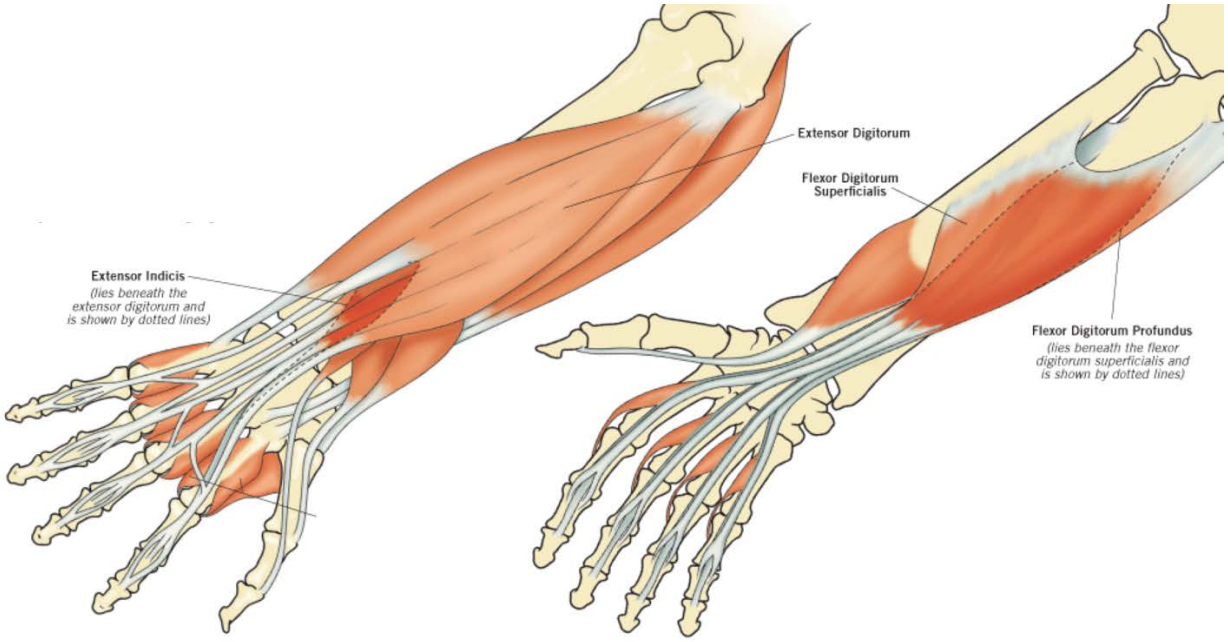

Figure 2.3. Overview of the extrinsic finger muscles of the fingers (Adapted from (Neumann et al., 2017)

In addition to the extrinsic finger muscles there are intrinsic finger muscles, the lumbricals and dorsal and palmer interossei, that originate in the hand and attach distally to the finger mainly via the extensor mechanism (Figure 2.4A). The primary actions of the intrinsic finger muscles are to abduct and adduct the fingers but they also play an important role in acting synergistically with the extrinsic muscles to balance and modulate the torques about the finger joints during flexion

and extension movements via the complex extensor mechanism (Figure 2.4B) (Darling and Cole, 1990; Palti and Vigler, 2012; Srinivasan, 1976).

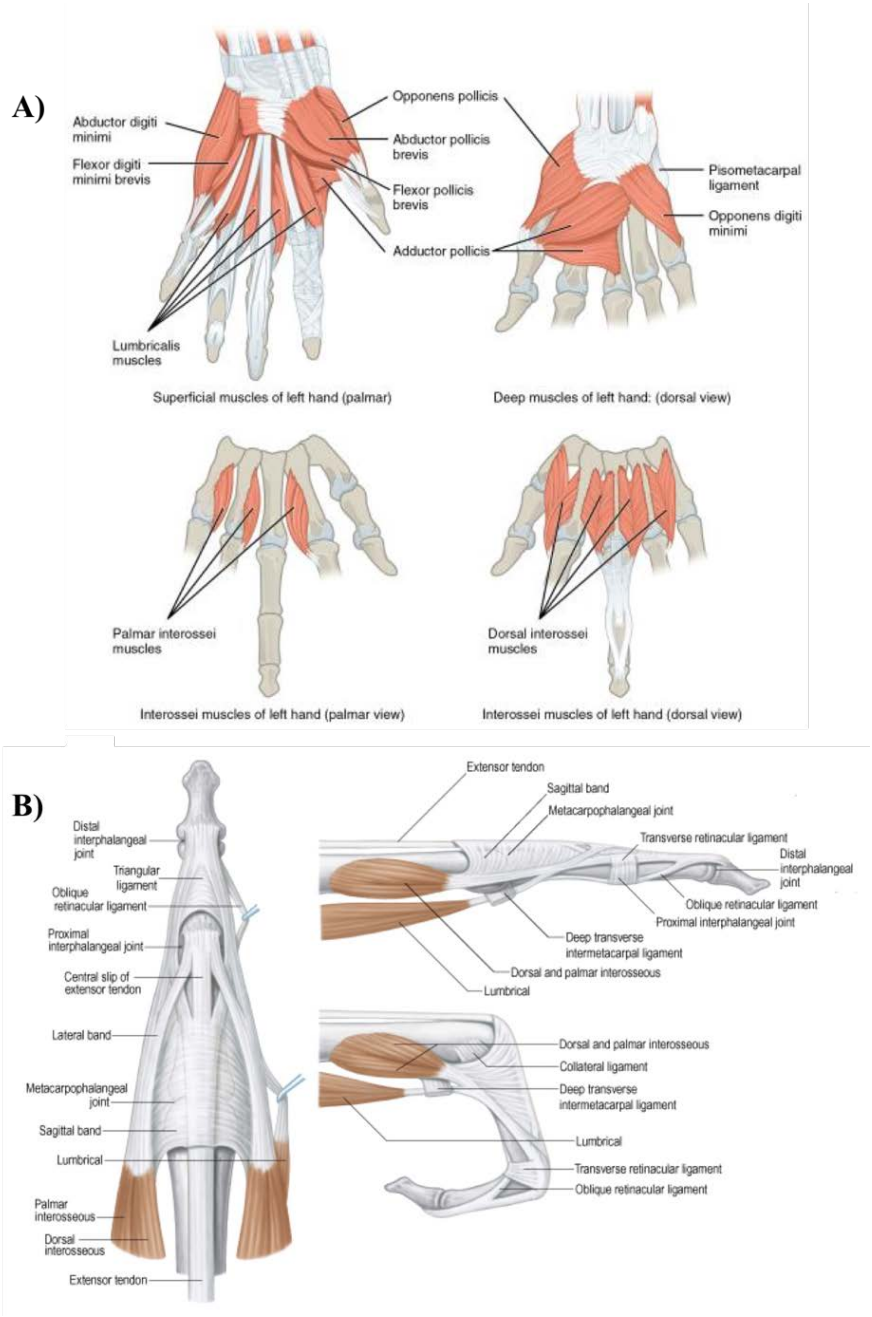

Figure 2.4. Overview of the A) intrinsic finger muscles and B) the extensor mechanism of the finger (Adapted from (Shatz) and (Standring, 2016)

The active force produced by the muscles is not the only contributor to coordinated finger flexion and extension. The passive torques produces by the soft tissue structures that surround a joint (including passive muscles) play a crucial role in the control and stabilization of dynamic finger movements. The importance of these passive torques to control dynamic movements in small mass and inertia systems, like the fingers whose masses of each segment range in the order of 2 grams to 16 grams, have been demonstrated in previous experimental work in systems ranging from insect legs to human wrists (Charles and Hogan, 2012; Hooper et al., 2009; Souza et al., 2009; Wu et al., 2012). The findings of these studies emphasize the importance of the passive joint torques in such systems for the passive torques influence the dynamic movement trajectories of the segments more than the momentum and inertia of the segments. Additionally, the inclusion of passive torques are critical for coordinated and controlled dynamic movements of the hand and fingers (Esteki and Mansour, 1997; Kamper et al., 2002). Within the fingers the structures contributing to the passive torques about each finger joint are the ligaments, joint capsules, and other soft tissues surrounding the joint (Figure 2.2B). Due to this complexity if there are any imbalances of the forces within the hand due to an injury of any of the structures or muscles, hand function will likely be impaired.

2.5 Computational musculoskeletal modeling

In a complex system like the hand, it is often difficult to distinguish the consequences of biomechanical changes on dynamic movements within experimental studies. Computational musculoskeletal models can be utilized to predict the mechanical consequences of biomechanical changes that would otherwise be impossible to distinguish in a biologic experiment and can be used to inform future focused experimental designs. Upper-extremity biomechanical models have

been used to probe the biomechanics of many pathologic conditions and predict surgical outcomes. Specific examples include the evaluation of tendon transfer procedures (Mogk et al., 2011b; Murray et al., 2002), the consequences of nerve injuries (Cheng et al., 2015; Crouch et al., 2011; Crouch et al., 2013, 2014), and the mechanics of orthopedic injuries to the wrist, elbow, and shoulder (Buffi et al., 2015; Nichols et al., 2017; Slowik et al., 2016).

The computational modeling platform used within this dissertation is OpenSim (Delp et al., 2007) an open source platform that is the product of over 40 years of research and development originating from the original platform called SIMM (Simulation In Musculoskeletal Modeling) (Delp et al., 1990). OpenSim allows for the development, analysis, and dynamic simulations of computational musculoskeletal models. Within this platform users to build models by defining the kinematic and kinetic properties of the system of interest, for our purposes the upper extremity, by defining the geometric anatomy, masses, and inertias of the individual segments and how each segment is linked to each in a kinematic chain using specified joints defined by the user. Muscles can be added to the system by defining their architectural and force-generating properties.

The muscles within these models are defined as generic Hill-type muscle models. In Hill-type muscle models the force produced by a muscle is defined by four normalized curves which include the (1) active and (2) passive force-length relationship, (3) force-velocity relationship, and (4) tendon force-strain curve (Zajac, 1989) (Figure 2.5). These four normalized curves may be adjusted for different implementations of the normalized Hill-type muscle model (Millard et al., 2013; Schutte, 1992; Thelen, 2003). These normalized Hill-type model curves are then scaled by muscle specific parameters to define the force output of each individual muscle. These muscle specific parameters are each muscle's optimal fiber length (L_{fo}), tendon slack length (L_{ts}), peak

isometric force (F_o), and pennation angle (α).

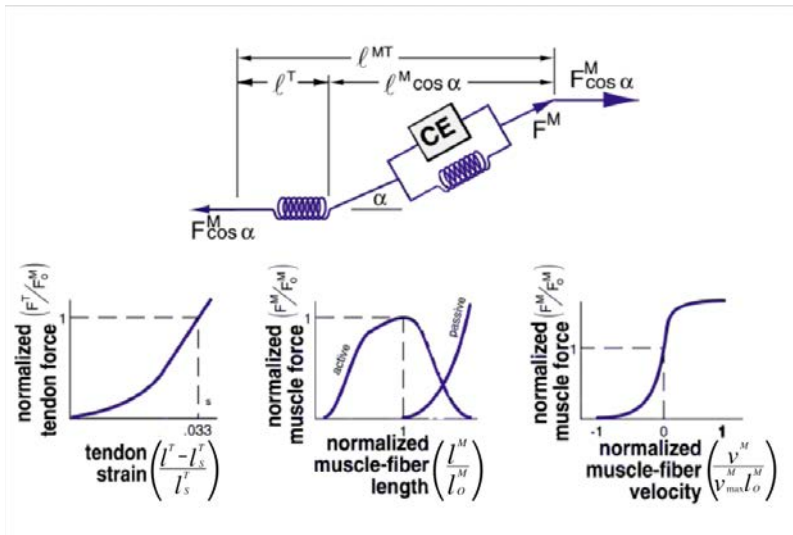

Figure 2.5. Schematic of the Hill-Type muscle model and the normalized tendon force-length curve, muscle fiber active and passive force-length curves, and muscle fibers force-velocity curve.

The computational model of the upper extremity used as the basis of all the models developed within this dissertation was first described as a kinematic model (Holzbaur et al., 2007a; Holzbaur et al., 2005; Holzbaur et al., 2007b) and then was updated to include the masses and inertias of the upper extremity segments, thereby allowing dynamic simulations (Saul et al., 2015). The model includes 7 degrees of freedom at the glenohumeral, elbow, forearm and wrist joints with the anthropometrical, mass, and inertia characteristics of a 50th percentile male for each segment. The model includes 32 muscles and muscle compartments crossing the glenohumeral, elbow, forearm and wrist joints (Saul et al., 2015). The force generating parameters for each muscle within the model were experimentally collected (Holzbaur et al., 2007a; Holzbaur et al., 2007b; Murray et al., 2000; Murray et al., 1995). The initial model developed by Holzbaur 2005 and the dynamic upper extremity model by Saul 2015 have been used extensively within and outside of our lab with at least 320 citations between the two models (Web_Of_Science, 2017).

3 INCORPORATING THE LENGTH-DEPENDENT PASSIVE-FORCE GENERATING MUSCLE PROPERTIES OF THE EXTRINSIC FINGER MUSCLES INTO A WRIST AND FINGER BIOMECHANICAL MUSCULOSKELETAL MODEL

Dynamic movement trajectories of low mass systems have been shown to be predominantly influenced by passive viscoelastic joint forces and torques compared to momentum and inertia. The hand is comprised of 27 small mass segments. Because of the influence of the extrinsic finger muscles the passive torques about each finger joint becomes a complex function dependent on the posture of multiple joints of the distal upper limb. However, biomechanical models implemented for the dynamic simulation of hand movements generally don't extend proximally to include the wrist and distal upper limb. Thus, they cannot accurately represent these complex passive torques. The purpose of this short communication is to both describe a method to incorporate the length-dependent passive properties of the extrinsic index finger muscles into a biomechanical model of the upper limb and to demonstrate their influence on combined movement of the wrist and fingers. Leveraging a unique set of experimental data, that describes the net passive torque contributed by the extrinsic finger muscles about the metacarpophalangeal joint of the index finger as a function of both metacarpophalangeal and wrist postures, we simulated the length-dependent passive properties of the extrinsic finger muscles. Dynamic forward simulations demonstrate that a model including these properties passively exhibits coordinated movement between the wrist and finger joints, mimicking tenodesis, a behavior that is absent when the length-dependent properties are removed. This work emphasizes the importance of incorporating the length-dependent properties of the extrinsic finger muscles into biomechanical models to study healthy and impaired hand movements.

3.1 Introduction

The forces produced by soft tissue structures that surround a joint (including passive muscles) play a crucial role in the control and stabilization of dynamic movements of low mass and inertia systems. Experimental work on biomechanical systems ranging from insect legs to human wrists (Charles and Hogan, 2012; Hooper et al., 2009; Souza et al., 2009; Wu et al., 2012) has demonstrated that passive viscoelastic forces, and the joint torques that result, influence dynamic movement trajectories of low mass systems more than the momentum and inertia of the segments.

Comprised of 27 bones with masses ranging between 0.002 and 0.04 kilograms (Le Minor and Rapp, 2001; McFadden and Bracht, 2003; Mirakhorlo et al., 2016; Saul et al., 2015), the hand is a small mass and inertia system. As a result, the inclusion of passive viscoelastic forces are critical for the simulation of controlled dynamic movements of the hand and fingers (Esteki and Mansour, 1997; Kamper et al., 2002). Passive viscoelastic forces in the hand are produced by soft tissue structures, either those that act within the hand (e.g., ligaments, joint capsules, skin, and intrinsic finger muscles) or the extrinsic finger muscles, which originate proximally, cross the wrist, and attach distally on the fingers (Knutson et al., 2000; Kuo and Deshpande, 2012). Because the force a muscle produces depends on length, it varies as a function of the posture of every joint the muscle crosses. Thus, forces produced by the passive extrinsic finger muscles are a complex, multi-dimensional function of joint postures of the distal upper limb (Bhardwaj et al., 2011; Knutson et al., 2000; O'Driscoll et al., 1992; Richards et al., 1996).

Biomechanical models that are implemented for dynamic simulations of finger movements include passive torques about each finger joint; however, most commonly these models exclude the wrist and distal upper limb (e.g. Babikian et al., 2016; Brook et al., 1995; Esteki and Mansour,

1997; Goislard de Monsabert et al., 2012; Kamper et al., 2002; Li and Zhang, 2009; Sancho-Bru et al., 2003; Sancho-Bru et al., 2001). While previous simulation work integrating the wrist and hand included active muscle properties that varied with proximal joint posture, the passive viscoelastic torques about each finger joint were defined as a function of a single joint, independent of other joint postures (Adamczyk and Crago, 2000). Here, we incorporate the length-dependent passive forces of the extrinsic index finger muscles into a biomechanical model of the hand and demonstrate their influence on combined passive movements of the wrist and hand.

3.2 Methods

3.2.1 Dynamic biomechanical musculoskeletal model development

A dynamic biomechanical model was developed in OpenSim v3.2 (Delp et al., 2007) by adapting an existing dynamic model of the upper extremity (Saul et al., 2015). The original model included the kinematics of the shoulder, elbow, and wrist, without additional degrees of freedom distal to the wrist. As described previously (Blana et al., 2016), the kinematics of the original model were augmented to include degrees of freedom for digits 1 (thumb) through 5 (pinky finger) (Figure 3.1).

Mass and inertia properties of the individual hand bone segments were distributed (Le Minor and Rapp, 2001; McFadden and Bracht, 2003) such that the sum of the individual bones are equal to the total mass of the hand segment from Saul et al., 2015 (Table 3.1). Because critical data needed for the hand model (e.g., moment arms, passive joint torques) currently only exist for the index finger (digit 2), the simulations of wrist and hand movement described here only involve the index finger. Muscle-tendon paths of the four extrinsic index finger muscles, flexor digitorum superficialis indices (FDSI), flexor digitorum profundus indices (FDPI), extensor digitorum

communis indices (EDCI), and extensor indicis proprius (EIP), defined by Saul et al. (2015) were edited so that the moment arms replicated experimental data about the metacarpophalangeal (MCP), proximal-interphalangeal (PIP), and distal-interphalangeal (DIP) joints of the index finger (Figure 3.2) (Buford et al., 2005; Fowler et al., 2001).

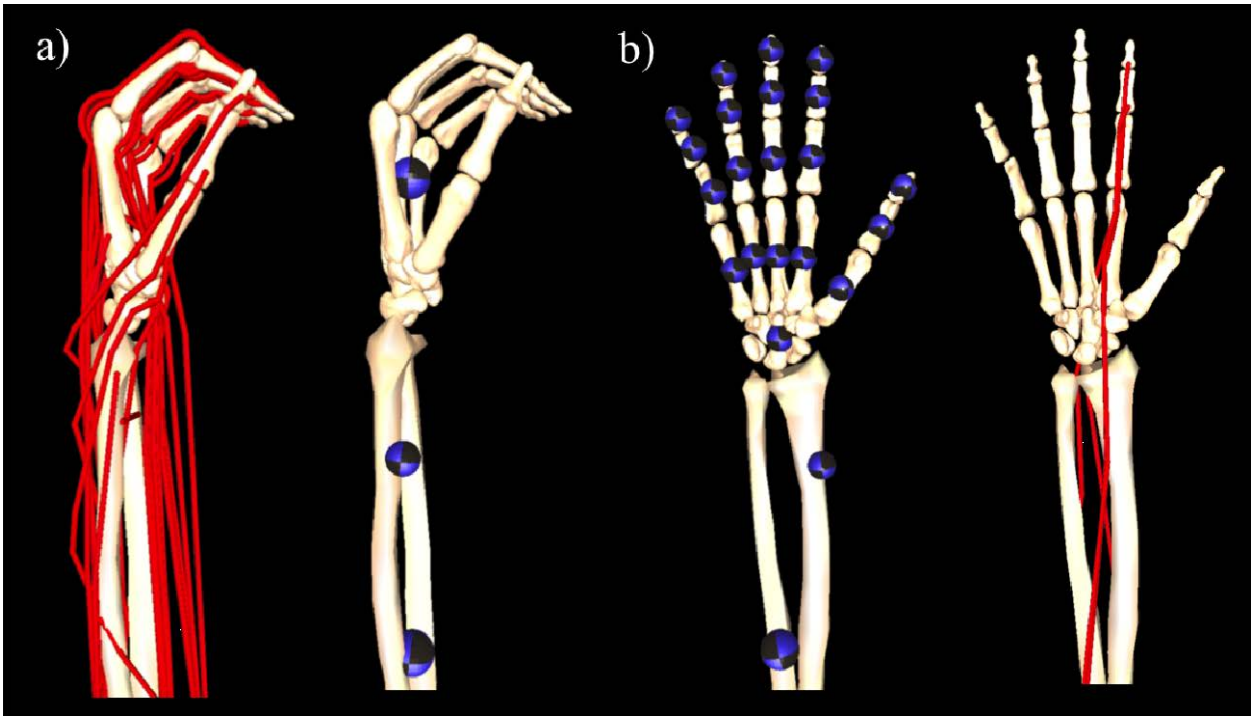

Figure 3.1. To enable simulation of combined wrist and finger motions, (a) the kinematic tree of the dynamic model described in Saul et al. (2015) was augmented to (b) include the degrees of freedom and kinematics of the fingers, thumb, and carpal-metacarpal joints. Location of the colored spheres represent the location of center of mass of each individual segment in the distal upper limb within the original model (Saul et al., 2015) and the adapted model; the diameter of each sphere indicates the mass of the modeled segment (see Table 3.1). Red lines represent simulated muscle-tendon paths within the model; for the purposes of this study, we only included the extrinsic muscles of the index finger.

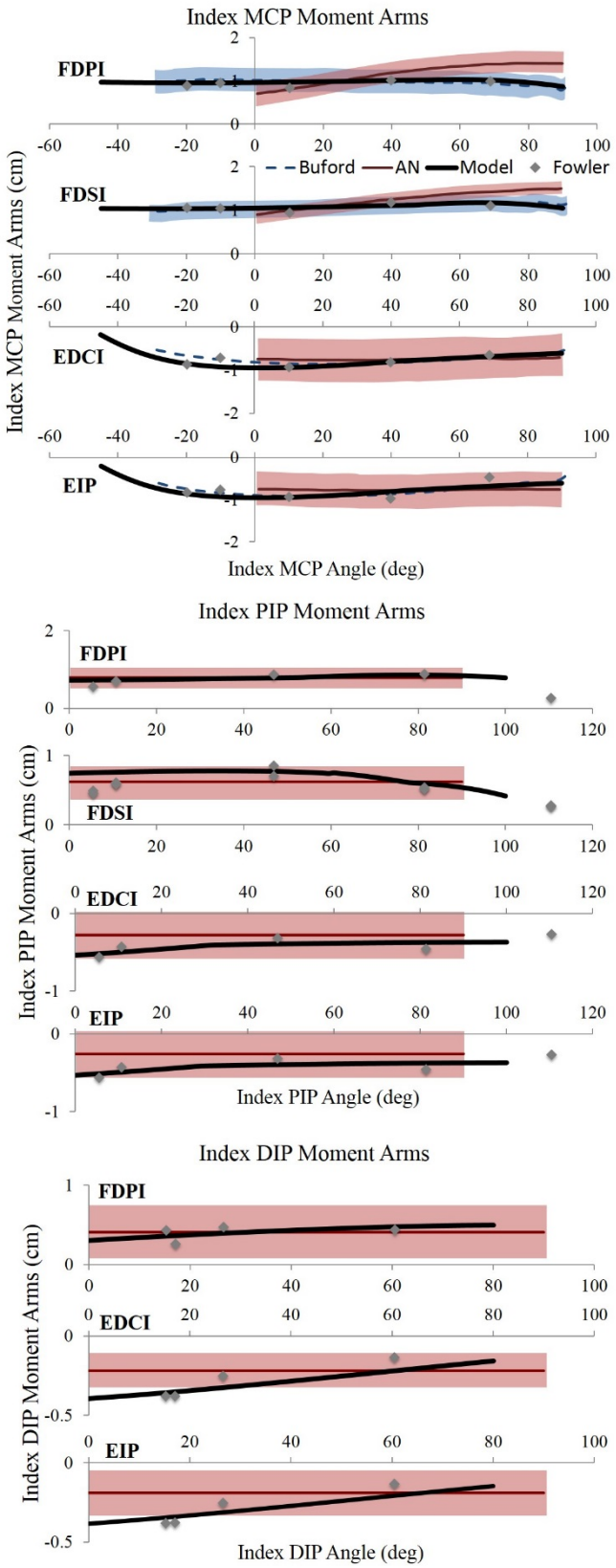

Figure 3.2. Moment arm data about the metacarpophalangeal (MCP), proximal interphalangeal (PIP), and distal interphalangeal (DIP) joints of the current model (solid black), Buford et al. (blue line), An et al. (red line), and Fowler (grey diamonds) of the flexor digitorum superficialis indices (FDSI), flexor digitorum profundus indices (FDPI), extensor digitorum communis indices (EDCI), and extensor digitorum proprius (EIP) muscles. Shaded area indicates two standard deviations when data was available.

Table 3.1. Interial Parameters For Bone Segments

Segment	Mass (kg)	Center of Mass in Segment Reference Frame (m)			Inertia about Center of Mass (kg m)					
		Rx	Ry	Rz	Ixx	Ixy	Ixz	Iyy	Iyz	Izz
Carpal Bones*	0.3274	-0.0003	0.0033	-0.0045	1.51E-05	0.00E+00	0.00E+00	3.37E-05	0.00E+00	3.96E-05
First metacarpal	0.0160	0.0078	-0.0147	-0.0060	2.38E-06	9.44E-07	5.02E-07	1.42E-06	-8.17E-07	2.52E-06
Second metacarpal	0.0364	0.0000	0.0000	0.0000	9.78E-06	1.45E-06	-2.40E-07	5.29E-07	1.56E-06	9.74E-06
Third metacarpal	0.0381	0.0000	0.0000	0.0000	8.89E-06	1.28E-07	-1.68E-08	2.95E-07	1.12E-06	8.74E-06
Fourth metacarpal	0.0333	-0.0020	-0.0214	0.0034	6.85E-06	-7.04E-07	1.00E-07	3.49E-07	9.37E-07	6.79E-06
Fifth metacarpal	0.0296	-0.0061	-0.0177	0.0054	4.77E-06	-1.06E-06	2.23E-07	5.73E-07	9.36E-07	4.82E-06
Thumb proximal phalanx	0.0079	0.0096	-0.0163	-0.0063	5.21E-07	1.89E-07	7.52E-08	3.19E-07	-1.25E-07	5.85E-07
Thumb distal phalanx	0.0031	0.0056	-0.0104	-0.0044	9.21E-08	2.84E-08	1.31E-08	6.45E-08	-2.09E-08	1.00E-07
Second proximal phalanx	0.0158	0.0044	-0.0253	0.0040	2.41E-06	3.31E-07	-6.25E-08	5.63E-07	3.59E-07	2.40E-06
Second middle phalanx	0.0049	0.0022	-0.0154	0.0002	2.83E-07	2.39E-08	-1.13E-09	7.30E-08	1.01E-08	2.85E-07
Second distal phalanx	0.0018	0.0013	-0.0100	0.0000	4.55E-08	5.53E-09	-5.75E-10	1.58E-08	3.20E-09	4.62E-08
Third proximal phalanx	0.0193	0.0010	-0.0262	0.0037	3.52E-06	8.59E-08	-6.42E-09	6.16E-07	2.17E-07	3.51E-06
Third middle phalanx	0.0064	0.0007	-0.0168	0.0013	5.25E-07	1.99E-08	-8.17E-10	1.01E-07	1.74E-08	5.25E-07
Third distal phalanx	0.0025	0.0005	-0.0102	-0.0003	8.08E-08	4.06E-09	-3.80E-10	2.65E-08	5.10E-09	8.06E-08
Fourth proximal phalanx	0.0137	-0.0022	-0.0238	0.0035	1.95E-06	-2.02E-07	2.31E-08	3.91E-07	1.81E-07	1.96E-06
Fourth middle phalanx	0.0057	-0.0020	-0.0147	0.0012	3.60E-07	-2.37E-08	2.13E-09	9.43E-08	2.41E-08	3.60E-07
Fourth distal phalanx	0.0029	-0.0004	-0.0102	0.0020	9.91E-08	-5.72E-09	1.26E-09	3.64E-08	1.39E-08	9.65E-08
Fifth proximal phalanx	0.0111	-0.0081	-0.0211	0.0021	1.18E-06	-3.28E-07	2.81E-08	3.72E-07	7.93E-08	1.29E-06
Fifth middle phalanx	0.0037	-0.0049	-0.0121	-0.0002	1.57E-07	-4.00E-08	3.69E-09	6.14E-08	1.01E-08	1.70E-07
Fifth distal phalanx	0.0022	-0.0036	-0.0089	0.0003	5.06E-08	-1.24E-08	1.15E-09	2.89E-08	2.53E-09	5.59E-08

Passive force-generating properties of the extrinsic muscles were simulated by scaling a generic, Hill-type muscle-tendon model (Millard et al., 2013). Force-generating parameters were taken from Saul et al. with the exception of tendon slack lengths (L_{ts}). L_{ts} was optimized (Table 3.2) to replicate length-dependent, passive force-generating properties of the extrinsic finger muscles determined experimentally (see section 3.2.2). L_{ts} was chosen as the optimization parameter because when all other parameters are held constant for a given muscle-tendon actuator, L_{ts} alters the relationship between joint position and fiber length, influencing the passive muscle forces produced over a given range of joint motion (Arnold et al., 2010; Holzbaur et al., 2005).

Of note, to improve both computational efficiency and numerical stability, the default, normalized, active force-generating curve ($\tilde{f}_a(\tilde{l}_m)$) in the "Millard2012EquilibriumMuscle" model, recommended for general use in OpenSim, yields small active forces at fiber lengths where no active force can be generated (e.g., normalized force = 0.1, 10% of maximum isometric force, at normalized fiber lengths of less than 0.5) (Millard et al., 2013). For similar computational reasons, the default minimum muscle activation is defined as 0.01 (1% of full activation). We altered these default settings, sacrificing computational robustness to enable simulations of purely passive muscle forces. Specifically, the default $\tilde{f}_a(\tilde{l}_m)$ curve in the "Millard2012EquilibriumMuscle" tool in OpenSim 3.2 was modified to replicate the $\tilde{f}_a(\tilde{l}_m)$ curve we have implemented previously (Holzbaur et al., 2005; Saul et al., 2015). Additionally, minimum muscle activation level was defined to be zero. To prevent numerical singularities under these conditions the fiber damping coefficient was defined to be 0.1 (Millard et al., 2013). For consistency, we also modified the default, normalized passive force-length ($\tilde{f}_p(\tilde{l}_m)$) and tendon

force-strain ($\tilde{f}_t(\varepsilon_t)$) curves to replicate our previous work. See Appendix A for validation of the muscle model.

3.2.2 Incorporation of the extrinsic finger muscles' length-dependent passive properties

Parameter values for L_{ts} for the four extrinsic finger muscles (Table 3.2) were defined by solving an optimization problem that matched simulated passive torques about the MCP joint of the index finger to experimental data (Knutson et al., 2000). An optimization algorithm was coded within MATLAB (Natick, MA) to minimize the difference between experimental torques ($T_E(\theta,\omega)$) and the net simulated passive torque ($T_M(\theta,\omega)$) produced by the extrinsic finger muscles, defined as:

$$T_M(\theta,\omega) = \sum_{i=1}^{4} \tilde{f}_{t,i}\left(\varepsilon_{t,i}\left(\theta,\omega,L_{ts,i}\right)\right) \cdot ma_i(\theta) \cdot F_{o,i} \qquad (1)$$

where, for the ith actuator: $\tilde{f}_{t,i}\left(\varepsilon_{t,i}\left(\theta,\omega,L_{ts,i}\right)\right)$ is the normalized tendon force at tendon strain ($\varepsilon_{t,i}$), which is a function of MCP angle (θ), wrist angle (ω), and $L_{ts,i}$; ma_i is the moment arm; $F_{o,i}$ is the maximum isometric force.

The difference between $T_M(\theta,\omega)$ and $T_E(\theta,\omega)$ was minimized using a 3 degree-of-freedom optimization (Eq. (2) and (3)), solving for L_{ts} for each of the four extrinsic muscles, subject to a constraint (J), intended to limit changes from initial parameter values.

$$\min\left[\left[\sum_{\omega=-60}^{60}\sum_{\theta=-45}^{90}\left(T_E(\theta,\omega) - T_M(\theta,\omega)\right)^2\right] + J(L_{ts})\right] \qquad (2)$$

$$J(L_{ts}) = \frac{1}{100}\left(\left|\frac{L_{ts,FDSI}-L^I_{ts,FDSI}}{L^I_{ts,FDSI}} - \frac{L_{ts,FDPI}-L^I_{ts,FDPI}}{L^I_{ts,FDPI}}\right| + \left|\frac{L_{ts,EDCI}-L^I_{ts,EDCI}}{L^I_{ts,EDCI}} - \frac{L_{ts,EIP}-L^I_{ts,EIP}}{L^I_{ts,EIP}}\right|\right) \qquad (3)$$

L^I_{ts} is the initial tendon slack length from Saul et al. (2015).

For the optimization, passive forces and torques produced by the extrinsic muscles about the MCP joint of the index finger were explicitly calculated in MATLAB (Natick, MA); $\tilde{f}_p(\tilde{l}_m)$ and $\tilde{f}_t(\varepsilon_t)$ curves, all muscle force-generating parameters, muscle-tendon lengths, and moment arms needed for the calculations were exported from the OpenSim v3.2 model.

Normalized passive forces for a given iteration of L_{ts} parameter values were computed by solving a non-linear system of equations (Equations 4-7) using the MATLAB *fsolve* function. Each actuator was assumed to be passive and static, simplifying the model to two elastic elements, the tendon and the muscle fibers, arranged in series at a relative orientation specified by the muscle's pennation angle (α). Thus, for all joint postures, muscle fiber length, $L_{m,i}(\theta,\omega)$, and tendon length, $L_{t,i}(\theta,\omega)$, must satisfy:

$$L_{mt,i}(\theta,\omega) = L_{t,i}(\theta,\omega) + \cos(\alpha_i)L_{m,i}(\theta,\omega) \tag{4}$$

where the muscle-tendon length, $L_{mt,i}(\theta,\omega)$, is explicitly defined by the muscle-tendon lengths exported from OpenSim. The force outputs of the muscle and tendon at a given normalized fiber length, $\tilde{l}_{m,i}$, and tendon strain, $\varepsilon_{t,i}$, are specified by the generic $\tilde{f}_p(\tilde{l}_m)$ and $\tilde{f}_t(\varepsilon_t)$ curves exported from OpenSim, and also must satisfy:

$$\tilde{f}_{t,i}\left(\varepsilon_{t,i}(\theta,\omega,L_{ts,i})\right) = \cos(\alpha_i)\tilde{f}_{p,i}\left(\tilde{l}_{m,i}(\theta,\omega)\right) \tag{5}$$

where $\tilde{l}_{m,i}(\theta,\omega)$ and $\varepsilon_{t,i}(\theta,\omega,L_{ts,i})$ are functions of $L_{m,i}(\theta,\omega)$ and $L_{t,i}(\theta,\omega)$ from Eq. (4), respectively. Specifically,

$$\tilde{l}_{m,i}(\theta,\omega) = \frac{L_{m,i}(\theta,\omega)}{L_{fo,i}} \tag{6}$$

$$\varepsilon_{t,i}(\theta,\omega,L_{ts,i}) = \frac{L_{t,i}(\theta,\omega)-L_{ts,i}}{L_{ts,i}} \tag{7}$$

$L_{fo,i}$ is the optimal fiber length.

In passive conditions the muscle-tendon actuator can only generate forces at joint angles where both the tendon is longer than its slack length and the muscle fibers are longer than optimal length. That is:

$$\tilde{f}_{t,i}\left(\varepsilon_{t,i}(\theta,\omega,L_{ts,i})\right) = \begin{cases} \tilde{f}_{t,i}\left(\varepsilon_{t,i}(\theta,\omega,L_{ts,i})\right) & if \quad L_{mt,i}(\theta,\omega) \geq L_{ts,i} + \cos(\alpha)L_{fo,i} \\ 0 & otherwise \end{cases} \quad (8)$$

Table 3.2. Optimized Tendon Slack Lengths And Precent Changes

	FDPI	FDSI	EIP	EDC
Initial tendon slack length	0.3015	0.275	0.21	0.365
New optimized tendon slack length	0.3044	0.2772	0.1911	0.3486
Percent change	0.95%	0.79%	-9.89%	-4.70%

3.2.3 Incorporation of passive torques produced by soft tissue structures intrinsic to the hand

The optimization of L_{ts} allows us to simulate passive torques for the extrinsic muscles that replicate the work of Knutson et al. (2000). The net passive torques contributed by the intrinsic soft tissue structures (e.g., ligaments, joint capsules, skin, and intrinsic finger muscles) that cross the MCP, PIP, and DIP joints of the index finger are implemented into the model as three, torsional, spring-dampers, each acting independently about a single joint. In each case, the relationship between passive joint torque and joint angle was specified via the “FunctionBasedBushing” tool (DeMers, 2015) in OpenSim. A cubic spline curve parameterized additional data reported in Knutson et al. (2015) to define the constitutive relationship between the net, passive, elastic torques produced by intrinsic hand structures and MCP joint angle. Similarly, the constitutive torque-angle

relationship for the PIP and DIP joints, and the viscous property of each spring-damper acting about the three joints were defined from the literature (Kamper et al., 2002).

3.2.4 Forward dynamic simulation of wrist and finger motion

Forward dynamic simulations of combined wrist and finger motion were performed in two forearm postures. The hand was oriented horizontally; gravity either opposed (pronated forearm) or assisted (supinated forearm) wrist extension. Wrist motion was prescribed (Figure 3.3a). First, 60° extension, maintained for one second, yielded the initial equilibrium position of the index finger. Second, wrist flexion was prescribed at 20°/second, until achieving 60° flexion. The remaining unconstrained degrees of freedom in the model (MCP, PIP, and DIP joint angles) were simulated with time.

Simulations were repeated with all length-dependent passive properties removed from the hand model. In these simulations, passive torques about each finger joint were implemented only by the torsional spring-dampers. Torque magnitudes were re-defined using the sum of the passive torques produced by the intrinsic structures and those produced by the extrinsic finger muscles at a single wrist posture (0° wrist extension).

3.3 Results and Discussion

Simulation of length-dependent passive force-generating properties of extrinsic finger muscles yielded coupled movements between the wrist and index finger during dynamic forward simulations (Figure 3.3). With the forearm pronated, prescribed wrist flexion produced coordinated MCP extension (initial position: 83° flexion, final position: 21.8° extension) and PIP extension (11.1° to 1.7° flexion; Figure 3b-d), mimicking tenodesis (Johanson and Murray, 2002;

Su et al., 2005). With the forearm supinated, the finger joints followed similar trajectories but were more flexed (Figure 3.3b-d). Muscle-tendon lengths of the extrinsic finger flexors increase by 1-2% with supination, increasing the passive flexion torques generated. Without length-dependent passive properties, the posture of the index finger was determined by gravity; coupled motion was absent and the finger joints were more extended with the forearm supinated (Figure 3.3).

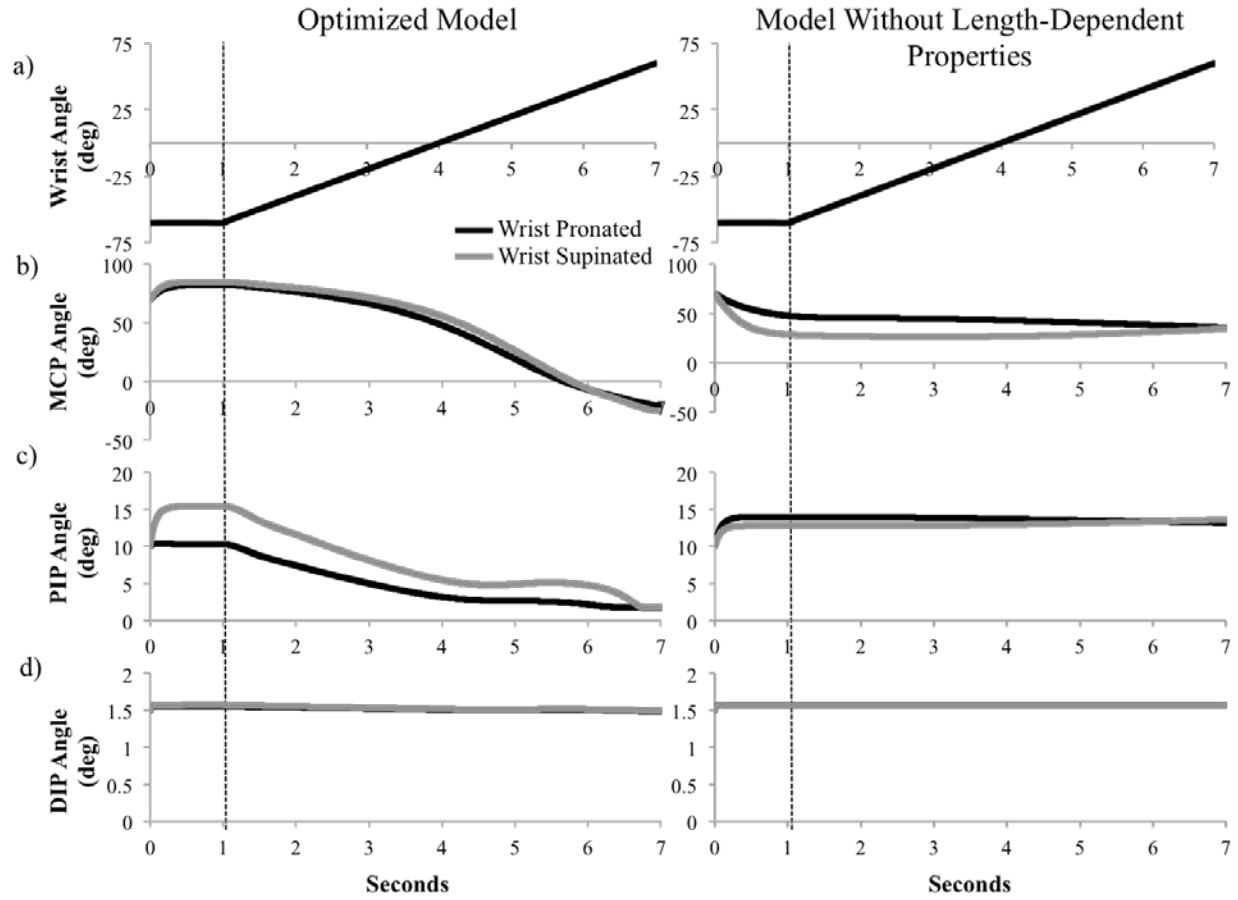

Figure 3.3. Wrist and index finger joint postures as a function of time in a pronated (black lines) and supinated (grey lines) forearm position; optimized model results on the left, model without the length-dependent passive properties on the right. (a) Wrist posture was prescribed identically in both sets of simulations, (b) metacarpophalangeal (MCP), (c) proximal interphalangeal (PIP), and (d) distal interphalangeal (DIP) joints postures were simulated. The dotted line indicates start of wrist motion.

3.4 Conclusion

Passive torques are critical to achieve controlled and stabilized dynamic free movements of the wrist and fingers (Babikian et al., 2016; Blana et al., 2016; Charles and Hogan, 2012; Kamper et al., 2002). Additionally, passive coupling of the fingers and wrist is a fundamental component of hand function in the severely disabled hand, such as following tetraplegia (Johanson and Murray, 2002; Su et al., 2005). The methods implemented in this study are novel in that they enable incorporation of experimentally measured, length-dependent passive torques produced by the extrinsic muscles in biomechanical models of the hand. Given experimental data for both healthy and impaired hands, the methods described here will enable simulation-based analysis of healthy hand function and evaluation of how musculoskeletal alterations after an injury, that are often associated with increases in passive joint stiffness, affect impaired populations. The extent to which the passive coupling between the hand and distal upper limb joints affects both endpoint force production with the fingers and high-speed movements is unknown; the tools described here facilitate future work in this direction.

4 THE BIOMECHANICAL BASIS OF THE CLAW FINGER DEFORMITY: A COMPUTATIONAL SIMULATION STUDY

During attempted finger extension, the claw finger deformity is commonly present in many populations whose intrinsic finger muscles are weakened or paralyzed due to peripheral or central neural impairments. Though, the claw finger deformity is not acutely present following intrinsic muscle palsy. Rather, the impairment has a delayed onset and the severity progresses over time. This delay and progression of the deformity leads to the assumption that biomechanical property changes exacerbate the loss of intrinsic muscle function and advance the deformity. The postulated biomechanical changes include increased joint laxity, stretching of the extensor mechanism, and contracture of the extrinsic finger flexors. However, current surgical interventions focus primarily on restoring the actions of intrinsic muscles and these critical biomechanical changes, contributing to the development and severity of the claw finger deformity, are neglected and unaccounted for the during surgical interventions. Therefore, within this study we simulated varying levels of individual and combined changes of the biomechanical property changes within the hand to evaluate their effects on the development and severity of the claw finger deformity during finger extension using a computational musculoskeletal model. Our results suggest that the claw finger deformity is most sensitive to shortening of the extrinsic finger flexors and neither changes of increased laxity nor a stretched extensor mechanism independently produce the claw finger deformity. When all three changes were combined the most severe deformity becomes present indicating a significant interaction between all three mechanisms. These results suggest that in both the acute and chronic stages of intrinsic finger paralysis maintaining the length of the extrinsic

finger flexors should be an area of focus of rehabilitation to prevent the formation of the deformity and in pre-habilitation for surgical interventions to achieve optimal outcomes.

4.1 Introduction

The claw finger deformity is present in many populations whose intrinsic finger muscles are weakened or paralyzed due to central (i.e., stroke, spinal cord injury) or peripheral (i.e., ulnar nerve injury, leprosy) neural impairments. During healthy finger extension, the intrinsic finger muscles act synergistically with the extrinsic finger muscles to prevent metacarpophalangeal (MCP) hyperextension and, via the extensor mechanism, couple proximal and distal interphalangeal (PIP and DIP, respectively) extension (Brand, 1958; Brand and Hollister, 1993; Darling and Cole, 1990; Kozin et al., 1999; Li et al., 2000; Palti and Vigler, 2012; Srinivasan, 1976). The claw deformity occurs during attempts to extend the fingers; instead, the MCP joints hyperextend while the PIP and DIP joints concomitantly flex. This dis-coordination subsequently impedes finger extension and limits the ability to grasp objects and functional use of the hand.

The claw finger deformity is not acutely present following intrinsic muscle palsy (Sapienza and Green, 2012; Schreuders et al., 2007). Rather, the impairment occurs with a delayed onset and the severity progresses over time. As a result, biomechanical soft tissue properties are postulated to exacerbate the loss of intrinsic muscle function and, as they change over time, advance the deformity (Schreuders et al., 2007). For example, individuals who have lax MCP joints develop the claw finger deformity before those with stiffer fingers and often present more severely (Sapienza and Green, 2012; Schreuders et al., 2007; Zancolli, 1957), Additionally, as use of the hand decreases, the fingers remain in a flexed resting posture for extended periods which is postulated to cause contracture (or adaptive shortening) of the extrinsic finger flexor muscles,

similar to muscle shortening following limb immobilization (Tabary et al., 1972; Williams and Goldspink, 1978). Adaptive shortening of the extrinsic flexor muscles would add to the severity of the deformity because, at a given finger position, the shortened flexors would generate relatively large passive flexion forces, resisting finger extension (Brand, 1958; Schreuders et al., 2007). Finally, a prolonged, flexed, resting hand posture is also thought to lead to stretching of the extensor mechanism (Schreuders et al., 2007). Specifically, the central slip and the dorsal hood of the extensor mechanism surrounding the PIP joint are thought to stretch (Sapienza and Green, 2012; Schreuders et al., 2007), resulting in anterior translation of the lateral slips during PIP joint flexion (Schreuders et al., 2007). Anterior translation of the lateral slips would decrease the extensor mechanism's mechanical advantage about the PIP joint and, therefore, the extension torque generated at the PIP joint.

Clinical interventions to mitigate the claw finger deformity focus on replacing critical functions of the paralyzed intrinsic muscles. For example, the synergistic intrinsic muscle activity that prevents MCP hyperextension during finger extension is emulated clinically either via orthoses (Chan, 2002; Colditz, 2002; Sousa and de Macedo, 2015) or surgical procedures that include bone blocks (Mikhail, 1964), tenodeses (Riordan, 1953; Smith, 1984; Srinivasan, 1973), and volar plate capsulodesis (Zancolli, 1957). Additionally, numerous active tendon transfers have been developed in order to improve coordination of distal finger joint extension following loss of intrinsic muscle function (Brand and Hollister, 1993; Sapienza and Green, 2012). In these procedures, the paths of functioning muscle-tendon units, commonly wrist muscles (Brand, 1958; Littler, 1949; Riordan, 1953; Taylor et al., 2004) or the flexor digitorium superficialis (Bunnell, 1942; Littler, 1949), are attached distally to the dorsal aspect of the fingers, after first being routed

on the palmar side of the MCP joint, to mimic the actions of the intrinsic muscles at the MCP, DIP, and PIP joints.

While current clinical interventions focus primarily on finding substitutes for active intrinsic muscle function, they commonly neglect the secondary, but critical, biomechanical changes that contribute to the development of the deficit. The objective of this study is to simulate the effects of soft tissue biomechanical properties on coordinated finger extension using a computational model and to evaluate the contributions of: (i) increased joint laxity, (ii) decreased mechanical advantage of the extensors about the PIP joint, and (iii) shortening of the flexor muscles on the development of claw finger deformity. From clinical observations indicating MCP joint stiffness limits the severity of the deformity as well as many successful clinical interventions focusing on the prevention of MCP hyperextension we will test the hypothesis that joint laxity is the primary factor in the development and severity of the claw finger deformity using computational musculoskeletal models. Upper-limb computational models have previously been used to probe the biomechanics of pathologic conditions and surgical outcomes; including the evaluation of tendon transfer procedures (Mogk et al., 2011a; Murray et al., 2006; Saul et al., 2003), the consequences of nerve injuries (Cheng et al., 2015; Crouch et al., 2011; Crouch et al., 2013, 2014), and mechanics of orthopedic injuries to the wrist, elbow, and shoulder (Buffi et al., 2015; Nichols et al., 2013, 2016; Nichols et al., 2017; Slowik et al., 2016). These computational musculoskeletal models allow for the assessment of the consequences following biomechanical changes on dynamic motions which would be otherwise difficult to distinguish an experimental set up. This analytic ability is especially desirable within the complex system of the hand in order to discern

how soft tissue biomechanical property alterations may affect coordinated finger extension as the claw finger deformity develops.

4.2 Methods

4.2.1 Musculoskeletal Model

To evaluate the sensitivity of coordinated finger extension to soft tissue biomechanical properties that are postulated to advance claw finger deformity, a previously described biomechanical model of the index finger and distal upper limb (Binder-Markey and Murray, 2017) was used to generate forward dynamic simulations of active finger flexion and extension within the OpenSim platform v3.3 (Delp et al., 2007). A 'one-at-a-time' factorial analysis (Hogg and Ledolter, 1987) was performed to evaluate to what extent (i) increased joint laxity, (ii) decreased mechanical advantage of the extensors about the PIP joint, and (iii) shortening of the flexor muscles contributed to the development of claw finger deformity. As described in more detail below, parameter values in the biomechanical model were adapted to reflect a broad range of soft tissue biomechanical properties for each factor, first in isolation (see sections 4.2.3.1-3), then combined (see section 4.2.3.4).

The biomechanical model for the distal upper limb we implemented[32] includes the radius, ulna, carpal, metacarpal, and phalangeal bones of the hand with mass and inertial properties defined to be consistent with a 50th percentile male (Binder-Markey and Murray, 2017; Le Minor and Rapp, 2001; McConville et al., 1980). Kinematics of wrist flexion/extension, and index finger MCP, PIP, and DIP flexion/extension were implemented as defined previously (Binder-Markey and Murray, 2017; Blana et al., 2016). Similarly, muscle-tendon paths and force-generating properties (both active and passive) of the four extrinsic index finger muscles; flexor digitorum superficialis indicis

(FDSI), flexor digitorum profundus indicis (FDPI), extensor digitorum communis indicis (EDCI), and extensor indicis proprius (EIP); are explicitly defined as previously described (Binder-Markey and Murray, 2017). The net passive torques contributed by intrinsic muscles and soft tissue structures (e.g., ligaments, joint capsules, and skin) that cross the MCP, PIP, and DIP joints of the index finger are implemented into the model as three torsional spring-dampers, each acting independently about each joint (Binder-Markey and Murray, 2017). Consistent with an "instrinsic-minus" hand, active force-generating properties of the intrinsic finger muscles were excluded from the model.

4.2.2 Dynamic Simulations

Two sets of simulations were performed with the hand oriented horizontally so that gravity opposes extension. Within the first set of simulations the wrist was locked at 30° of extension, reflecting a wrist posture adopted during daily reaching and grasping activities (de los Reyes-Guzman et al., 2010; Reghem et al., 2014; Ryu et al., 1991). The second set of simulations repeated a subset of the first set with the wrist locked to 30° of flexion, mimicking the Andre-Thomas sign, a strategy often adopted by individuals with mild claw finger deformities to achieve finger extension (Sapienza and Green, 2012; Schreuders et al., 2007). The remaining unconstrained degrees of freedom in the model (MCP, PIP, and DIP joint angles) were simulated with time during the forward dynamic simulation process. The forward dynamic simulation process involves the input of muscle excitations that are then transformed into resultant force of each muscle and their torques about the joints of the system that then drive the motion of those joints through solving a system of the differential equations that define the dynamics of the system (Figure 4.1).

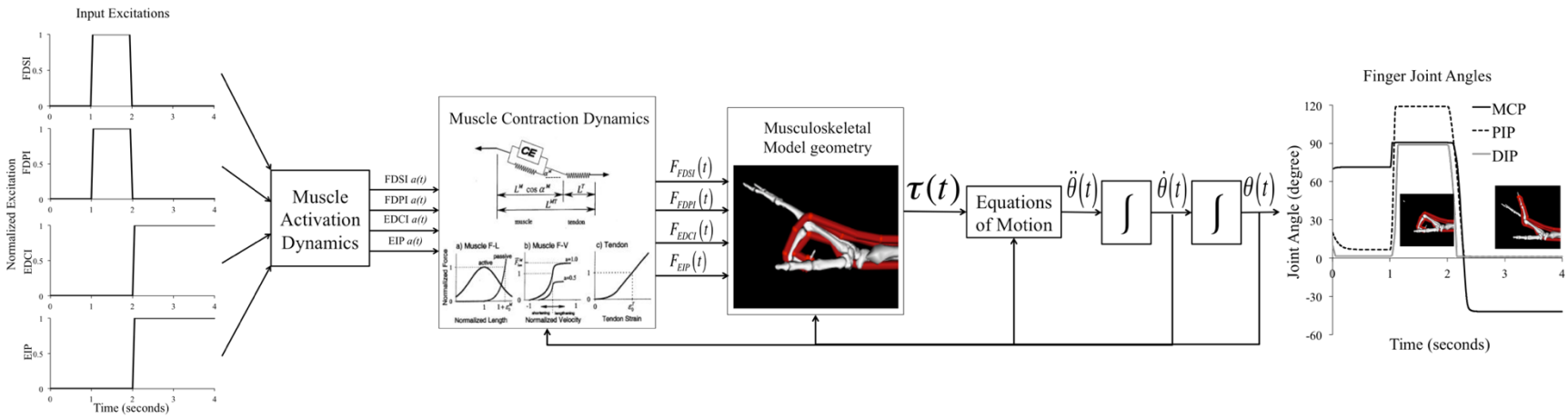

Figure 4.1: Flow chart demonstrating the process of the forward dynamic simulations from the input of the muscles excitations of the flexor digitorum superficialis indicis (FDSI), flexor digitorum profundus indicis (FDPI), extensor digitorum communis indicis (EDCI), and extensor indicis proprius (EIP) to the output of the joint kinematics. The process begins with inputs of muscle activations that then are transformed into muscle forces through the muscle activation and contraction dynamics these forces are then converted into the torques within the system based on the musculoskeletal model geometry. These torques then dictate the joint kinematics through the equations of motion which solve for the acceleration, velocity, and position of each joint over the simulation throughout time.

Regardless of wrist posture, an individual simulation trial involves muscle excitation inputs, defined over a 4 second interval, using a simple step input function. For a specific simulation, 4 muscle excitation inputs were specified, with identical input functions for the extrinsic flexors (FDSI & FDPI) and identical functions for the extrinsic extensors (EDCI & EIP) (Figure 1). The timing of muscle excitation inputs for the extrinsic flexors and extensors was constant across all simulations, and were chosen qualitatively, defined to generate a single cycle of index finger flexion followed by index finger extension with the nominal model. At the completion of the flexion-extension simulation the equilibrium postures of the MCP, PIP, and DIP joints were recorded. The claw finger deformity was defined to be present if both hyperextension (extension beyond 0 degrees) of the MCP and concurrent flexion greater than 20 degrees of the PIP joint were observed.

4.2.3 One-factor-at-a-time Sensitivity Analysis

A one-factor-at-a-time analysis was completed for the three postulated soft tissue biomechanical properties that advance the claw finger deformity, as described below. For the factor analysis, the same forward dynamic simulations were repeated with the input excitations defined as simple step functions scaled to three magnitudes (20%, 50%, and 100% of the maximum excitation) (Table 2).

4.2.3.1 Increased joint laxity

To evaluate the isolated effects of increased joint laxity on coordinated finger extension, forward dynamic simulations were repeated with four different sets of parameter values: the nominal set of parameters (Binder-Markey and Murray, 2017) defined based on experimental data (Kamper et al., 2002; Knutson et al., 2000), and three additional sets of values that decrease the

magnitudes of the passive joint torques contributed by the intrinsic muscles and soft tissue structures about the three finger joints (Figure 4.2). Specifically, the passive joint torques in the nominal model were uniformly scaled to magnitudes equal to 75%, 50%, or 25% of the nominal torques.

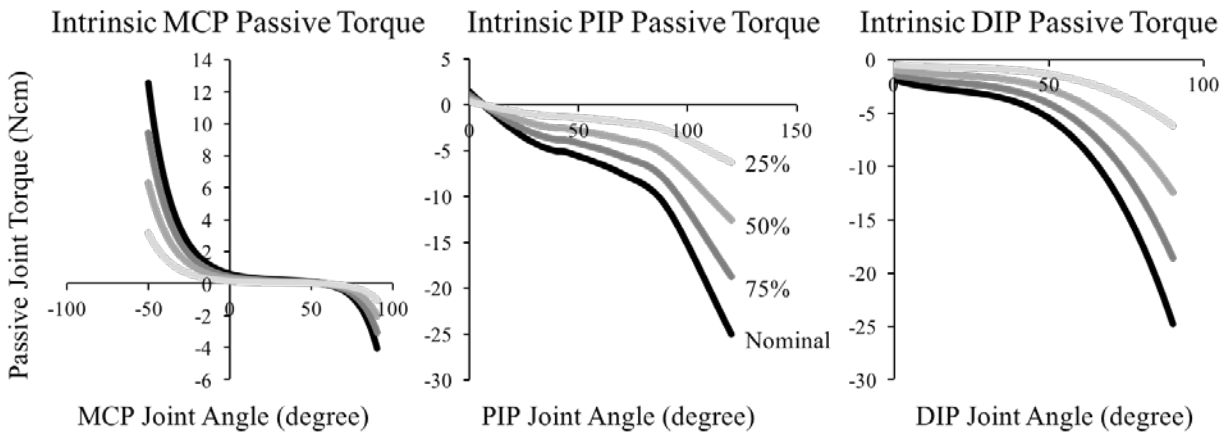

Figure 4.2: The nominal elastic torques produced by intrinsic muscles and joint structures (black) about the MCP, PIP, and DIP joints within the model and the elastic torques mimicking increased laxity of the joints with decreasing nominal torques to 75%, 50%, and 25% (shades of grey) about the MCP, PIP, and DIP joints. (+ flexion/- extension)

4.2.3.2 Decreased extensor mechanical advantage

While our biomechanical model does not include an extensor mechanism, we evaluated the sensitivity of coordinated finger extension to decreased mechanical advantage of the extrinsic index extensor muscles about the PIP joint, a mechanical consequence of the postulated stretching of the extensor mechanism (Brand and Hollister, 1993; Sapienza and Green, 2012) and concomitant anterior translation of the lateral slips of the extensor mechanism in PIP flexion (Schreuders et al., 2007). Forward dynamic simulations were repeated with the PIP extension

moment arms of both extrinsic extensor muscles defined to represent four differing magnitudes in PIP flexion: the nominal magnitude (Binder-Markey and Murray, 2017) defined from a set of experimental parameters (Buford et al., 2005; Fowler et al., 2001) and three sets of decreased extensor moment arm magnitudes (Figure 4.3). The decreased extensor moment arm magnitudes in PIP flexion were simulated by reducing the diameter of the kinematic constraint that determines the distance between the muscle-tendon path and the PIP joint center in flexed postures; diameters of 75%, 50%, and 25% of the nominal diameter were simulated (Figure 4.3).

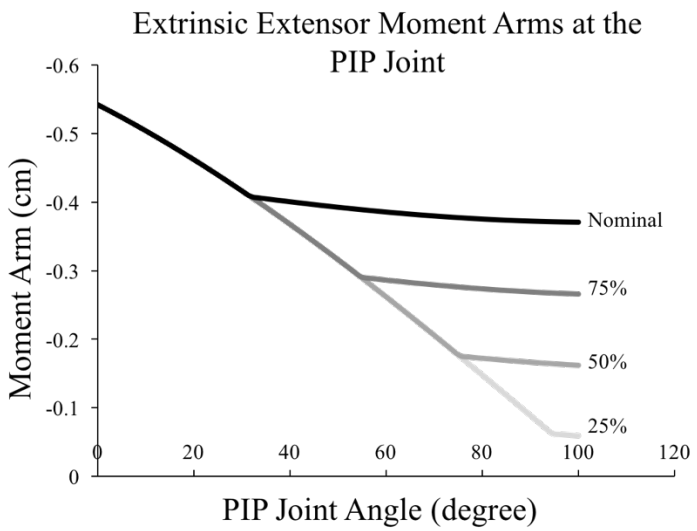

Figure 4.3: Moment arm plots about the PIP joint for the extrinsic extensors with the nominal wrapping surface radius (black) and decreased to 75%, 50%, and 25% of the nominal radius (shades of grey). The muscle tendon path is initially not in contact with the wrapping surface and all the simulations have the same moment arms until coming in to contact with the wrapping surface. As the PIP joint is flexed the path comes in to contact with the surface, as denoted by the flat portions, preventing the anterior translation of the path. As the radius of the surface is decreased the path is able to translate closer to joint center of rotation before making contact, decreasing the moment arms of the extensor muscles about the joint. (+ flexion/- extension)

4.2.3.3 Shortening of the Extrinsic Finger Flexors

The extent that shortening of the extrinsic flexor muscles advances the claw finger deformity following intrinsic muscle weakness or paralysis was also evaluated with forward dynamics simulations performed with four different sets of parameter values. Adaptive shortening of the extrinsic index finger muscles was simulated relative to the nominal "resting length" of the muscle (Binder-Markey and Murray, 2017). Here, we define "resting length" of a muscle-tendon unit based on the understanding that muscle-tendon actuators only generate passive forces at lengths where both the tendon is longer than its slack length (L_{ts}; the length where the tendon becomes taut and begins to transmit force (Zajac, 1989)) and the muscle fibers are longer than optimal length (L_{fo}; the length of a muscle's fibers at maximum active force (Zajac, 1989) which we also define to correspond to the onset of passive force generation). Resting muscle-tendon length, $L_{mt,r}$, is defined mathematically as:

$$L_{mt,r} = L_{ts} + \cos(\alpha) L_{fo}$$

where α is the pennation angle of the muscle fibers with respect to the tendon. To simulate shortening of the resting length of the extrinsic flexor muscles (FDSI and FDPI), the two parameters defining L_{ts} and L_{fo} were uniformly decreased to 98%, 95%, and 90% of the nominal lengths, thus shortening the resting lengths of the muscles (Table 4.1). In simulations where extrinsic flexor muscle-tendon resting lengths were defined to be shorter than nominal, the limb positions where these muscles generated passive forces shifts occurred in more flexed postures (Figure 4.4).

Table 4.1: Optimal Fiber, Tendon Slack, and Muscle-Tendon Resting lengths of the FDSI and FDPI at nominal lengths and shortened to 98%, 95%, and 90% of nominal length.

		Nominal	98%	95%	90%
FDSI	Optimal fiber length	0.0835	0.0818	0.0793	0.0752
	Tendon Slack Length	0.2772	0.2717	0.2633	0.2495
FDPI	Optimal fiber length	0.0749	0.0734	0.0712	0.0674
	Tendon Slack Length	0.3044	0.2983	0.2892	0.2740

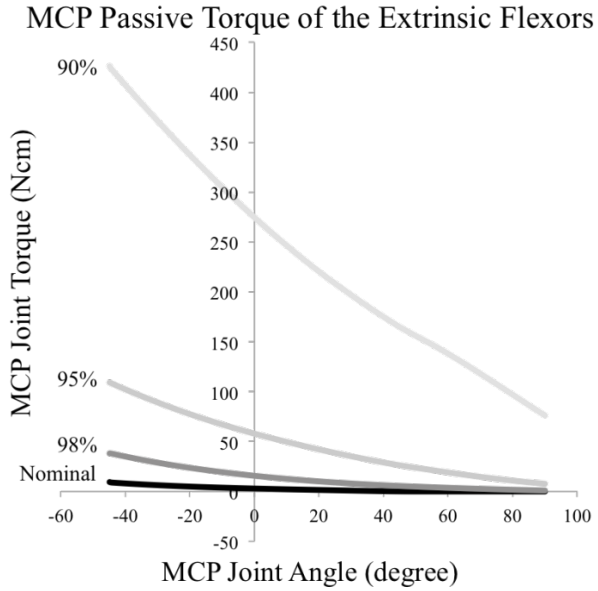

Figure 4.4: The sum of the FDSI and FDPI passive flexion torques throughout the MCP joint range of motion with muscle-tendon unit resting lengths at the nominal length and altered to 98%, 95%, and 90% of the nominal resting length. Note the increase in passive torques and shift of the equilibrium point as the resting lengths are shortened (+ flexion/- extension)

4.2.4 Sensitivity analysis of the interaction effects

After completion of the one-factor-at-a-time sensitivity analysis, where the effect of each the factors was evaluated independently the sensitivity of finger extension to the interaction effects of combined changes was evaluated under three conditions. Those three conditions include either when all the (i) small (75% laxity, 75% moment arm, 98% shortening), (ii) medium (50% laxity, 50% moment arm, 95% shortening), or (iii) large (25% laxity, 25% moment arm, 90% shortening) changes of each postulated biomechanical change to occur in the hand are combined. Forward dynamic simulations with these combined conditions were repeated using the same input excitation step functions (20%, 50%, and 100% of the maximum excitation) and with the wrist extended to 30° as in the "one-factor-at-a-time" analysis. An additional set of simulations with the combined interactions were run with the wrist posture flexed to 30° mimicking the Andre-Thomas sign (Table 4.2).

A total of 48 simulations were completed within this analysis (Table 4.2). With 39 simulations with the wrist at an extended posture with the nominal parameters, the 'one-factor-at-a-time' analysis, and the combined interaction analysis. The remaining nine simulations were run with a flexed wrist posture mimicking the Andre-Thomas sign with the combined interactions only (Table 4.2).

Table 4.2: Summary counting the simulations run during the sensitivity analysis. Set one consists of the simulations with an extended wrist posture within the nominal model, the 'one-at-a-time' analysis, and the combined models. Set two of the simulations run with a flexed wrist posture mimicking the Andre-Thomas sign was run with the combined models only.

	Wrist extended to 30°													Wrist flexed to 30°		
	Nominal Model	"One at a time"									Combined			Combined		
		Increased Laxity			Decreased Mechanical Advantage			Flexor Shortening			Small	Medium	Large	Small	Medium	Large
		75%	50%	25%	75%	50%	25%	98%	95%	90%						
20%	1	1	1	1	13	16	19	22	25	28	31	34	37	40	43	46
50%	1	1	1	1	14	17	20	23	26	29	32	35	38	41	44	47
100%	1	1	1	1	15	18	21	24	27	30	33	36	39	42	45	48
													39			9

4.3 Results

4.3.1 Individual Biomechanical Changes

The claw finger deformity only became present when the extrinsic finger flexors' resting lengths were shortened (Figure 4.5). Even small changes to 98% of the nominal resting length of the muscles produced the claw finger deformity at the 20% activation level; with greater activations finger extension was achieved (Figure 4.5g). Medium length changes to 95% of the nominal resting length demonstrated the deformity across all activation levels (Figure 4.5h) and larger changes to 90% of the nominal resting length resulted in the inability to extend any of the finger joints (Figure 4.5i). Neither changes from increased laxity nor decreased extensor mechanical advantage individually produced the claw finger deformity and full extension of all the joints were achieved across all activation levels (Table 4.3).

4.3.2 Combined Biomechanical Changes

The most severe claw finger deformity, greatest MCP hyperextension with flexion of PIP and DIP joints, was demonstrated within the model including all three of the medium structural changes suggesting a significant interaction between all three mechanisms (Figure 4.6b). These models mimic the progression of the biomechanical changes after intrinsic muscle paralysis. Within the combined model including the small changes, low activations of 20% demonstrated the claw finger deformity but increases in the activation to 50% and 100% extension of all three joints was produced (Figure 4.6a). In models combining the medium and large changes with the wrist extended full finger extension was not achievable across all activation levels. Either the finger joints were unable to extend or the claw finger deformity became present (Figure 4.6c&e). As the

wrist was flexed the models including the small and medium changes achieved finger extension across all activation levels (Figure 4.6b&d). In the model consisting of large changes, the most severe model, the fingers were unable to extend and the deformity was present even with the wrist flexed and full muscle activation (Figure 4.6f).

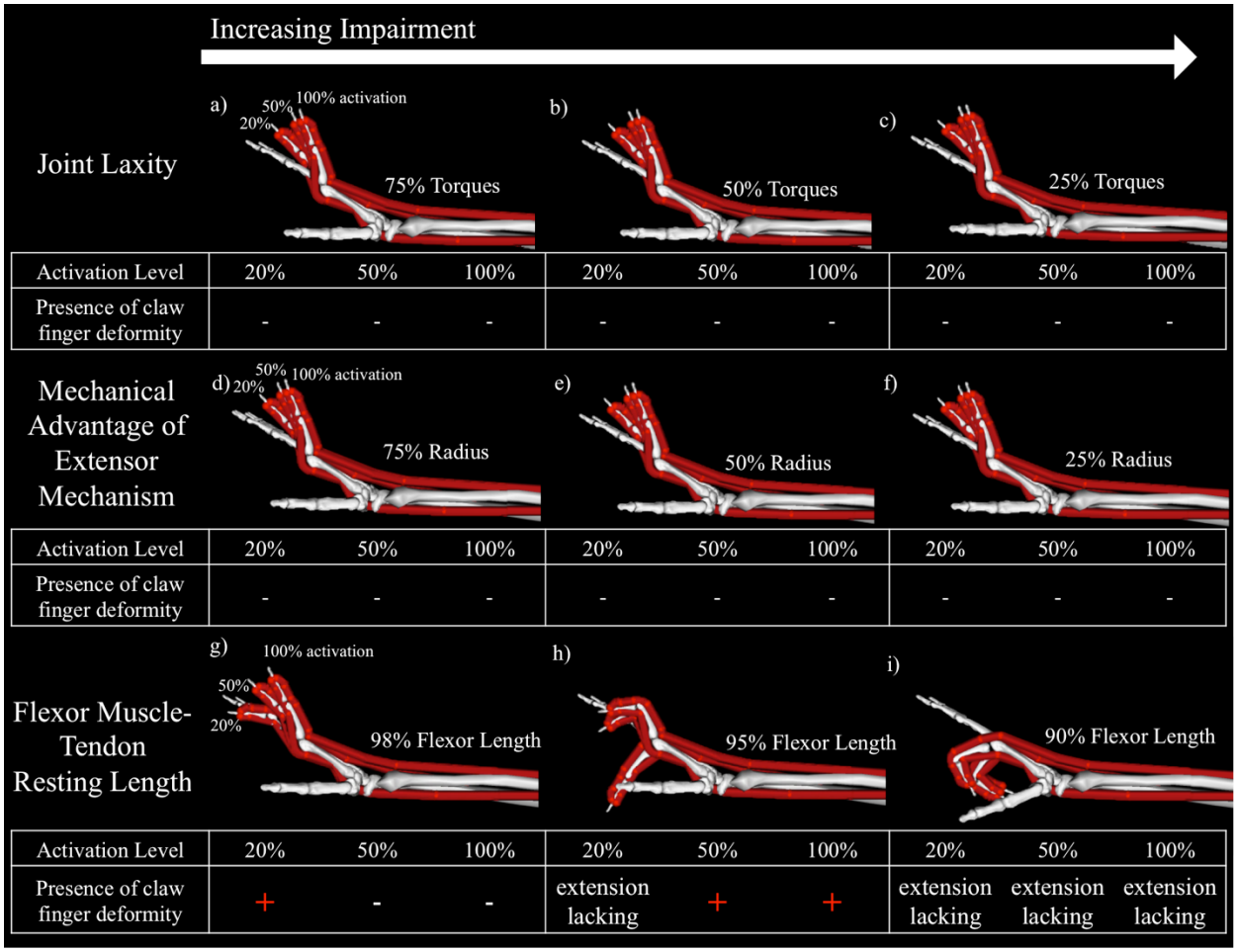

Figure 4.5: Final equilibrium position for extension of the forward simulations with increased laxity (a-c), stretched extensor mechanism (d-f), and shortened flexor muscles (g-i) with the muscle activated to 20%, 50%, and 100%. The results of this one-at-a-time analysis demonstrates that even small shortening of the finger flexor muscle resting length causes the development of the claw finger deformity (red "+"), which becomes more severe as the resting length decreases and limiting the extension of the finger even with full activation in the most severe cases. These impairments are not demonstrated with any of the other changes.

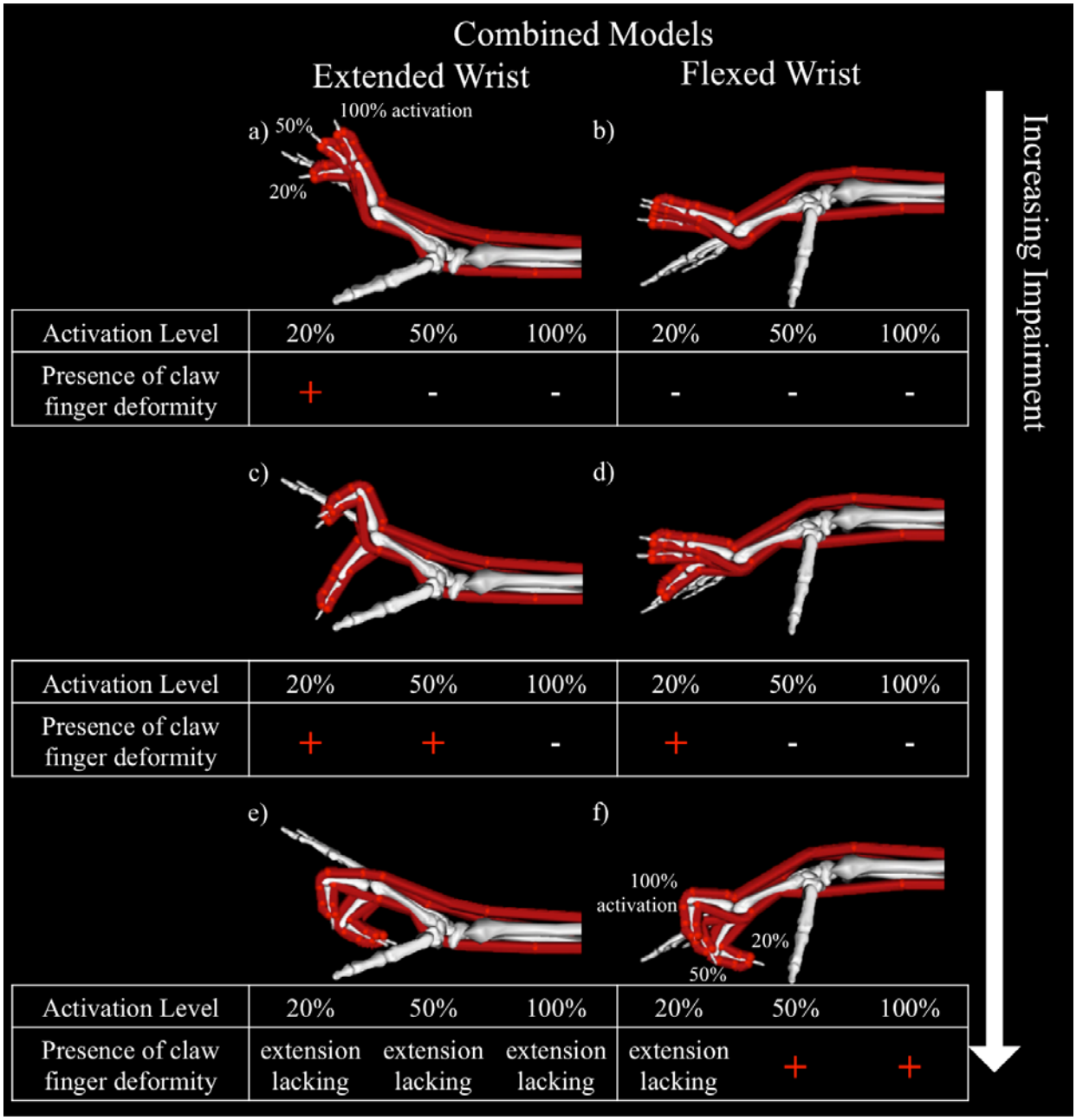

Activation Level	20%	50%	100%	20%	50%	100%
Presence of claw finger deformity	+	-	-	-	-	-

Activation Level	20%	50%	100%	20%	50%	100%
Presence of claw finger deformity	+	+	-	+	-	-

Activation Level	20%	50%	100%	20%	50%	100%
Presence of claw finger deformity	extension lacking	extension lacking	extension lacking	extension lacking	+	+

Figure 4.6: Final equilibrium position for extension of the forward simulations with an extended (a,c,e) and flexed wrist (b,d,f) of the models combining the small (a,b), medium (c,d), and large changes (e,f) demonstrating the claw finger deformity (red "+") becomes more severe with increasing impairment limiting the ability to extend of the finger even with full activation of the muscles. When the wrist is flexed to mimic the Andres-Thomas compensation reversal of the claw finger deformity is achieved as the wrist is flexed with mild and moderate impairments, however when the impairments become severe, wrist flexion is unable to reverse the deformity.

4.3.3 Nominal model

Simulations of the original intrinsic-minus model, including the nominal parameter values based on experimental data of non-impaired hands, did not produce the claw finger deformity (Figure 4.7) mimicking the acute phase of intrinsic muscle paralysis when individuals are still able to achieve finger extension and the claw finger deformity has not yet developed (Schreuders et al., 2007). During the flexion and extension phases of the fingers there was coordinated flexion and extension across all three finger joints (Figure 4.7).

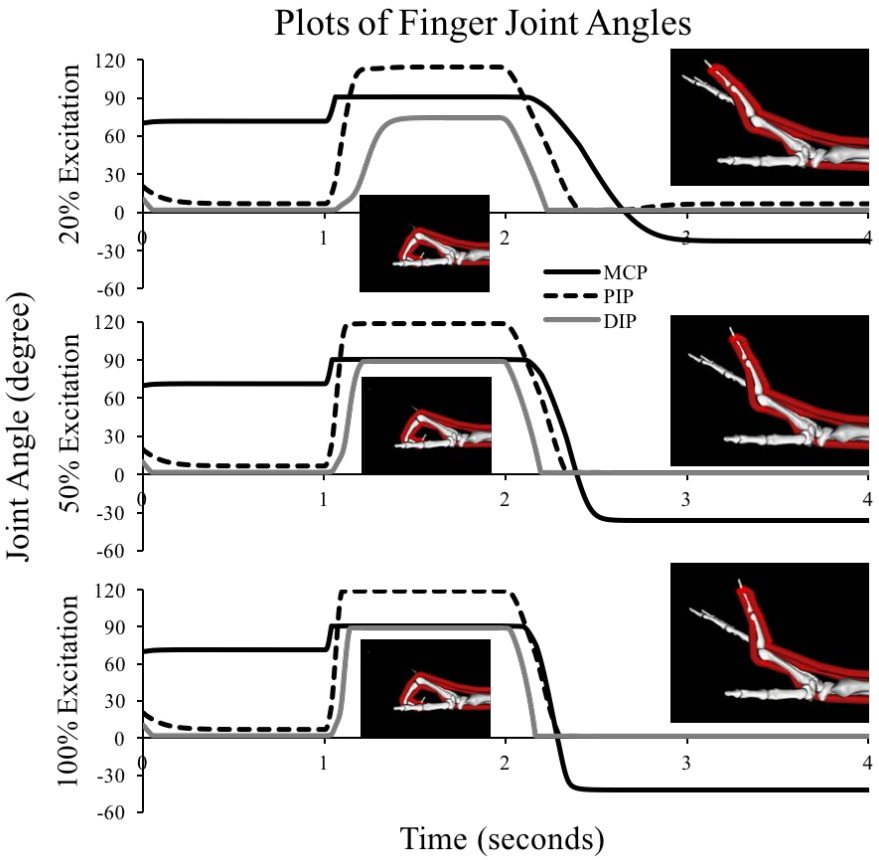

Figure 4.7 Joint angle plots of the non-impaired model of the metacarpophalangeal (MCP), proximal interphalangeal (PIP), and distal interphalangeal (DIP) joints throughout the forward dynamic simulations with 20%, 50%, and 100% input excitations (+ flexion/ - extension). Coordinated finger flexion is demonstrated, in which all three joints flex simultaneously, along with full and coordinated finger extension at all activation levels within the nominal model.

Table 4.3: Final equilibrium postures of the MCP, PIP, and DIP joints at the end of extension for the simulations with the single parameter changes and combined changes.

		Small Changes			Medium Changes			Large Changes		
	Activation	MCP	PIP	DIP	MCP	PIP	DIP	MCP	PIP	DIP
Increased Joint Laxity	20%	-22.83	6.54	1.38	-22.83	6.54	1.38	-22.83	6.54	1.38
	50%	-36.26	1.33	1.23	-36.26	1.33	1.23	-36.26	1.33	1.23
	100%	-41.85	1.10	1.08	-41.85	1.10	1.08	-41.85	1.10	1.08
Decreased Mechanical Advantage	20%	-23.99	7.56	1.39	-25.60	9.77	1.40	-28.91	17.11	1.41
	50%	-36.84	1.33	1.23	-37.46	1.33	1.24	-38.11	1.33	1.25
	100%	-42.26	1.10	1.08	-42.69	1.10	1.09	-43.14	1.10	1.09
Shortening of the Muscle-Tendon Resting Length	20%	-10.26	35.31	1.39	82.12	6.67	1.38	90.31	98.78	1.49
	50%	-27.11	14.52	1.25	-22.08	85.25	1.26	90.20	87.15	1.29
	100%	-35.27	1.27	1.11	-32.51	71.20	1.11	54.26	91.29	1.12
Combined Extended Wrist	20%	-24.29	64.79	1.38	82.12	6.67	1.38	90.29	118.38	1.49
	50%	-28.86	19.24	1.26	-27.02	118.71	1.50	81.71	118.38	1.27
	100%	-35.59	1.27	1.11	-38.09	113.19	1.08	27.36	118.74	1.14
Combined Flexed Wrist	20%	-33.91	1.47	1.36	-12.73	26.74	1.40	37.10	114.48	1.43
	50%	-41.99	1.21	1.20	-28.81	1.57	1.25	-8.06	118.56	1.32
	100%	-45.29	1.00	1.04	-38.37	1.16	1.08	-32.61	118.65	1.11

4.4 Discussion

The claw finger deformity is demonstrated in many individuals who have weakened or paralyzed intrinsic finger muscles. However, this deformity is not acutely present and the delayed onset and progression of the deformity is postulated to be due to biomechanical properties that exacerbate the loss of intrinsic muscle functions (Schreuders et al., 2007). These postulated biomechanical changes include: increased joint laxity, decreased extensor mechanical advantage of the extensor mechanism, and shortening of the extrinsic finger flexors. However, current surgical interventions focus primarily on restoring the actions of intrinsic muscles and often neglect these potentially critical biomechanical changes and their effects on the development of the deformity. Therefore, we simulated the effects of the postulated biomechanical property changes to finger extension using a computational model to evaluate the contribution of these factors to the claw finger deformity.

Contrary to our initial hypothesis our results suggest, of the mechanisms studied, the claw finger deformity is most sensitive to shortening of the extrinsic finger flexors. Neither changes of increased laxity nor decrease of extensor mechanical advantage, following extensor mechanism stretching, independently produced the claw finger deformity. The claw finger deformity was present with even small decreases in flexor muscle length to 98% of the nominal resting length and low levels of activation mimicking weakened extensors that are likely to accompany intrinsic muscle paralysis. However, increased extensor muscle activation was able to reverse the deformity to achieve finger extension with small changes in flexor muscle resting length. Larger decreases of flexor muscles' resting length to 95% or 90% of the nominal length full finger extension was not achievable. The increased passive forces and resistance torques about the finger joints from

the shortened muscle-tendon unit resting length resulted in either the development of the claw finger deformity or the inability to extend the finger joint (Figure 4.5h & i).

As further demonstration of the sensitivity of the claw finger deformity to the tension and length of the extrinsic finger flexor muscles the deformity reverses with wrist flexion. This reversal occurs as the wrist is flexed and the muscle-tendon length, the distance between origin and insertion, of the extrinsic finger flexors shortens enough to decrease the passive tension being produced by the muscles allowing the extensor muscles to extend the fingers. However, with large changes of the muscle's resting length wrist flexion does not sufficiently shorten the muscle tendon length to decrease the tension within the muscles and the claw finger deformity becomes present.

Notably, this wrist flexion technique is adopted by individuals with intrinsic muscle paralysis and mild claw finger deformities to help achieve finger extension and, as noted previously, is called the Andre-Thomas or Thomas sign. The compensation is successful acutely with mild deformities but as the deformity progresses the technique becomes less effective (Sapienza and Green, 2012; Schreuders et al., 2007). The current clinical explanation for the success of this technique is that the technique improves finger extension by lengthening the extrinsic finger extensors and theoretically placing them on a more advantageous portion of the force length curve (Sapienza and Green, 2012; Schreuders et al., 2007) and hence they are able to produce more force to extend the fingers. However, the results from this study indicate that the more likely explanation is that the technique decreases the tension of the extrinsic finger flexors resulting in decreased flexion torques about the finger joints allowing extension at the IP joints. Additionally, within our model and previous experimental work (Lieber and Friden, 1998) it has been demonstrated that the extrinsic finger extensor and wrist extensor muscles operate on the plateau and descending portions of the

force length curve (Figure 4.8). This is problematic for the current clinical explanation of increased extensor muscle force, for operating on this portion of the force length curve implies that the extensor muscles' optimal forces are produced when the muscles are in a shortened position with the wrist and fingers are in extended postures. Therefore, by flexing the wrist, and lengthening the extensor muscles, the muscle's fiber length would shift further from the optimal fiber length, moving to a less advantageous portions of the force length curve and thereby decreasing the force the muscles can produce (Figure 4.8).

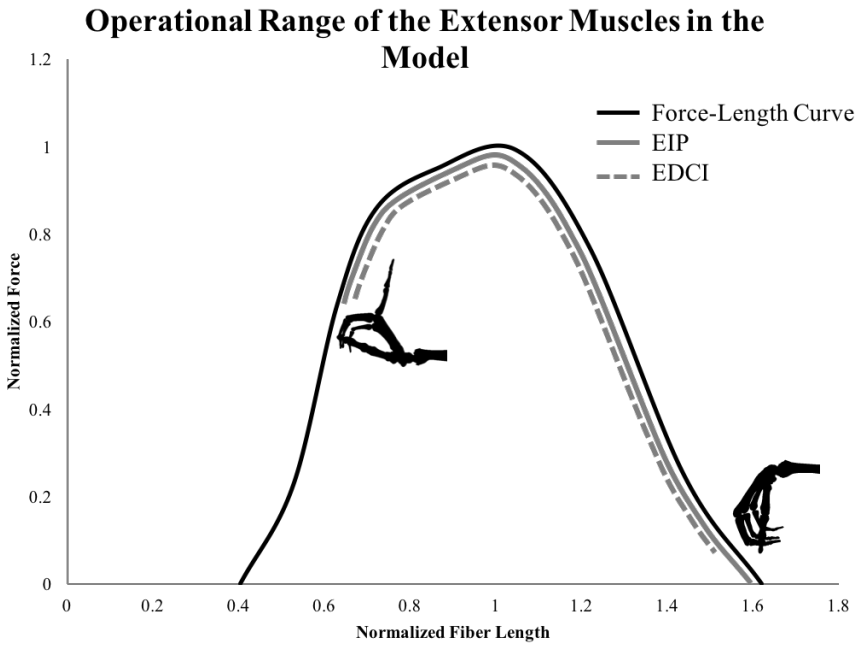

Figure 4.8: The operational range of the Extensor Indicis Profundus (solid grey) and Extensor Digitorium Communis Indicis (dashed grey) throughout the full finger and wrist range of motion within the biomechanical musculoskeletal model. The normalized fiber lengths of the muscles from full wrist and finger extension to full wrist and finger flexion are overlaid on the normalized active force-length curve (black) used within from the musculoskeletal model. The muscles both operate mainly on the plateau and descending portions of muscles force length curves within the model.

The findings from this simulation study indicate that maintaining the length of the finger flexors could be an area of focus for rehabilitation interventions preventing the development or

progression of the claw finger deformity. This is especially important for those who are able to voluntarily extend their fingers; i.e. low ulnar nerve lesions and lower level SCI, for they may have the residual extrinsic finger extensor capacity to extend the fingers if there is not substantial resistance from the flexors. Yet in these individuals the current inventions are focused primarily on orthotics and surgical techniques aimed at restoring the actions of the intrinsic muscles and do not account for the altered biomechanics that may be contributing to the deformity. The surgeries have short-term success rates of "fair to excellent" outcomes in 85%-96% of cases (Anderson, 2006) but long term success rates decrease to a maximum of 86% (Anderson, 2006). These outcomes may be suboptimal if the fundamental changes within extrinsic finger flexors is not addressed. In addition to our demonstration that shortening of these muscles is likely a critical factor in the development of claw finger deformity, shortening or contractures of the flexors have been shown to correlate with unsuccessful outcomes of claw finger surgeries (Ebenezer et al., 2012). Therefore, in both the acute stage as well as in patients who have the developed the claw finger deformity and are considered pre-surgical candidates, stretching and maintaining the length of the extrinsic finger flexors should be an area of focus to increase the likelihood of a successful surgical outcome.

4.4.1 Limitations

Some limitations to our study are that our model does not include the active component of the intrinsic muscles as well as the complex structure of the extensor mechanism with its complex network of force transmission to the distal segments of the fingers. Because we were simulating intrinsic muscle paralysis we do not believe the absence of these components of the intrinsic muscles to have an impact on the findings of this study especially the effects of the shortened

flexor muscles. If the active components of the intrinsic muscles were incorporated into the model it is likely that they would prevent the deformity from occurring for it is the combination of the intrinsic paralysis and the biomechanical changes that truly contribute to the formation of the deformity. A limitation of not including the extensor mechanism within our simulations may be the relatively unchanged equilibrium posture of the DIP joint over the simulations. This is likely because the passive torques incorporated about the joint dominate the dynamics and the extrinsic finger flexor muscles did not produce insufficient forces at the DIP joint to affect the resting posture.

4.5 Conclusion

This simulation study establishes that, in addition to intrinsic muscle paralysis and of the postulated biomechanical changes of (i) increased joint laxity, (ii) decreased mechanical advantage of the extensors about the PIP joint, and (iii) shortening of the flexor muscles, the development and progression of the claw finger deformity is most sensitive to the shortening of extrinsic finger flexors. Suggesting that the relationship of flexor muscle shortening and the development of the claw finger deformity should be the focus of future experimental or clinical studies. Additionally, these findings suggest that in both the acute and chronic stages of intrinsic finger paralysis maintaining the length of the extrinsic finger flexors should be an area of focus of rehabilitation and pre-habilitation of surgical candidates.

5 PASSIVE ELASTIC TORQUES WITHIN THE HAND CHANGE MINIMALLY IN INDIVIDUALS WITH CHRONIC HEMIPARETIC STROKE

Loss of function of the upper extremity is the most common physical impairment following stroke, with over two-thirds of survivors never regaining normal use of the upper extremity. Impairments to the upper limb and hand stem initially from damage to the corticospinal pathways but secondary biomechanical changes of the muscles and joints could further impair hand function, although current evidence of these changes is inconclusive. This is likely due to background muscle hyperactivity that obfuscates the underlying biomechanical changes even during "passive" or "relaxed" conditions. Therefore, we designed an experimental protocol that minimizes the effects of muscle hyperactivity to quantify and compare the *in vivo* biomechanical passive elastic torques of the hand. The passive elastic torques about the wrist and all four MCP joints were quantified in the paretic and non-paretic hands of 27 chronic stroke individuals with severe (n=9), moderate (n=9), and mild (n=9) hand impairments. To quiet the muscle hyperactivity the subjects were in a sleep or near sleep state during data acquisition. Our results indicate that there are not substantial differences in the passive torques between the paretic and nonparetic hands in individuals with chronic hemiparetic stroke for we only found small, 0.3 Ncm, to medium, 8.1 Ncm, average differences in torques across impairment levels at the wrist and MCP joints. We were also able to quantify the relative contribution to the total joint torques of the extrinsic finger muscles from the soft tissue structures surrounding each joint. We found unsubstantial and inconsistent changes across impairment levels. These finding indicate that after a stroke there are no substantial increases of passive torques about either the wrist or the fingers. Increased stiffness

observed clinically and in previous studies is likely a result of muscle hyperactivity and not secondary biomechanical changes of the muscles or other soft tissue structures.

5.1 Introduction

Loss of function of the upper extremity is the most common physical impairment following stroke, with over two-thirds of survivors never regaining normal use of the upper extremity (Broeks et al., 1999; Lawrence et al., 2001). In addition, more than half of these individuals have such severe long-term impairments that they cannot open or control their paretic hand (Broeks et al., 1999; Nakayama et al., 1994; Parker et al., 1986). The loss of hand function requires an increased reliance on the other hand or caregivers to perform activities of daily living, which decreases an individual's independence and quality of life.

Impairments to the upper limb and hand stem initially from damage to the corticofugal pathways in the lesioned hemisphere resulting in weakness (Hoffmann et al., 2016; Kamper et al., 2006; Kamper et al., 2003), loss of independent joint control (Brunnstrom, 1970; Dewald et al., 1995; Dewald et al., 2001; Miller and Dewald, 2012; Sukal et al., 2007), and muscle hyperactivity, which manifests as hypertonicity (a persistent muscle activity) and spasticity (hyperactive stretch reflexes) (Bhadane et al., 2015; Kamper and Rymer, 2000; McPherson et al., 2008; McPherson et al., 2017; O'Dwyer et al., 1996). A proposed mechanism of this muscle hyperactivity after a stroke is an upregulation of the reticulospinal pathways causing increased monoaminergic signaling to the spinal cord increasing motoneuron excitability (Fedirchuk and Dai, 2004; Heckman et al., 2008; Johnson and Heckman, 2014; McPherson et al., 2008; McPherson et al., 2017; Owen et al., 2017). This motoneuron hyperactivity, especially during awake hours, leads to persistent muscle

tone and increased joint torques and stiffness of the hand that further impede the opening and use of the hand even while the individual is in a relaxed or passive state (Kamper et al., 2003).

In addition to the neurological impairments, prolonged disuse and hyperactivity may produce biomechanical changes in the muscles and peri-articular structures of individuals with chronic hemiparetic stroke that could further impair hand function (Malhotra et al., 2010) but the current evidence of these changes is inconsistent. A majority of studies primarily indicate that within the paretic limb there are increases in passive joint torques and stiffness at the ankle (Gao et al., 2009; Given et al., 1995; Kwah et al., 2012; Mirbagheri et al., 2008), elbow (Eby et al., 2016), wrist (de Gooijer-van de Groep et al., 2016), and hand (Kamper et al., 2006). However a couple of studies have demonstrated no increase in passive torques and stiffness of the paretic joints of the ankle (Freire et al., 2017) or elbow (Given et al., 1995). The inconsistencies in these results may be due to the use of experimental designs that increase the likelihood of eliciting the muscle hyperactivity. The studies either use continuous motion of the joint, do not pre-stretch the muscles to attenuate the hyperactive motoneurons (Schmit et al., 2000), and/or lack EMGs to monitor muscle activity during data collection. These approaches increase the likelihood of muscle hyperactivity being present during the collection of data even during “passive” or “relaxed” conditions that can obfuscate the underlying biomechanical changes.

The purpose of this study is to use an experimental protocol that minimizes the effects of muscle hyperactivity to quantify and compare the *in vivo* biomechanical passive elastic torques of the wrist and finger joints in the paretic and non-paretic limbs of individuals with chronic hemiparetic stroke. With this information we should be able to determine if structural biomechanical changes occur about the wrist and MCP joints and how these changes may impact

function of the hand in individuals with chronic hemiparetic stroke. Additionally, our methods will allow us to assess the torques contributed by the extrinsic finger muscles separate from all other soft tissue structures at the wrist and fingers. The driving hypotheses, based on the prevailing findings in previous literature indicating increased torques about paretic joints and the clinical presentation of increasingly stiff flexed wrist and finger postures in many chronic stroke survivors: 1) within severely and moderately impaired individuals the passive torques of the paretic hand will be greater than that of the non-paretic hand, and 2) this increase in torque will be muscular in origination and specifically arising from the extrinsic finger muscles.

5.2 Materials and Methods

5.2.1 Participants

An interdepartmental research database, the Clinical Neuroscience Research Registry from Northwestern University and the Shirley Ryan AbilityLab (formerly Rehabilitation Institute of Chicago), was used to pre-screen individuals with chronic hemiparetic stroke based on inclusion criteria (Table 5.1) and prior assessment of hand impairment resulting in the recruitment of 28 individuals to participate in this study. The data of one individual was excluded from the analysis due to the inability to fully relax both their paretic and non-paretic arm muscles. The remaining 27 subjects were stratified into 3 groups by hand impairments (severe, moderate, or mild) using the Chedoke McMaster Stroke Assessment Hand Score (CMSA-HS) (Gowland et al., 1993) (see Table 5.2). CMSA-HS of 1-3 were considered severe impairments, 4-5 moderate impairments, and 6-7 mild impairments. Clinical tests of CMSA-HS and Modified Ashworth Scale (MAS) were administered by the same trained and licensed physical therapist across all subjects to eliminate inter-rater errors.

The study protocol was approved and participants gave informed consent for participation using a form approved by the Institutional Review Board of Northwestern University. Clinically relevant subject demographics were gathered from all subjects in a brief questionnaire prior to data collection (Table 5.2).

Table 5.1: Table of Inclusion Criteria for Subjects

Subject Inclusion Criteria
Paralysis confined to one side of the body
Stroke occurred at least one year prior to participation in the study
Stroke did not occur in the cerebellum or brainstem
Absence of impairment or injury in the unimpaired limb
Lack of severe atrophy of the impaired limb
Lack of severe concurrent medical problems
Ability to give informed consent
No history of botulinum neurotoxin injections to the hand or forearm

Table 5.2: Subject Demographics.

(CMHS – Chedoke McMaster Stroke Assessment Hand Score, MAS – Modified Ashworth Scale)

Impairment Level	Sex	Age in years (SD)	Time Since Stroke in years (SD)	Paretic Side	CMHS	MAS	Weight in pounds (SD)	Height in inches (SD)
Severe (n=9)	6-M, 3-F	60.28 (10.40)	17.1 (7.91)	5-L, 4-R	2.44 (0.73)	2.17 (0.87)	175.89 (47.20)	67.11 (3.10)
Moderate (n=9)	5-M, 4-F	64.3 (7.95)	13.2 (7.96)	6-L, 3-R	4.22 (0.44)	1.78 (0.94)	188.44 (31.95)	67.11 (3.18)
Mild (n=9)	5-M, 4-F	56.93 (12.18)	8.41 (3.71)	1-L, 8-R	6.44 (0.53)	0.28 (0.57)	185.33 (22.41)	67.78 (3.87)

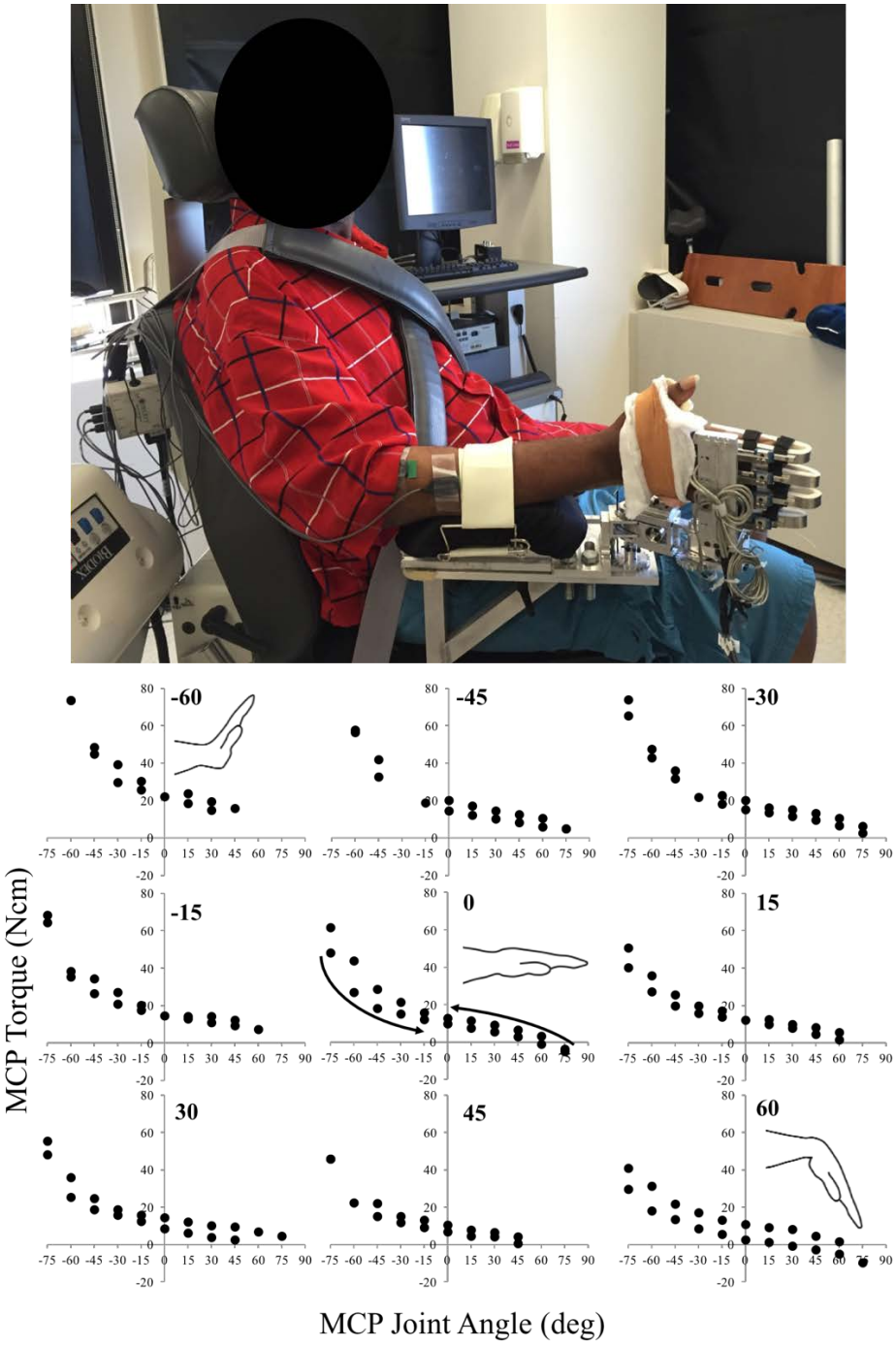

Figure 5.1: Top: Picture of the experimental set-up with the subject seated upright with their hand attached to the WFTS device. Bottom: A schematic of the data points collected as the MCP joint was ranged through its range of motion from full extension to full flexion and back to extension at each wrist position from 60 degrees of extension to 60 degrees of flexion. Each dot represents a collection position. (+ flexion/- extension)

5.2.2 Experimental Set-up

Subjects were seated in an upright position and their hand secured to a custom built version of the Wrist and Finger Torque Sensor (WFTS) (Stienen et al., 2011). Their arm was positioned comfortably at their side so that the forearm was parallel to the ground and the hand vertical with the palm facing medially; this position eliminates the effects of gravity in the flexion and extension directions (Figure 5.1). The two distal finger joints for each finger were splinted, fixing the distal joints and ensuring isolated MCP and wrist movements. Muscle activity was monitored throughout the trials using surface EMGs electrodes (16-channel Bagnoli EMG System, Delsys Inc., Boston, MA; 1000 x gain, 20-450 Hz bandpass) placed over 4 muscles; Flexor Digitorium Superficialis, Flexor Carpi Ulnaris, Extensor Digitorium Communis, and Extensor Carpi Radialis.

5.2.3 Muscle Hyperactivity Inhibition Protocol

Muscle hyperactivity was successfully reduced and quieted during data collection by having the subjects in a sleep or near sleep state throughout the protocol. The theory is that while in this state the reticulospinal tracts become down regulated, decreasing spinal motoneurons excitability and muscle hyperactivity (Fraigne et al., 2015; Hodes and Dement, 1964; Krenzer et al., 2011). This state was facilitated by creating a dark relaxing atmosphere in which a video or music was played to occupy the subjects; diverting their attention from the experiment.

Each session began with 10 minutes of stretching of the wrist and fingers into both full flexion and extension within the device. These stretches accommodated the individual to the device as well as accommodated the muscle hyperactivity (Schmit et al., 2000). After the stretching protocol, the device was unlocked so the hand could rest at its equilibrium posture and baseline trials were collected to zero out the device and set the passive EMG baseline. Zeroing torques and EMG

baseline data were collected during three 15-second trials where no evidence of motor unit firing was present. This critical EMG baseline was used to ensure that the muscles were passive with no detectable muscle activity throughout the remainder of the experiment by using the methods described in section 5.2.5 below.

5.2.4 Experimental Procedure

The passive elastic torques were collected at multiple combinations of wrist and MCP posture for each subject. The wrist was positioned randomly between 60° flexion and 60° extension, in 15 degree increments resulting in 9 wrist postures. At each of the randomly set wrist postures the MCP joints were ranged throughout their ROM, starting in full extension, to full flexion, and back to full extension in static 15 degree increments (Figure 5.1). MCP ROM at each wrist posture was determined by the subject's comfort level and the device's ROM.

The torques were collected at static postures to prevent muscle hyperactivity by eliminating the Ia afferent velocity dependent component of the stretch reflex elicited during even slow continuous motions (Kamper et al., 2003). At each static position of wrist and MCP posture the data was collected for 15 seconds and visually inspected for evidence of muscle activity or deviations within the torque, if present the trial was discarded and another trial at that position was collected. This protocol was completed on two separate days, on the first day data from the non-paretic hand was collected and on the second day data from the paretic hand was collected.

5.2.5 Data processing:

The raw torque and EMGs were collected and digitized at a sampling frequency of 1kHz. The torque and rectified EMG data were then digitally filtered using a zero-phase infinite impulse response 4th-order Butterworth low-pass filter with a 4Hz corner frequency.

The processed baseline trials were used to set the torque offset and EMG threshold. Torque offset was set as the average of the means of the torque during the three baseline trials. EMG threshold, EMG_t, was set as:

$$EMG_t = \bar{x}_{EMG_base} + 3 \cdot \sigma_{EMG_base} \tag{1}$$

where $\bar{x}_{EMG_base}$ is the average over the three EMG baseline trials and σ_{EMG_base} is the average standard deviation of the EMG of the three baseline trials.

At each passive torque trial the processed torque and EMG data were divided into 1-second bins, for a total of 15 bins per trial. In each bin the mean torque and EMG value was found, if the mean EMG signal from any muscle went above EMG_t or if the torque deviated more than 5% from the mode of the torques across the entire trial, the bin was discarded. The mean of the remaining bins for each trial were used to create the total torque versus wrist and MCP posture data set for each subject.

5.2.6 Separation of the structures contributing to the total torque:

Using the total torque data set collected at all combinations of wrist and MCP posture an analytical model that separates the extrinsic finger muscles from the other muscles and joint structures about each joint was created (Knutson et al., 2000). This allows for the determination of the relative contributions made by the extrinsic finger muscles' passive properties for each subject relative to the contributions made by the other joint structures.

The analytical models were fit to each subject's total wrist and MCP torque data set using a previously described method described by Knutson and colleagues (2000). The total torque, $T_t(\theta, \omega)$, in the analytical model is comprised of two components.

$$T_t(\theta, \omega) = T_{sj}(\theta) + T_e(\theta, \omega) \tag{2}$$

$T_{sj}(\theta)$, consists of the torques contributed by the single-joint structures (wrist or intrinsic hand muscles, ligaments, joint capsules, etc.) that are a function of either the wrist or MCP joint posture only and $T_e(\theta, \omega)$, representing the extrinsic finger muscles, that is a function of both MCP and wrist posture. Where θ is the angle of the joint of interest (wrist or MCP) and ω is the angle of the co-varying joint:

$$T_{sj}(\theta) = A_1\left(e^{-k_1(\theta-\theta_1)} - 1\right) - A_2\left(e^{k_2(\theta-\theta_2)} - 1\right) \tag{3}$$

$$T_e(\theta, \omega) = A_3\left(e^{-k_3(\theta-\theta_3)} - 1\right) - A_4\left(e^{k_4(\theta-\theta_4)} - 1\right) \tag{4}$$

$$\theta_j = B_j \cdot \omega + \emptyset_j \;\; (j = 3,4) \tag{5}$$

From this analytical model (Knutson et al., 2000), each subject's total torque about the wrist and the MCP joints can be described as a function of the wrist and MCP posture and 14 constants ($A_{1\text{-}4}$, $k_{1\text{-}4}$, $\theta_{1\text{-}4}$, *and* $B_{3\text{-}4}$). To create a data set describing the contributions of the single-joint structures and extrinsic finger muscles for use in the data analysis, $T_{sj}(\theta)$ and $T_e(\theta, \omega)$ at the wrist and MCP were interpolated in 15 degree increments of the wrist and MCP posture within the subject's ROM collected.

5.2.7 Analysis of Data

To determine the effect of the paretic vs. non-paretic hand a generalized linear-mixed model analysis in the SPSS software (v24.0 IBM Corp Armonk, NY) was used to analyze the data sets

described above (measured total joint torque data, modeled single-joint structures, and modeled extrinsic finger muscles) of the subjects grouped by impairment level. Across all analyses the dependent variable used was torque. For the total joint torque and extrinsic finger muscles torques, a four-factor analysis including subject, hand (paretic/non-paretic), MCP position, and wrist position was used. For the single-joint torques a three-factor analysis including subject, hand (paretic/non-paretic), and MCP or wrist position was used. Subjects were set as a random intercept factor and all other factors were fixed factors.

The effect size of the changes between the paretic and non-paretic hand at each impairment level were found using the mean difference between torques of the paretic and non-paretic hands. The differences in torques were calculated by subtracting the torque of non-paretic from the torque of paretic hand at each combination of wrist and MCP joint posture. The difference at a posture was only calculated if a torque was present in both the paretic and non-paretic hand. Means and standard deviations of the differences were used in the effect size calculations.

5.3 Results

5.3.1 Measured Total Passive Torque about the Wrist and MCP joints

Across impairment levels there were no substantial increases in torque. The effect sizes of the differences in torques were small to medium (Cohen's d=0.02 to 0.66) about the wrist and MCP joints. About the wrist the mean difference in torques for the severely, moderately, and mildly impaired individuals were 0.5Ncm, 6.7Ncm, and 0.3Ncm, respectively. Only the severely and moderately impaired individuals demonstrated statistically significate differences in the total torques at the wrist ($p<0.001$ for both) (Figure 5.2). About the MCP joints the mean differences across the severely, moderately, and mildly impaired groups were 8.1Ncm, 5.0Ncm, and 2.1 Ncm,

respectively, and were statistically significantly different (p<0.001 for all three) (Figure 5.3). These mean differences in torques, however were very small when compared to the maximum average passive torques of wrist (137.7Ncm) and MCP joints (105.4Ncm) (Figures 5.2 & 5.3).

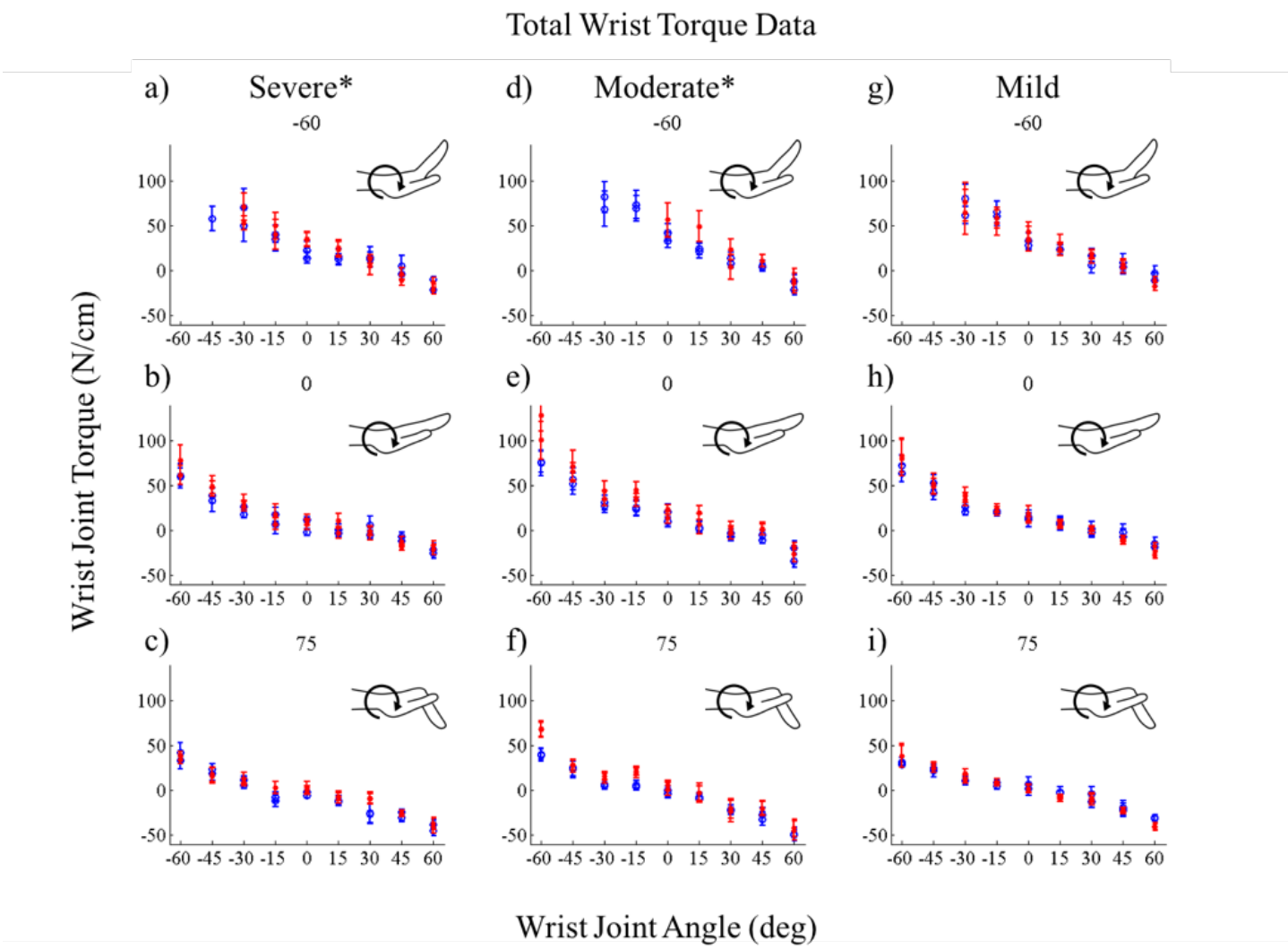

Figure 5.2: Wrist torque data over the wrist's range of motion with the MCP joints locked in -60, 0, and 75 degrees of the paretic (red) and non-paretic (blue) with standard error bars of individuals with severe, moderate, and mild hand impairments. Note the unsubstantial differences in passive wrist torques across all wrist and MCP joint angles and impairment levels as demonstrated by the overlapping standard error bars. (+ flexion/- extension) (* p<0.05)

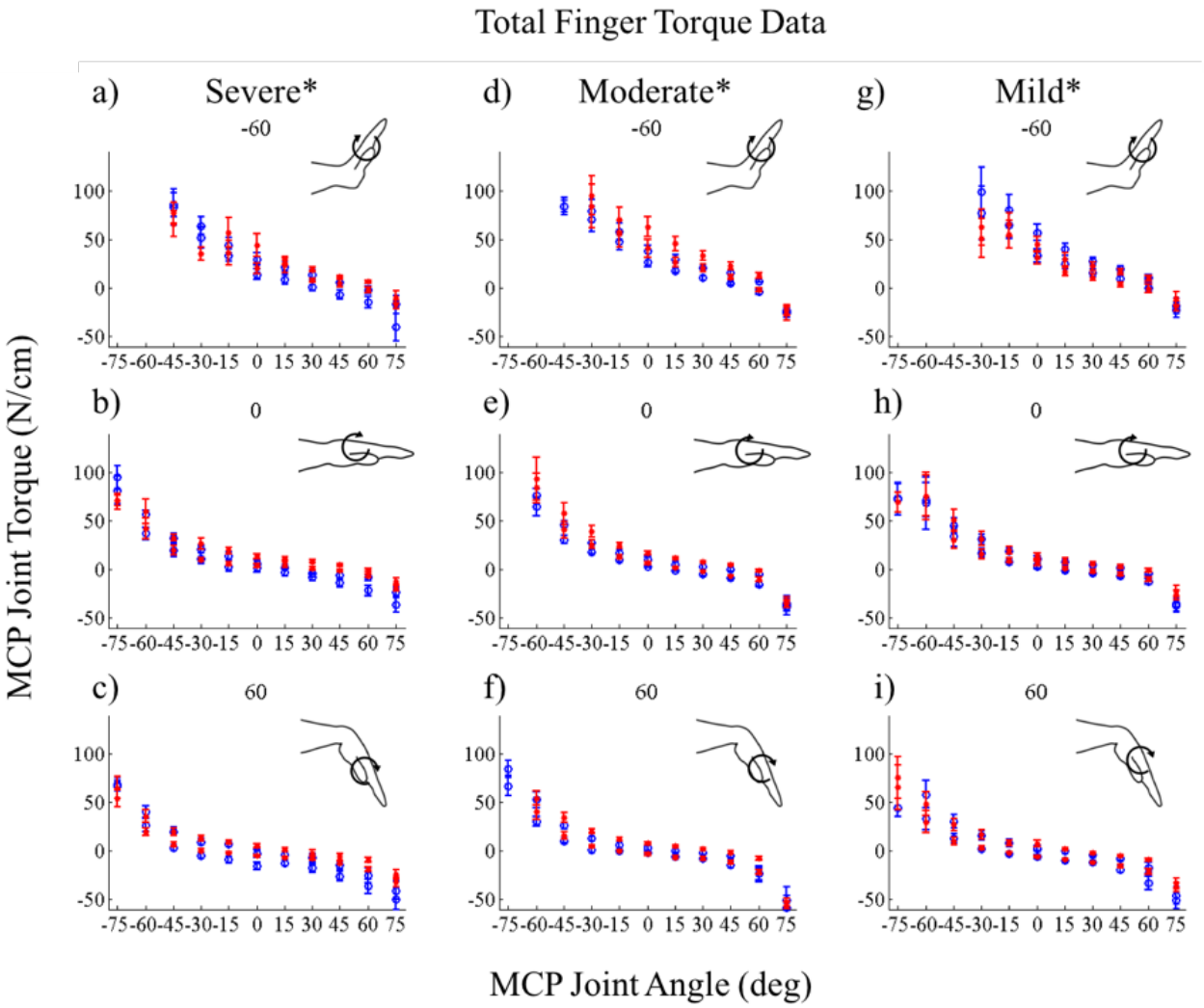

Figure 5.3: MCP torque data over the MCP joints' range of motion with the wrist locked in -60, 0, and 60 degrees of the paretic (red) and non-paretic (blue) with standard error bars of individuals with severe, moderate, and mild hand impairments. Note the lack of increase in flexion torques about the MCP joints as the fingers are extended across all impairment levels and that the difference in torques across the severe and moderate groups occur as the fingers are flexed demonstrating a decrease in passive extension torques. (+ flexion/- extension) (* $p<0.05$)

5.3.2 Analytical model separation of structures contributing to the total torque by impairment severity

The 14 constant parameters (see Table 5.3) defining the analytical model of the relative contributions of the extrinsic finger muscles and the single-joint structures about the wrist and the MCP joints of the paretic and non-paretic hand at each impairment level fit well to the experimentally collected data at the wrist (paretic r^2=0.907, non-paretic r^2= 0.877) and the MCP finger joints (paretic r^2=0.914, non-paretic r^2= 0.919).

In individuals with severe hand impairments the contribution from the extrinsic finger muscles to the total passive torque about the MCP joint was overall not substantially greater in the paretic hand as compared to the non-paretic hand. However, there was a statistically significant difference in MCP joints torques ($p< 0.001$) (Figure 5.6a-c) and this difference was demonstrated as a decrease in the amount of MCP extension torques in flexed wrist and finger postures (Figures 5.6c). There were no differences found for single-joint structures at the wrist or the MCP joint ($p=0.239$ and $p=0.131$, respectively) (Figures 5.4a & 5.5a).

In individuals with moderate hand impairments there were slight increases in flexion torques between the paretic and non-paretic limbs in the extrinsic finger muscles and single-joint structures at the MCP joint ($p<0.001$ for both) that were most evident at extended finger and wrist postures (Figures 5.6d-f & 5.5b). There were no significant differences between the paretic and non-paretic wrist single-joint structures ($p=0.568$) (Figure 5.4b).

Lastly, individuals with mild impairments did not demonstrate significant differences in either the single-joint structures at the MCP joint or the extrinsic finger muscles ($p=0.805$ and $p=0.089$, respectively) (Figures 5.6g-i & 5.5c). However, there were slight increases in flexion torques of the single-joint structures at the wrist in extended postures ($p=0.008$) (Figure 5.4c).

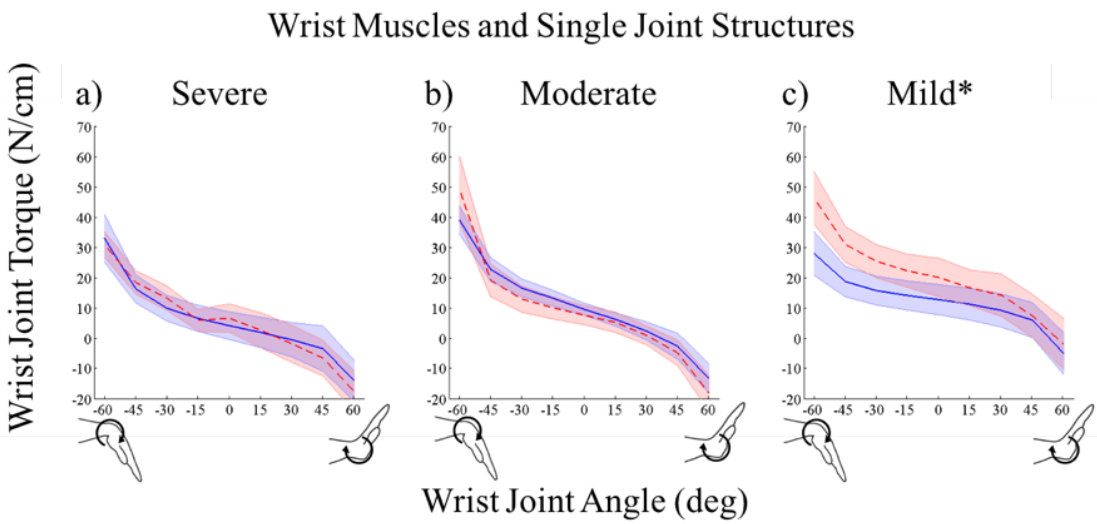

Figure 5.4: Wrist torque of the wrist muscles and other joint structures about the wrist over the wrist's range of motion of the paretic (red dashed line) and non-paretic (blue solid) with the shaded regions being standard error. Individuals with severe and moderate hand impairments do not demonstrate significantly different wrist torques, though there is a slight increase in flexion torque about the wrist in individuals with mild impairments (+ flexion/- extension) (* $p<0.05$)

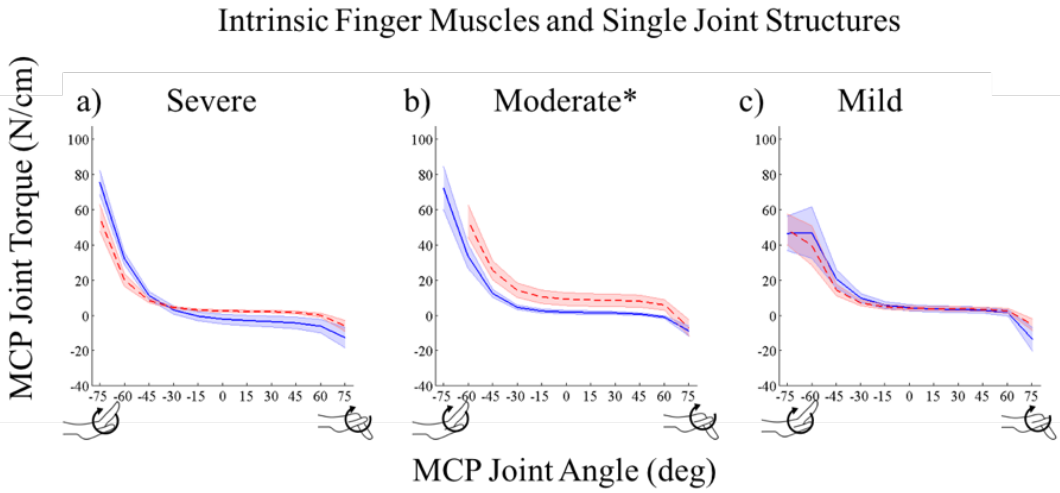

Figure 5.5: MCP torque of the intrinsic hand muscles and other joint structures about the MCP joints over the MCP range of motion of the paretic (red dashed line) and non-paretic (blue solid) with the shaded region being the standard error of individuals with severe, moderate, and mild hand impairments. The MCP single joint torques are not significantly different for individuals with either severe and mild hand impairment and for those with moderate impairments there is a with slight shift to increased flexion torques. (+ flexion/- extension) (* $p<0.05$)

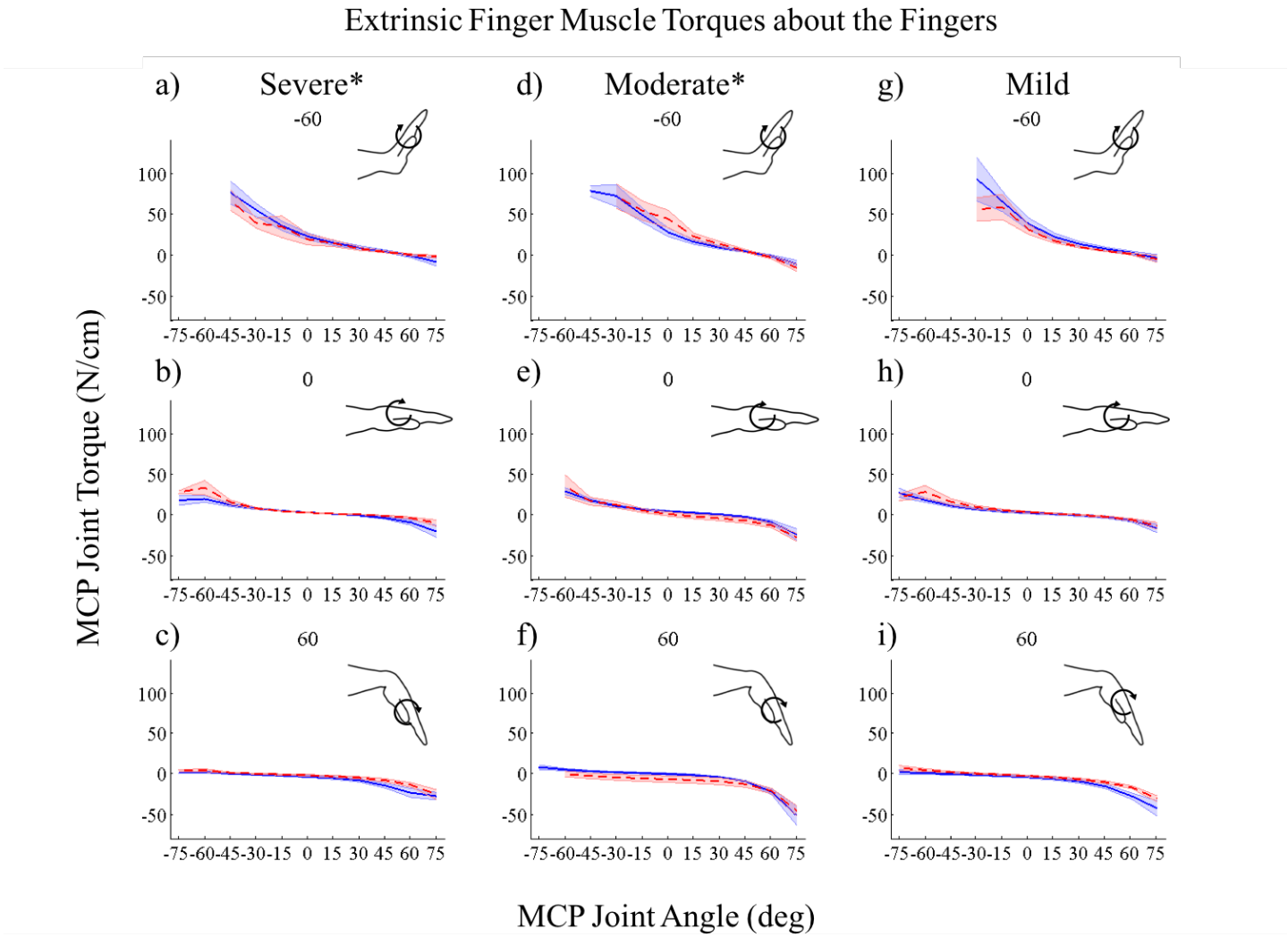

Figure 5.6: MCP torque of the extrinsic finger muscles about the MCP joints over the MCP range of motion with the wrist locked in -60, 0, and 60 degrees of the paretic (red dashed line) and non-paretic (blue solid) with standard error in the shaded region of individuals with severe, moderate, and mild hand impairments. There are unsubstantial difference across all impairment levels with overlapping error bars between both hand across the MCP and wrist joints range of motion (+ flexion/- extension) (* $p<0.05$)

Table 5.3: Median Parameters for the fit analytical models of paretic and non-paretic at the MCP and wrist at each impairment level. R^2 is the mean of R^2 values

	Parameter	A1	k1	theta1	A2	k2	theta2	A3	k3	B3	phi3	A4	k4	B4	phi4	R^2
Severe	Paretic MCP	1.13	0.0708	-27.43	3.20	0.1185	70.55	1.20	0.0393	-0.96	2.80	2.72	0.0323	-0.25	42.66	0.90
	Non-Paretic MCP	8.30	0.0579	-37.97	5.90	0.1692	69.59	1.93	0.0288	-1.20	3.35	2.61	0.0520	-0.31	39.39	0.92
	Paretic Wrist	2.72	0.0584	-39.66	20.33	0.0191	47.88	5.57	0.0319	-0.81	-9.74	17.27	0.0084	-2.02	95.50	0.91
	Non-Paretic Wrist	4.04	0.0664	-30.74	15.42	0.0538	53.61	4.98	0.0365	-0.88	-29.79	21.08	0.0093	-1.05	45.92	0.88
Moderate	Paretic MCP	1.70	0.0678	-17.14	7.19	0.1118	72.59	2.73	0.0363	-1.09	-6.71	2.05	0.0658	-0.14	42.14	0.92
	Non-Paretic MCP	2.13	0.0873	-23.73	2.27	0.1074	69.75	1.71	0.0370	-0.96	8.25	2.14	0.0602	-0.23	40.45	0.91
	Paretic Wrist	2.79	0.0793	-40.96	19.47	0.0353	34.10	6.43	0.0373	-0.87	5.05	27.39	0.0118	-2.60	145.51	0.90
	Non-Paretic Wrist	3.30	0.0565	-33.22	26.70	0.0301	51.12	6.10	0.0321	-0.86	-9.66	24.28	0.0098	-0.91	62.01	0.85
Mild	Paretic MCP	1.10	0.0787	-21.61	2.91	0.1743	70.36	1.36	0.0332	-1.18	4.96	2.24	0.0325	-0.50	38.05	0.93
	Non-Paretic MCP	2.16	0.0897	-20.07	5.27	0.2974	66.15	3.06	0.0361	-1.29	-4.39	4.66	0.0438	-0.69	37.90	0.93
	Paretic Wrist	3.38	0.0585	-33.99	23.89	0.0473	57.66	5.13	0.0419	-0.79	0.64	23.47	0.0065	-0.56	43.26	0.91
	Non-Paretic Wrist	3.28	0.0298	-38.58	16.58	0.0232	54.85	5.76	0.0464	-0.69	-13.40	32.74	0.0076	-0.67	87.57	0.90

5.4 Discussion

The purpose of this research was to quantify the differences of passive elastic torque between the paretic and non-paretic hands of individuals with chronic hemiparetic stroke. In testing our first hypothesis, our results indicate that there are not substantial increases in the passive torques between the paretic and non-paretic hands in individuals with chronic hemiparetic stroke with severe and moderate hand impairments. We only found small (0.5 Ncm) to medium (8.1 Ncm) average differences, with effect sizes of 0.05 to 0.66, in the torques at the wrist and MCP joints (Figures 5.2 & 5.3). Contrary to our second hypothesis, we did not find consistent increases of torques originating from the extrinsic finger muscles (Figures 5.6). Interestingly however, in individuals with severe hand impairments we found decreases in passive extension torque when the wrist and fingers were flexed (Figure 5.6).

The unsubstantial changes found are likely not large enough to impair hand function. In the moderately impaired individuals, we found mean increases of 6.8 Ncm at the wrist and 5.0 Ncm at the MCP joint when averaged across all postures and subjects. The largest mean increase of MCP torques, 29.9 Ncm, between the paretic and non-paretic hands was observed in 30° of wrist extension and 45° of MCP extension. The differences of passive torque observed are small when compared to the deficits in voluntarily finger extension of up to 90% (Hoffmann et al., 2016; Kamper et al., 2006) indicating that impairments are likely more closely related to neural deficits in activating muscle than the biomechanical changes.

5.4.1 Discrepancies from previous published work

The discrepancy between our findings and substantial increases of joint torque and stiffness found previously is likely due to differences in the methodology used to collect the data. The previous studies which reported increases in torque of the paretic upper extremity in chronic stroke individuals all utilized continuous motion to collect the passive torques (de Gooijer-van de Groep et al., 2016; Eby et al., 2016; Kamper et al., 2006). This presents a problem because, even at low constant velocities, hyperactive stretch reflexes can be elicited in the paretic muscle of chronic stroke individuals (Kamper et al., 2003). The effect of these hyperactivity stretch reflexes during even a slow continuous velocity of 10 deg/s can increase the torques of the paretic hand by at least 30% (Kamper et al., 2003). Furthermore, many of the previous upper extremity studies fail to mention whether stretching prior to data collection was utilized to attenuate the stretch reflex (de Gooijer-van de Groep et al., 2016; Gao et al., 2009; Kamper et al., 2006). Finally, in the few studies where EMGs were collected and monitored, they were not used to discard trials. Instead, the EMGs were used to calculate the passive torques as part of a dynamic analytical model used to decompose the recorded torque into active and passive components dependent on acceleration, velocity, and position using system identification methods (de Gooijer-van de Groep et al., 2016; Kamper et al., 2006). This can be problematic for underlying hyperactivity is not considered within these models and the positional component of the stretch reflex would then be considered as part of the passive elastic torques, confounding the results.

The inconsistencies between our study and the previous studies underscore the importance of ensuring that there is no muscle activity, even when a subject is in a “relaxed” state. Merely asking

patients to relax is not sufficient for many of these individuals are unable to fully relax due to the hyperexcitability of their motoneurons resulting in muscle hypertonicity.

5.4.2 Strength of Experimental Methods Utilized

The strength of our study lies in the rigor used to ensure passive torque collection even in individuals with hyperactive muscles. We found that having study participants in a relaxed sleep or near sleep state was an ideal condition and reduced hyperactivity and promoted passive muscles. Additionally, to reduce the effects of the velocity Ia or length driven type Ia or II afferent stretch reflexes, we collected the torques at static joint postures while closely monitoring the EMG signals. Any data that contained evidence of muscle activity was discarded at the time of data collection and the EMG signals were again verified within the data processing protocol. To ensure a truly passive EMG baseline reference real-time unfiltered EMG data were analyzed and if a single motor unit was firing the baseline trial was discarded and repeated. In addition, to ensure the changes were due to natural progression following the neural deficits and not the result of pharmacological interventions that may have an effect on the structure of the muscles and its passive properties, we excluded any individual who had ever received botulinum toxin injections within the forearm or hand (Minamoto et al., 2015; Thacker et al., 2012; Ward et al., 2017).

5.4.3 Study Limitations

A limitation to our study is that we are unable to tell how the difference or lack of difference in torques are related to atrophy (loss of contractile material), adaptations of extra-cellular matrix (ECM) structure of the muscle, tendon compliance, or any combination of these changes. We do not believe atrophy would have a substantial affect for previous work has demonstrated relatively

little atrophy in the paretic muscles of the index finger (Triandafilou and Kamper, 2012). Additionally we measured the volume of each subjects forearms and verified that there was no significantly difference for any impairment level (severe p=0.244, moderate p=0.885, mild p=0.604) using a paired t-test. Though future studies could use MRI imaging to further quantify the muscle volume changes to then calculate the normalized torque to volume of muscle. As for adaption in the ECM or tendon, we were only able to quantify the combined changes of the muscle tendon unit and were unable to separate any potential changes occurring in the architecture muscle, ECM, or tendon. Future studies should explore these potentially different changes and their impacts on function.

5.5 Conclusion

We believe this to be the most thorough investigation of *in vivo* passive elastic torques at the hand in the chronic hemiparetic stroke population. These finding indicate that after a stroke there are not substantial increases of passive torques about either the wrist or the fingers. Increased stiffness observed clinically and in previous studies is likely a result of neural hyperactivity resulting from increased monoaminergic neuromodulatory drive mediated via the reticulospinal tract (McPherson et al., 2008; McPherson et al., 2017) and not from mechanical changes of the muscles or other soft tissue structures of the hand. Therefore the loss of hand function post-stroke is likely due to weakness from voluntary activation deficits (Hoffmann et al., 2016) and impaired control of the muscles of the hand (Miller and Dewald, 2012) due to disruptions of the corticospinal pathways (Kuypers, 1964; Lawrence and Kuypers, 1968). Future studies and rehabilitation techniques should therefore focus on the neural deficits post stroke such as weakness and motoneuron hyperactivity to achieve improved hand function.

6 CHRONIC STROKE INDIVIDUALS WHO RECEIVED BOTULINUM TOXIN INJECTIONS HAVE LONG TERM INCREASES OF MUSCLE STIFFNESS

Botulinum neurotoxin (BoNT) is the preferred treatment to reduce muscle stiffness produced by muscle hyperactivity in the upper extremity and hand of individuals with chronic hemiparetic stroke. BoNT is preferred because it acts focally and is relatively long acting. It has also been demonstrated however, that muscles that have been injected with BoNT increase in collagen content in the short term (6 months) and long term (1 year +). The increases in collagen content would likely increase muscle stiffness, thereby having the opposite than desired effect on muscle stiffness having a detrimental effect on the recovery of hand function. However, the potential long-term effect of increased muscle stiffness due to the BoNT injections has never been studied previously. This study was designed to investigate the potential effects of BoNT on muscle stiffness and passive joint torques about the hand and wrist in individuals with chronic hemiparetic stroke. Passive wrist and finger torques were collected from 16 chronic hemiparetic stroke subjects with severe hand impairments of which 7 had in the past received BoNT injections in their forearms and/or hands. Our results demonstrate that individuals who had received BoNT injections had significantly reduced passive range of motion (ROM) ($p < 0.001$) with mean decreases of up to 68 degrees as compared to their non-paretic hand. Also contributing to this decrease in ROM, individuals who had received BoNT injections had substantially greater torques about the wrist and MCP joints of the paretic limbs with average increases in the flexion torque of 230% and 185%, respectively. Additionally, we found that the increases in total torque about the wrist and MCP joint in the BoNT group was the result of increased torques contributed by increased stiffness of the extrinsic finger flexor and wrist flexor muscles and not adaptions of the soft-tissue structures

surrounding the joint. These results demonstrate that BoNT injection likely cause long-term increases in torques within the hand which may be detrimental to the recovery of hand function post stroke. Therefore, innovative approaches other than BoNT injections need to be explored, including the development of pharmaceutical or rehabilitative therapeutic treatments that reduce or inhibit muscle hyperactivity without long-term increases in passive stiffness.

6.1 Introduction

Currently, botulinum neurotoxin (BoNT) is the preferred treatment to reduce muscle hyperactivity, hypertonicity and spasticity, in individuals with chronic hemiparetic stroke. BoNT is preferred because it acts focally and is relatively long acting. Whereas, alternative pharmaceutical therapies that treat the muscle hyperactivity work systemically, are short acting, and are not well tolerated by individuals because of side effects including lethargy and general weakness (Gallichio, 2004; Ozcakir and Sivrioglu, 2007). In individuals with hemiparesis due to a stroke, BoNT injections have shown short-term improvements in passive range of motion and clinically evaluated spasticity (Kaku and Simpson, 2016; Shaw et al., 2011). These improvements aid in decreasing pain, self-care burden, and caregiver burden, but there is very limited evidence that BoNT injections improve functional outcomes (Kaku and Simpson, 2016; Shaw et al., 2011).

The mechanism by which BoNT works is well understood, but the effect of BoNT on muscle properties is just starting to be understood. At a mechanistic level, BoNT prevents the release of acetylcholine at the muscle's neuromuscular junction, thereby weakening and paralyzing the muscle in which it is injected (Dolly and Aoki, 2006). This paralysis initially causes a decrease in the size of muscle's fibers. Once the effects of the BoNT have dissipated, the fibers recover in size but not in force generating ability (Kim et al., 2003; Minamoto et al., 2007; Minamoto et al., 2015;

Thacker et al., 2012; Ward et al., 2017). Interestingly, it has also been demonstrated that muscles that have been injected with BoNT increase in collagen content in the short term (6 months) and long term (1 year +) (Minamoto et al., 2015; Thacker et al., 2012; Ward et al., 2017). The increased collagen content after BoNT may increase the muscle stiffness of the chronic stroke survivors who have received the injections that are not present in individuals who have never received BoNT, as demonstrated in the previous chapter.

If these injections cause long-term increases in muscle stiffness rather than reducing muscle stiffness, BoNT can have the reverse effect on long-term muscle stiffness than desired. However, the long-term changes in muscle stiffness following BoNT has never been reported. One common site of BoNT injections is to the wrist and finger flexors of individuals with chronic hemiparetic stroke with the goal of these injections is to aid hand hygiene and potential function by reducing the resistance from the hypertonia of the flexor muscles. If there were any increase in muscle resistance due to changes of muscles properties after BoNT injections, it may further impair these individuals' ability to extend their wrist and open their hands during reaching and grasping tasks because their extensor muscles are already weakened post-stroke (Kamper et al., 2006; Kamper et al., 2003). Thus the potential effects of increased muscle stiffness due to the BoNT injections could have substantial effects on the recovery of hand function post stroke in these individuals as compared to those who have not had BoNT injections.

In this study we investigate the potential effects of BoNT on muscle stiffness and passive joint torques in previously injected muscles about the hand and wrist in individuals with chronic hemiparetic stroke. We hypothesize, based on the previous literature indicating increased collagen content in the muscles after BoNT injection, that 1) individuals who have received BoNT

injections will have increased muscle stiffness and passive joint torques about the wrist and MCP joints as compared to their non-paretic non-injected side and 2) these increases are muscular in origin.

6.2 Materials and Methods

6.2.1 Participants

An interdepartmental research database, the Clinical Neuroscience Research Registry from Northwestern University and the Rehabilitation Institute of Chicago (now the Shirley Ryan AbilityLab), was used prescreen individuals who matched the inclusion criteria and recruit 20 individuals with chronic hemiparetic stroke with severe hand impairments as determined by the Chedoke McMaster Stroke Assessment Hand Score (CMSA-HS) (Gowland et al., 1993) to participate in this study (Table 6.1). CMSA-HS of 1-3 was considered as having severe hand impairments. Inclusion criteria was that paralysis be confined to one side of the body, the stroke occurred in the cortical or subcortical areas, the stroke occurred at least one year prior to participation in the study, absence of impairment or injury other than the stroke to either limb, lack of severe atrophy, lack of severe concurrent medical problems, and able to give informed consent. Data from three of the individuals were excluded from the analysis due to the inability to fully relax either their paretic and non-paretic arm muscles. Of the remaining 17 subjects, 8 had in the past received BoNT injections in their forearms and/or hands, however only one individual had BoNT injections in their extensor muscles and were therefore excluded from the analysis to standardize injection site (Table 6.1). Clinical tests of CMSA-HS and Modified Ashworth Scale (MAS) were administered by the same trained and licensed physical therapist across all subjects to eliminate inter-rater errors (Table 6.1).

The study was approved by the Institutional Review Board (IRB) of Northwestern University and participants gave informed consent for participation in the study using a form approved by the IRB. Clinical tests of CMSA-HS and Modified Ashworth Scale (MAS) were administered to verify impairment level and clinically relevant subject demographics were gathered from all subjects in a brief questionnaire prior to data collection (Table 6.1).

6.2.2 Experimental Set-up

As in the previous chapter subjects were seated comfortably in an upright position with their hand secured to a custom built version of the Wrist and Finger Torque Sensor (WFTS) (Stienen et al., 2011). The arm was positioned such that the forearm was parallel to the ground and with the palm facing medially eliminating the effects of gravity in the flexion and extension direction (Figure 6.1). The two distal finger joints for each finger were splinted to prevent distal joint movements and ensure isolated MCP and wrist movement. Muscle activity was monitored throughout the trials using surface EMGs electrodes (16-channel Bagnoli EMG System, Delsys Inc.; 1000 x gain, 20-450 Hz bandpass) placed over 4 muscles; flexor digitorium superficialis (FDS), flexor carpi ulnaris (FCU), extensor digitorium communis (EDC), and extensor carpi radialis (ECR).

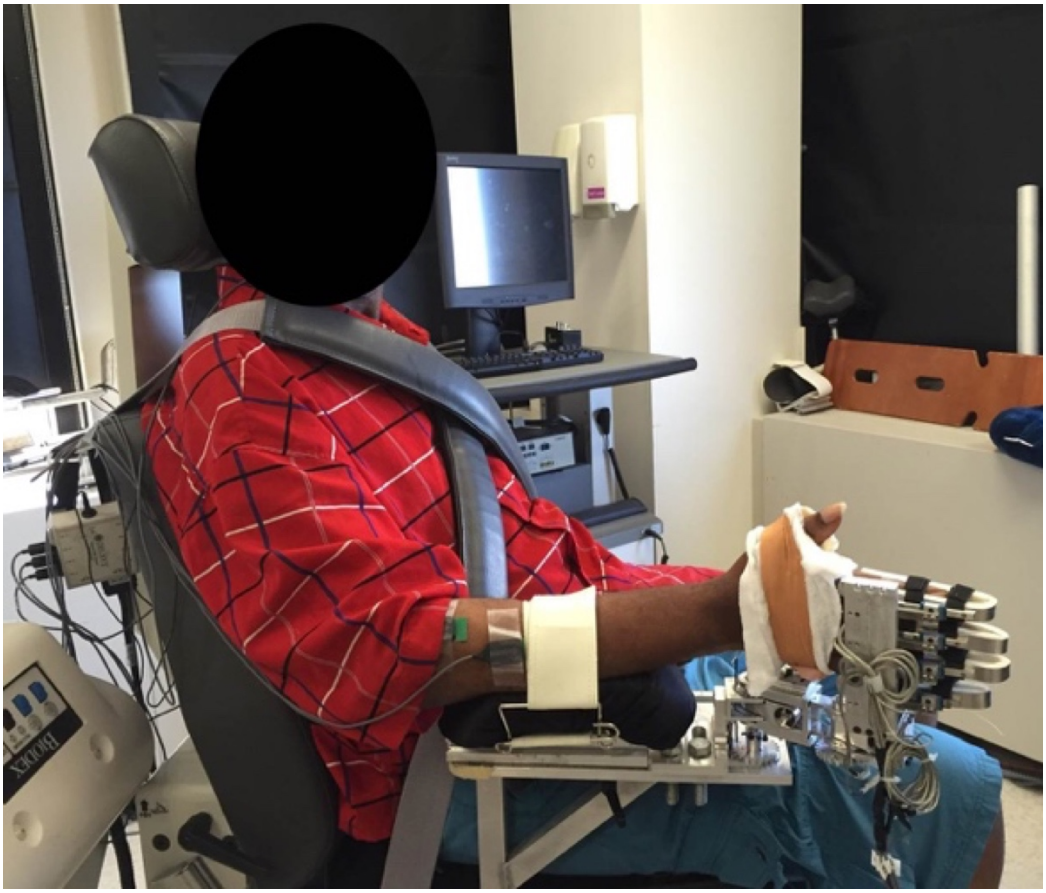

Figure 6.1: Picture of the experimental set-up with the subject seated upright with their hand attached to the Wrist Finger Torque Sensor.

Table 6.1: Subject Demographics. (CMHS – Chedoke McMaster Stroke Assessment Hand Score, MAS – Modified Ashworth Scale.)

Subject	Sex	Paretic Side	CMHS	MAS	Age in Years	Time Since Stroke in Years	Time Since Last BoNT Injection in Years	Location		
								Flexors	Extensors	Hand
b1	M	R	3	3	71	22.6	4.7	+		
b2	M	L	3	3	61.2	10.2	8.7	+		
b3	F	L	2	3	57.3	7.4	1.8	+		
b4	M	L	3	3	46.7	9.2	6.8	+		
b6	M	L	3	3	57.7	9.2	1	+		
b7	M	R	3	2	47.3	7.1	2.9	+		+
b8	M	R	3	2	55.7	9.5	5.8	+		
BoNT Mean (SD)			2.9 (0.4)	2.7 (0.5)	56.7 (8.3)	10.7 (5.3)	4.5 (2.8)			
nb1	M	L	1	3	49.2	16.9				
nb2	M	R	2	3	49.4	17.7				
nb3	M	R	2	3	74.7	15.2				
nb4	F	L	2	3	50.1	6.5				
nb5	M	L	3	2	69	13.5				
nb6	F	R	3	1	64	8.9				
nb7	M	L	3	1	50.9	28.5				
nb8	F	R	3	1+	63.9	30.3				
nb9	M	L	3	2	71.3	16.5				
No BoNT Mean (SD)			2.4 (0.7)	2.2 (0.9)	60.3 (10.4)	17.1 (7.9)				

6.2.3 Experimental Procedure

To eliminate hyperactivity within the muscles during data collection the protocol described in the previous chapter was used to reduce and acquiesce muscle hyperactivity during data collection. This protocol involves 10 minutes of pre-stretching within the device of the wrist and fingers into full flexion and extension, careful monitoring of EMG activity during trials, collecting the torques at static postures, and having the subject in a sleep or near sleep state to accommodate the hyperactive stretch reflexes.

This protocol was spaced over two days, the first day data consisted of collection from the non-paretic hand and the second day data consisted of collection from the paretic hand. The passive elastic torques were collected throughout multiple combinations of both the wrist and MCP joint postures as in the previous chapter. The wrist posture was randomly set in 15° increments between 60° of flexion and 60° of extension, resulting in 9 wrist postures. At each of the randomly set wrist postures the MCP joints were ranged throughout their range of motion, starting in full extension and then to full flexion and back to full extension in static 15° increments. MCP range of motion was determined by the subject's comfort level and the device's range of motion. At each static position of wrist and MCP posture the data was collected for 15 seconds and visually inspected for evidence of muscle activity or deviations within the torque, if present the trial was discarded and another trial at that position was collected.

6.2.4 Data processing

The raw torque and EMG data were collected and digitized at a sampling frequency of 1kHz. Torque data and rectified EMG data were then digitally filtered using a zero-phase infinite impulse

response 4th order Butterworth low-pass filter with a 4hz corner frequency. Baseline trials were used to set the torque offset and EMG threshold as previously described in Chapter 5.

At each combination of wrist and MCP joint posture, the processed torque and EMG data were divided into 1-second bins, for a total of 15 bins. In each bin the mean torque and EMG value was found, if the mean EMG signal from any muscle went above the EMG threshold or if the torque deviated more than 5% from the mode of the torques across the entire trial, the bin was discarded. The mean of the remaining bins for each trial were then used to create the total torque versus wrist and MCP posture data set for each subject at the wrist and the MCP joint to be used in the analysis.

6.2.5 Separation of the structures contributing to the total torque

Using the total torque data set collected at all the combinations of wrist and MCP postures we can create an analytical model that separates the extrinsic finger muscles from the other muscles and joint structures about each joint as done in the previous chapter (Knutson et al., 2000). The total wrist and MCP torque data set from section 6.2.4 were used to create an analytical model describing the total torque, $T_t(\theta, \omega)$, as comprised of two components.

$$T_t(\theta, \omega) = T_{sj}(\theta) + T_e(\theta, \omega) \tag{6.1}$$

$T_{sj}(\theta)$, consists of the torques contributed by the single-joint structures (wrist or intrinsic hand muscles, ligaments, joint capsules, etc.) that are a function of θ, either wrist or MCP joint angle. and $T_e(\theta, \omega)$, consists of the torques contributed by the extrinsic finger muscles that are a function of θ, either wrist or MCP joint angle, and ω, the co-varying joint angle. The methods used to fit this analytical mode are previously described in the last chapter (Knutson et al., 2000). From this analytical model each subject's total torque about the wrist and the MCP joints can be described as a function of the wrist and MCP posture and 14 constants. Then to create a data set describing

the contributions of the single joint structures and extrinsic finger muscle for use in the data analysis $T_{sj}(\theta)$ and $T_e(\theta, \omega)$ at the wrist and MCP were interpolated in 15 degree increments of the wrist and MCP posture within the subject's range of motion collected. Using these data sets we can analyze how the muscles separate from the other joint structures change.

6.2.6 Analysis of data

To determine the effect of the paretic vs. non-paretic hand; a generalized linear-mixed model analysis in the SPSS software (v24.0 IBM Corp Armonk, NY) was used to analyze the mean ROM of the MCP joints through all wrist angles and the data sets described above (measured total joint torque data, modeled single joint structures, and modeled extrinsic finger muscles) of the subjects in the BoNT group. Across all the analyses the dependent variable used was either ROM or torque. For the MCP ROM, total joint torque, and extrinsic finger muscles torques a four-factor analysis including subject, hand–paretic/non-paretic, MCP position, and wrist position was used. For the single joint torques a three-factor analysis including subject, hand–paretic/non-paretic, and MCP or wrist position was used. Subjects were set as a random intercept factor and all other factors were fixed factors. To test BoNT vs. No-BoNT differences in the paretic hands of each group linear-mixed model analyses were run using the same factors as before except with BoNT/No-BoNT as the hand factor.

Lastly, to understand the magnitude of the changes in the paretic hands the mean differences in torques and the percent change of the torques were calculated. For each subject the difference was calculated by subtracting the torque of non-paretic from the paretic hand at each of the wrist and MCP joint posture. The mean difference at each wrist and MCP posture were then averaged

across subjects in each group. The percent change at each wrist and MCP joint posture combination was found by dividing the mean difference by the mean non-paretic torque in each group.

6.3 Results

6.3.1 Impact on range of motion

Individuals who had received BoNT injections had significantly reduced passive ROM in their paretic hand as compared to the non-paretic hand ($p < 0.001$) with mean decreases in extension ROM of up to 68 degrees (Figure 6.2b) at full wrist extension. There was no difference in ROM between the paretic and non-paretic hands of individuals with no BoNT ($p=0.360$) (Figure 6.2a). The paretic hand of the BoNT group was also significantly different from the paretic hand of those without BoNT ($p < 0.001$) with up to group mean decrease of 60 degrees in ROM as compared between the paretic hands of each group, occurring at full wrist extension.

6.3.2 Measured total torque about the wrist and fingers

The BoNT group had substantial increases in total flexion torques of their paretic hands as compared to the non-paretic hands about the wrist ($p < 0.001$) and MCP joints ($p < 0.001$) (Figure 6.3d-f & 6.4d-f). There was an increase in the average flexion torque of 230% at the wrist and 185% at the MCP as compared to the non-paretic hand at the end of the paretic wrist and MCP joint extension. Additionally, there were significant increases of total flexion torque about the wrist ($p=0.005$) and MCP joints ($p=0.010$) of the paretic hands of the BoNT group as compared to the paretic hands of the no-BoNT group.

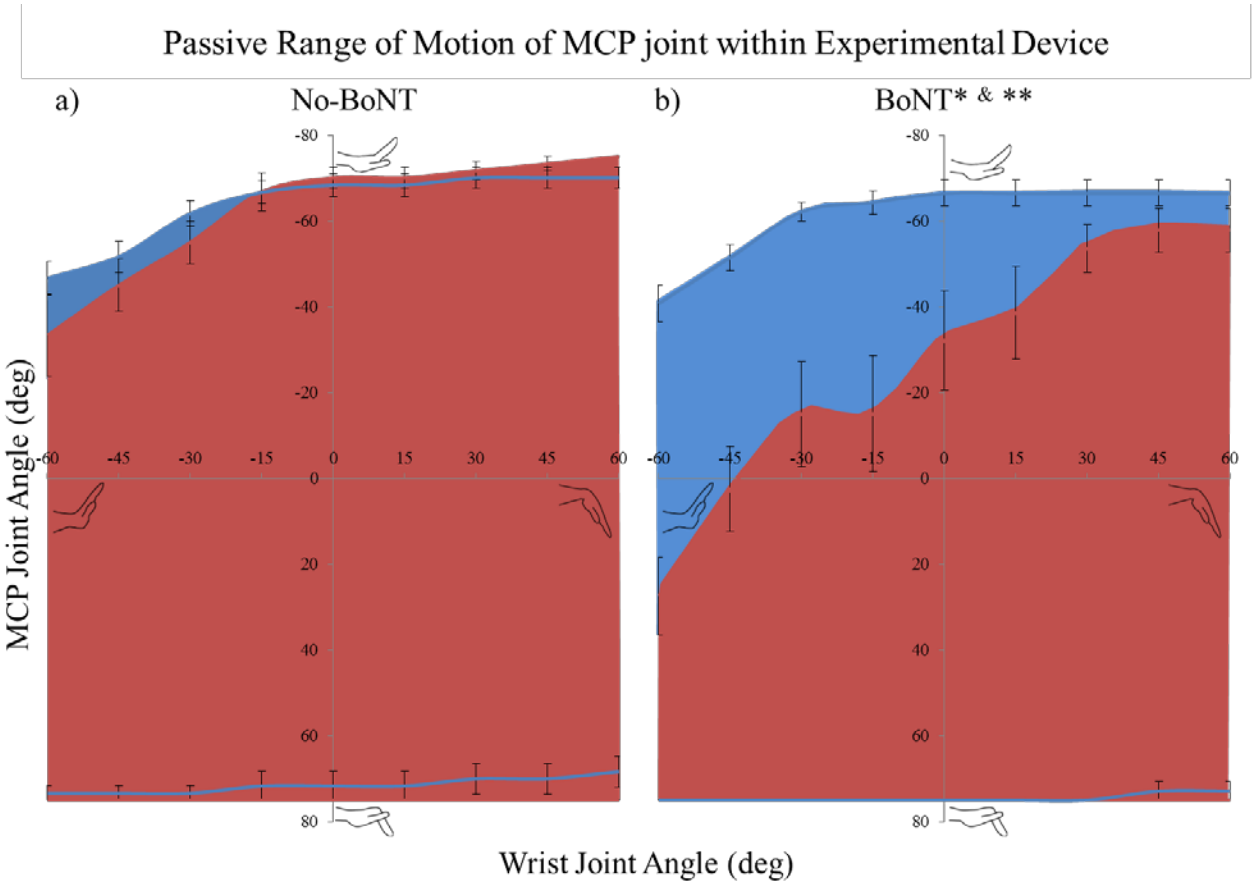

Figure 6.2: Mean end of MCP passive range of motion in extension (-, top lines) and flexion (+, bottom lines) throughout the wrist's ROM for the paretic (red) and non-paretic (blue) of the a) no-BoNT severe group and BoNT group within in the experimental device with standard error bars. The ROM of the paretic hand of the BoNT is significantly and substantially less than the non-paretic hand and paretic hand of the no-BoNT group. The greatest decreases in MCP ROM occurred in extended wrist postures. (*p <0.001 between paretic v non-paretic hands within group) (**p <0.001 between paretic hands across groups)

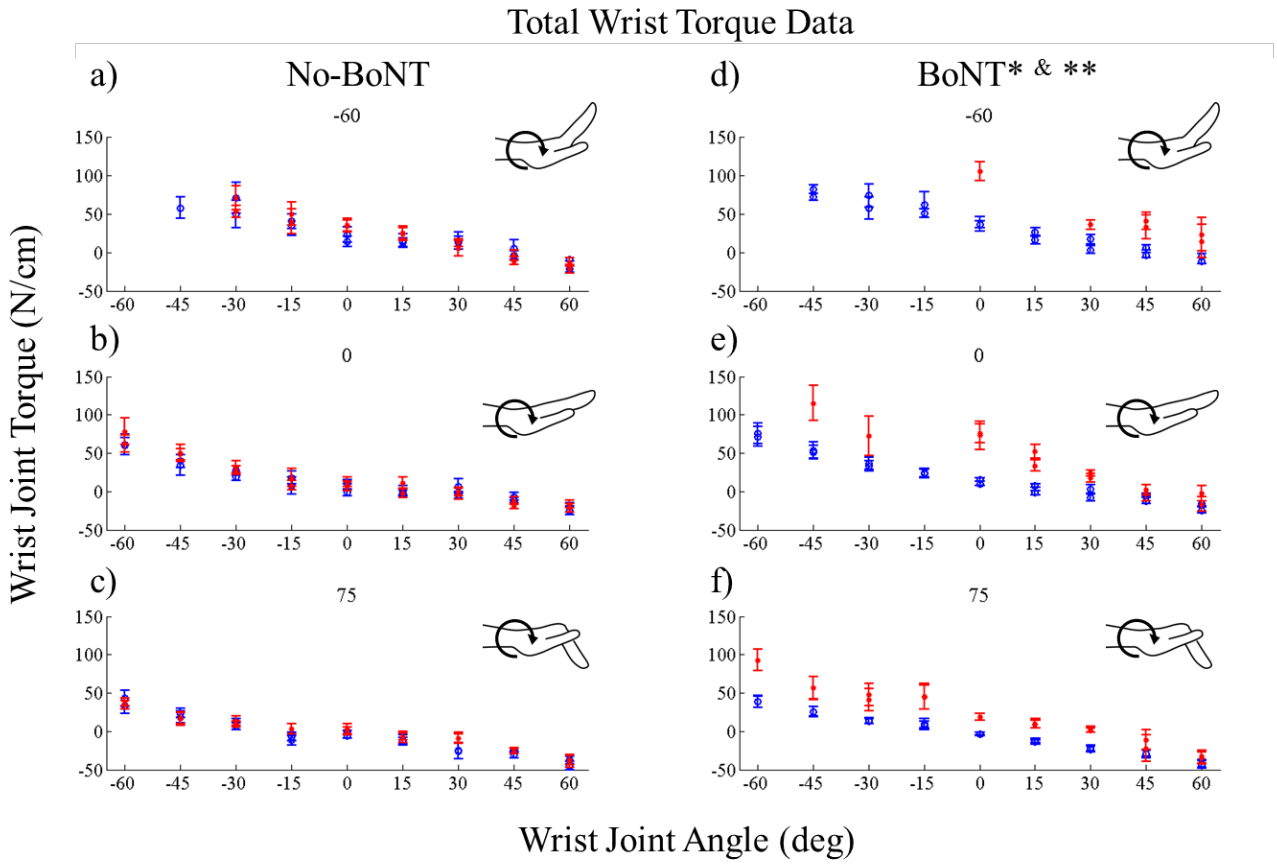

Figure 6.3: Wrist torque data versus over the wrist's range of motion with the fingers locked in -60, 0, and 75 degrees of the paretic (red) and non-paretic (blue) with standard error bars of the no-BoNT and BoNT groups. The BoNT group demonstrates increases of paretic wrist flexion torque that is not present in the paretic hand of the no-BoNT group. Data points are only displayed when there is individual data for 3 or more subjects at that specific posture. (+ flexion/- extension) (*p <0.05 between paretic v non-paretic hands within group) (**p <0.05 between paretic hands across groups)

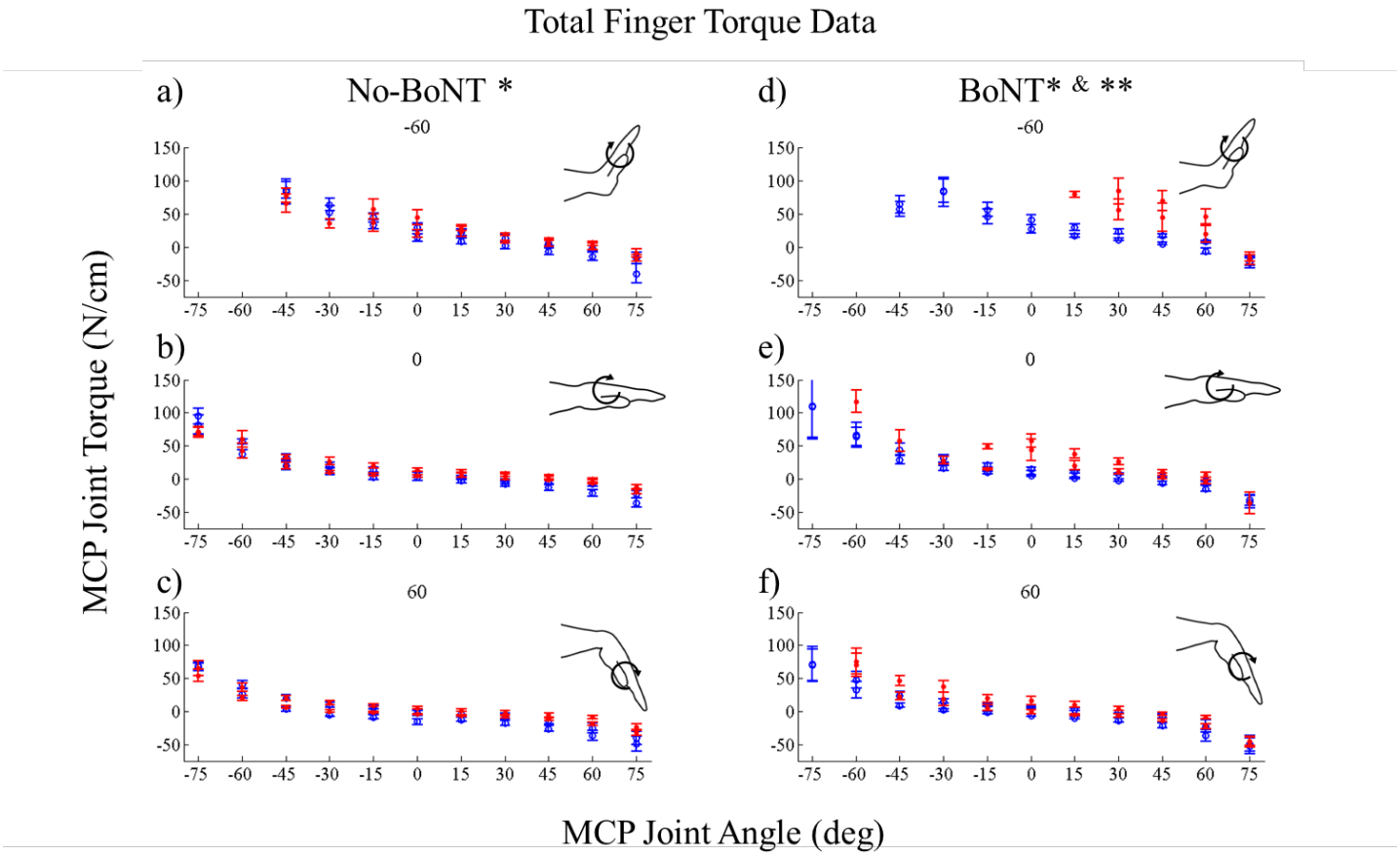

Figure 6.4: MCP torque data versus over the MCP joints' range of motion with the wrist locked in -60, 0, and 60 degrees of the paretic (red) and non-paretic (blue) with standard error bars of the no-BoNT and BoNT groups. Increases in finger flexion torque of the paretic hand within the BoNT group is demonstrated that is not present in the paretic hand of the no-BoNT group especially as the fingers are positioned in an extended posture. Data points are only displayed when there is individual data for 3 or more subjects at that specific posture. (+ flexion/- extension) (*p <0.05 between paretic v non-partic hands within group) (**p <0.05 between paretic hands across groups)

Table 6.2: Median Parameters for the fit analytical models of paretic and non-paretic at the MCP and wrist at each impairment level. R^2 is the mean of R^2 values

	Parameter	A1	k1	theta1	A2	k2	theta2	A3	k3	B3	phi3	A4	k4	B4	phi4	R^2
No-BoNT	Paretic MCP	1.04	0.0864	-9.78	6.22	0.0935	60.64	1.43	0.0384	-1.45	14.47	0.80	0.0533	-1.00	51.23	0.88
	Non-Paretic MCP	1.75	0.0990	-27.08	6.43	0.3819	65.05	1.86	0.0397	-0.95	4.02	14.16	0.0261	-0.63	31.63	0.95
	Paretic Wrist	3.65	0.0600	-28.18	27.17	0.0368	62.31	7.04	0.0373	-0.70	52.52	22.00	0.0003	-2.96	7.94	0.93
	Non-Paretic Wrist	3.23	0.0628	-41.92	38.83	0.0075	26.20	5.02	0.0332	-0.85	-10.61	27.30	0.0159	-0.78	54.44	0.92
BoNT	Paretic MCP	1.13	0.0743	-13.85	6.27	0.1074	62.81	1.49	0.0374	-1.33	11.00	0.93	0.0481	-0.72	45.03	0.90
	Non-Paretic MCP	1.44	0.0866	-23.37	4.64	0.1259	67.38	1.45	0.0357	-1.06	5.38	6.10	0.0240	-0.61	31.46	0.95
	Paretic Wrist	3.42	0.0518	-27.65	27.06	0.0347	57.78	7.17	0.0377	-0.72	41.61	21.92	0.0027	-2.28	24.83	0.93
	Non-Paretic Wrist	3.21	0.0689	-42.59	33.69	0.0081	23.98	5.15	0.0322	-0.84	-10.16	26.68	0.0130	-1.03	89.84	0.96

$T_t(\theta,\omega) = T_{sj}(\theta) + T_e(\theta,\omega)$ $T_{sj}(\theta) = A_1\left(e^{-k_1(\theta-\theta_1)} - 1\right) - A_2\left(e^{k_2(\theta-\theta_2)} - 1\right)$ $T_e(\theta,\omega) = A_3\left(e^{-k_3(\theta-\theta_3)} - 1\right) - A_4$ $\theta_j = B_j \cdot \omega + \emptyset_j$ $(j = 3,4)$

6.3.3 Analytical model separation of the structures contributing to the total torque

The 14 constant parameters (see Table 6.2) defining the analytical model of the relative contributions of the extrinsic finger muscles and the single joint structures about the wrist and the MCP joints of the BoNT group fit well to the total torque data of the BoNT group at the wrist (paretic r=0.93 & non-paretic r=0.96) and MCP joints (paretic r=0.90 & non-paretic r=0.95). Parameters for the no-BoNT group were calculated and used from the previous chapter.

The torques contributed by the extrinsic finger muscles about the MCP joints demonstrated significant differences in the BoNT group ($p< 0.001$) between the paretic and the non-paretic hands (Figure 6.5d-f). These differences were substantial in the BoNT group with mean increases of flexion torques at the end range of MCP extension across all wrist postures of 248% in the paretic hand as compared to the non-paretic as compared to increases of only approximately 45% in the no-BoNT group (Figure 6.5).

At the wrist, the BoNT group had substantial and significant increases in both the torques of both the single joint toques (wrist muscles, wrist ligaments, and other soft tissue structures) ($p< 0.001$) (Figure 6.6b). The single joint toques at the wrist, wrist muscles, wrist ligaments, and other soft tissue structures, demonstrated an average 26.1 Ncm shift towards greater flexion, which drastically shifts the equilibrium point of the wrist into approximately 50 degrees of greater flexion than that of the non-paretic wrist (Figure 6.6b).

There were small differences in the single joint structures (intrinsic hand muscles, ligaments, joint capsules, etc.) about the MCP joint in paretic vs. non-paretic hands of the BoNT (4.4 Ncm, p=0.044) (Figure 6.7b) or between the BoNT and no-BoNT paretic hands (7.4 Ncm p=.003) (Figure 6.7).

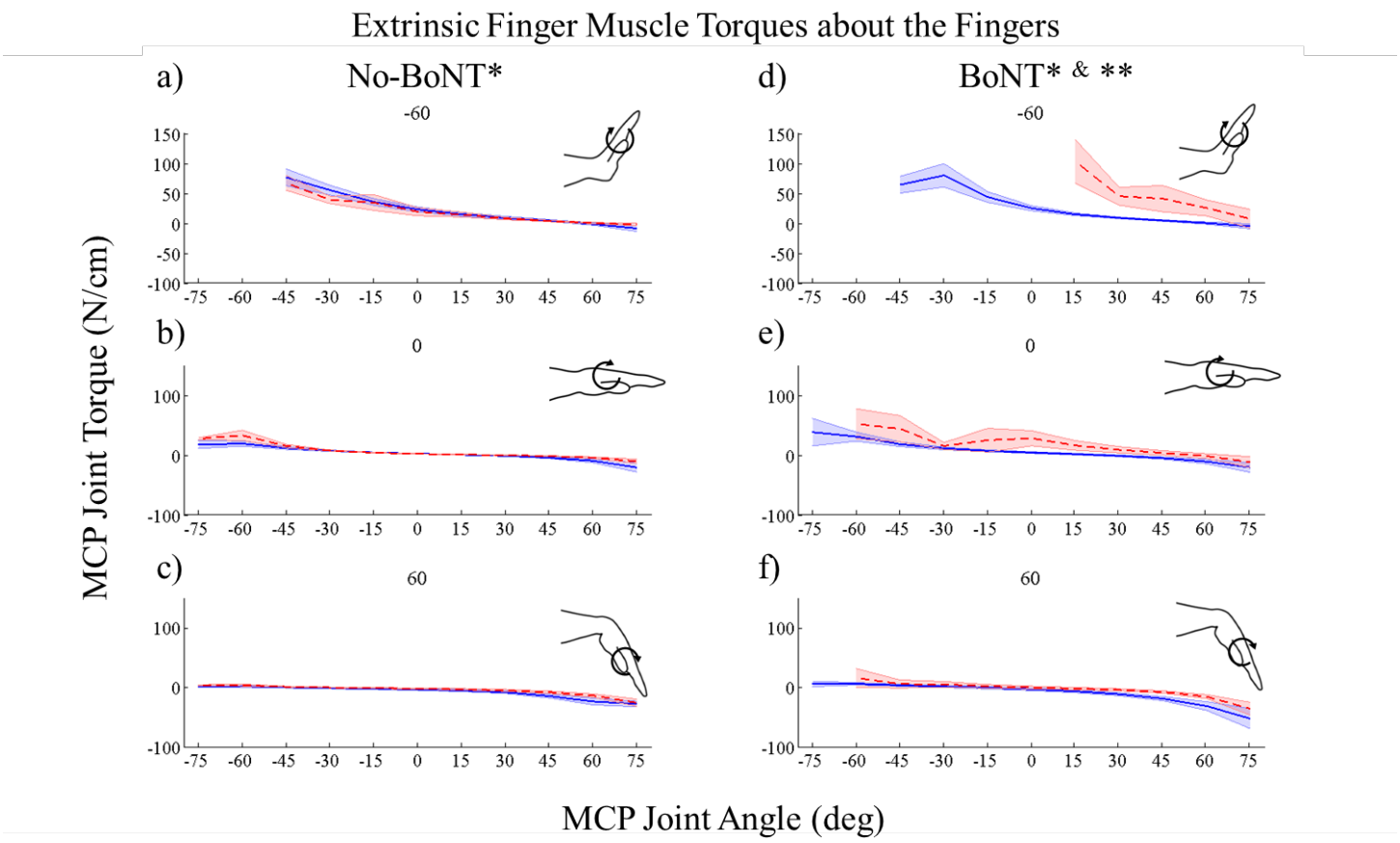

Figure 6.5: MCP torque of the extrinsic finger muscles about the MCP joints versus over the MCP range of motion with the wrist locked in -60, 0, and 60 degrees of the paretic (red dashed line) and non-paretic (blue solid) with standard error in the shaded region of the no-BoNT and BoNT groups. Increases in finger flexion torque contributed by the extrinsic finger muscles of the paretic hand within the BoNT group is demonstrated that is not present in the paretic hand of the no-BoNT group especially as the fingers are positioned in an extended posture indicating that the flexor muscles have increased in stiffnes. Data points are only displayed when there is individual data for 3 or more subjects at that specific posture. (+ flexion/- extension) (*p <0.05 between paretic v non-partic hands within group) (**p <0.05 between paretic hands across groups)

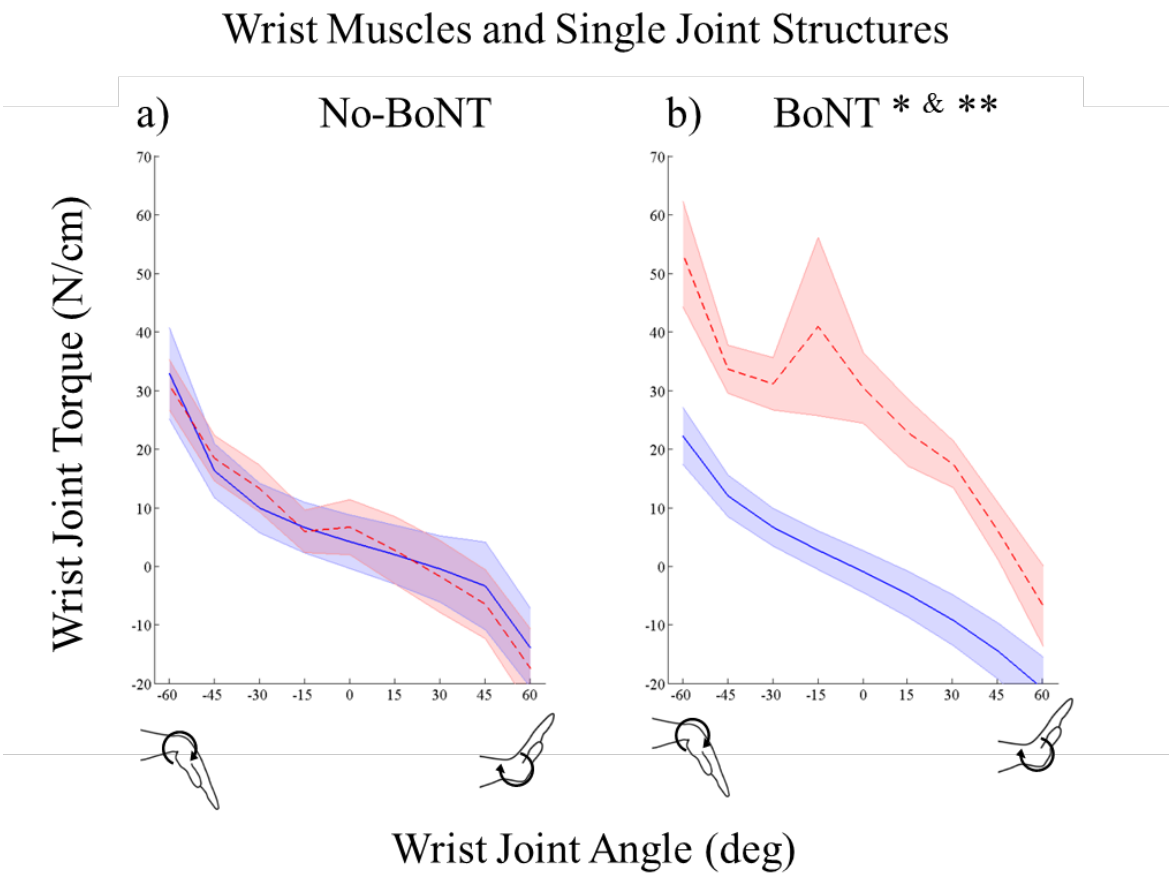

Figure 6.6: Wrist torque of the wrist muscles and other joint structures about the wrist joint's range of motion of the paretic (red dashed line) and non-paretic (blue solid) with standard error in the shaded region of the no-BoNT and BoNT groups. Increases in wrist flexion torque of the paretic hand within the BoNT group is demonstrated that is not present in the paretic hand of the no-BoNT group throughout the wrist's ROM that increases as the wrist is extended, indicating an increase in stiffness of the flexor muscles that is not present in the no-BoNT group. Data points are only displayed when there is individual data for 3 or more subjects at that specific posture. (+ flexion/-extension) (*p <0.05 between paretic v non-partic hands within group) (**p <0.05 between paretic hands across groups)

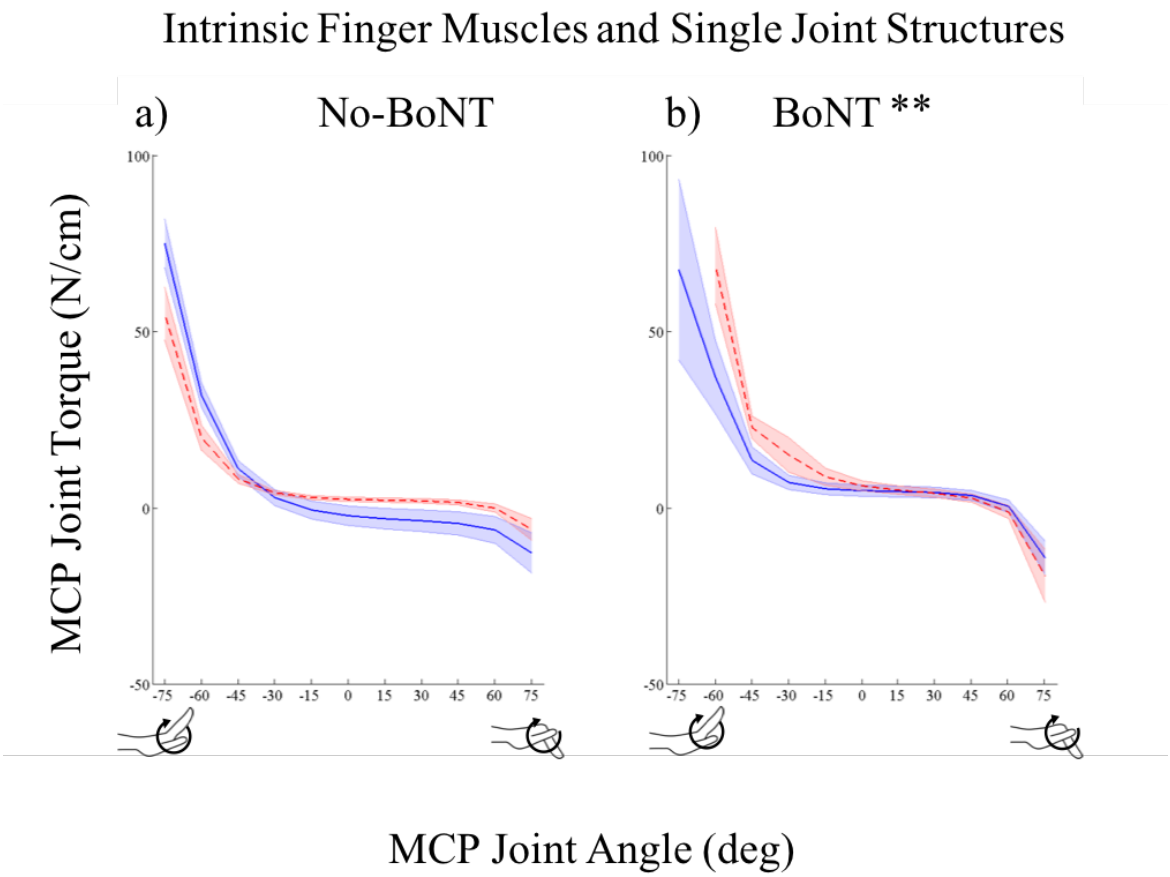

Figure 6.7: The MCP torque of the intrinsic hand muscles and other joint structures about the MCP joint's range of motion of the paretic (red dashed line) and non-paretic (blue solid) with standard error in the shaded region of the no-BoNT and BoNT groups. In both groups the BoNT and no-BoNT group the single joint structures of the paretic hand are not significantly different from the non-paretic hand. Data points are only displayed when there is individual data for 3 or more subjects at that specific posture. (+ flexion/- extension) (**p <0.05 between paretic hands across groups)

6.4 Discussion

The purpose of this study was to begin to understand the effects of BoNT on muscle stiffness and the resultant passive torques that are produced in the hand and wrist in individuals with chronic hemiparetic stroke. We believe this to be the first study exploring the potential long-term effects of BoNT on passive properties of hand and wrist muscles within humans.

The results from this study confirmed our first hypothesis that individuals who have received BoNT injections in their paretic limbs had substantially greater torques about the wrist and MCP joints of the paretic limbs as compared to their non-paretic side (Figures 6.3d-f & 6.4d-f) and the paretic limb of individuals who did not receive BoNT injections (Figures 6.3 & 6.4). Our second hypothesis was also confirmed that the origins of the increased total torque about the wrist and MCP joint in the BoNT group was the result of increased torques contributed by the extrinsic finger flexors and wrist flexor muscles (Figures 6.5d-f & 6.6b) for the increases in torques were only observed when the wrist and extrinsic finger flexor muscles were stressed into extended postures. Additionally, supporting this supposition is a lack of substantial difference in torques of the single joint structures about the MCP joint (intrinsic finger muscle, ligaments, joint capsule, etc.) (Figure 6.7b). The conclusion that the increases in torques originate in the flexor muscles is also consistent with the location where these individuals received BoNT injections. All of the individuals received injections in their wrist and finger flexors (Table 6.1).

The consequence of these increases in flexion torque within the BoNT group is evident as we observed mean decreases of up to 60 degrees in the passive range of motion of MCP joints when subjects were measured within our device of the BoNT group as compared to the other groups (Figure 6.2). These ROM limitations seen in the passive condition would be likely be further compromised in active ROM as the chronic stroke individuals attempt to actively open their hand and their weakened extensor muscles (Kamper et al., 2006; Kamper et al., 2003) cannot generate the torques required to reach the end of the ROM as seen in the device.

6.4.1 Origin of the increased torques from muscles injected with BoNT

The increased flexion torques and decreased ROM suggest that those individuals who have received BoNT injections undergo long lasting muscular property changes. These biomechanical changes within the muscles are likely an effect of the BoNT and not related to the neural impairments post stroke. The neural impairments likely do not have biomechanical changes that increased the passive torques of the muscles because in the previous chapter we found that post-stroke individuals across all impairment levels, who have never received a BoNT injection, do not have the substantial increases in passive torques about fingers or wrist as demonstrated in the previous chapter. It is only in those individuals that have had BoNT injections that we see this increase in passive torques. Interestingly, in the individual who had received BoNT injections within their extensor muscles of their paretic limb, that was excluded from the analysis, we found increases in passive extensor torque as the fingers were flexed and the increases originated from the wrist and finger extensors muscles. This further implicates BoNT as the likely cause of the increases in joint torques for whether the flexors or the extensors were injected the resulting increases in torque corresponded with the location of the injection.

The source of the increased torque is likely from increased muscle stiffness that is the result of increased collagen within the extra cellular matrix (ECM) of the muscles that have been injected with BoNT. In animal models, increases in collagen content in the ECM is present 6 months following 2 BoNT injections and lasts potentially for the lifespan of the animal (Minamoto et al., 2015; Thacker et al., 2012; Ward et al., 2017). However, the underlying mechanism of this increased collagen content is unknown. Two potential mechanisms are that the increases in collagen are a consequence of the BoNT induced muscle paralysis or a reaction within the muscle

to the BoNT compound itself. Parallels can be drawn between the effect of BoNT on muscle and muscle denervation, both eliminate neural input to the muscle; denervated muscle has been shown to demonstrate increases in collagen content within a month after the denervation (Faturi et al., 2016; Liu et al., 2016; Nikolaou et al., 2014; Russo et al., 2008). This time frame fits well within the three month timeframe of BoNT induced muscle paralysis, indicating that the muscle adaptation is likely to occur during that time. Unfortunately, to date there are no studies that have tested the hypothesis that the BoNT compound itself reacts with the muscles to increase collagen content. Further study into these mechanisms would greatly enhance our understanding of the long-term effects of BoNT on muscle.

6.4.2 Clinical Relevance of increased muscles stiffness following BoNT

BoNT is often used with post-stroke individuals who display hypertonicity and spasticity within their upper limbs as a treatment to improve cosmetic appearances, hygienic care, or reduce caregiver burden by relaxing the muscle and allowing for the ranging of the limb or hand through a greater ROM. The BoNT injections have this desired short-term benefit, but as our findings suggest the long-term effects of the injections may be detrimental to the maintenance of ROM. We observed decreases in passive ROM of the paretic hand of individuals who received BoNT, which would make opening of the hand exceedingly more difficult for themselves or their caregiver.

The long-term increases in muscle stiffness after BoNT injections may also be a barrier for improved hand function for patients who have some residual motor control of their hand. The increases in passive torque, when combined with the muscle weakness (Kamper et al., 2006; Kamper et al., 2003) would make hand opening exceedingly difficult. Additionally, we observed increases of passive torque in neutral and flexed postures of the MCP joints at wrist postures of 30

degrees extension to 30 degrees of flexion with the average passive torque increases of 209% in these ranges for the BoNT group whereas the increase in the no-BoNT was only 57%. This is particularly problematic, because a majority of functional tasks occur within these wrist and MCP joint postures (Bain et al., 2015; Hume et al., 1990; Ryu et al., 1991). Once again, these substantial increases in passive torque would further impede the already weakened ability to extend the fingers and open the hand.

For individuals who do not have sufficient residual motor control to volitionally open their hand, these increases in passive flexion torques are especially important to consider while developing therapies and devices aimed at resorting hand function. For example, individuals who have not received BoNT injections and have negligible increases in passive torques, a viable intervention may be functional electrical stimulation (FES) because the residual capacity of the extensor muscles exceeds the passive forces and stiffness of the flexor muscles. But in individuals who have received BoNT injections the adaptions within the muscles and resulting increases in flexion torques may be insurmountable for the weakened extensors, making FES a less viable option. In such cases, mechanical devices may be necessary to assist the individuals to go through a functional ROM and need to be designed with these limitations in mind.

6.4.3 Strengths and Limitations

This study utilizes an experimental method that eliminates muscles hyperactivity during the evaluation of the passive mechanical elastic properties of the structures of the wrist and hand. This allowed us to explore how the passive mechanical torques, which are often masked by the hyperactivity of the muscles in individuals with chronic hemiparetic stroke, are changing post stroke. However, we only monitored the EMG from superficial muscles (FPS, FCU, EDC, and

ECR) and did not specifically monitor the muscles within the deep compartments of the forearm. However, it is unlikely that these deeper muscles would be selectively and differentially active from the superficial muscles. Thus, we do not believe that the deeper muscles were active and contributing substantially to the torques we recorded.

This study was a cross-sectional study looking at changes within the muscles of individuals who previously had BoNT injections in their forearms and/or hands versus those who did not. It was not a longitudinal randomized control study to determine whether BoNT increases stiffness or not. Though we believe the increases in torques are due to the cascade effects of the BoNT, it may be argued that different levels of hyperactive stretch reflexes could influence the passive biomechanical torques. This is likely not the case in our study for the MAS scores between the two groups were not different from each other (BoNT 2.7±0.5, No-BoNT 2.2±0.9, $p=0.158$). We also were not able to correlate dosage and usage of BoNT to increases in torques for we did not have accurate enough data for such an analysis because we did not have permission to access the medical records of these individuals. Future studies should include the use of a longitudinal study and medical records to deduce any causal or dosage dependent effects of BoNT on muscle stiffness.

6.5 Conclusion

We believe this to be the first study to explore the potential long-term effects of BoNT on the passive muscle properties within humans. Within muscles of the hand and wrist we found that individuals with chronic hemiparetic stroke who received BoNT injections have substantial increases in the torques about their wrist and MCP finger joints versus their non-paretic hands and versus the torques of the paretic hands of individuals who had not received BoNT. We also found that these effects last for years after stopping the injections with the mean time since their last

injection being approxiamtely about 4.5 years. The origins of these increases are likely due muscle property changes of increased collagen content occurring within the ECM of the muscles following the BoNT injections. These long-term increases in torques have the opposite effect of the initial desired goal of the BoNT injections to reduce passive resistance from hyperactive muscles and increase ROM. Therefore, other innovative approaches other than BoNT injections need to be explored. These new approaches could include pharmaceutical or other rehabilitative therapeutic treatment approaches that reduce or inhibit muscle hyperactivity without the long-term increases in passive stiffness. With these findings, and our limited understanding of the long-term effects of BoNT on muscle, BoNT should be used with discretion until there is a better understanding of the mechanisms of the long-term effects of BoNT. Finally, additional research is needed to further explore the mechanisms by which BoNT produces its long-term effects on muscle stiffness.

7 INCREASED FLEXION TORQUES LEAD TO HAND IMPAIRMENTS IN CHRONIC HEMIPARETIC STROKE: A SIMULATION STUDY

In individuals with chronic hemiparetic, stroke finger extension and consequently hand opening is the most commonly impaired and difficult task to perform. The main impediment to finger extension is the inability to generate sufficient forces required to overcome the increased flexion torques about the finger joints. These increased flexion torques may be the result of an upregulation of reticulospinal pathways following a hemiparetic stroke resulting in involuntary flexor muscle activity or hypertonicity, at rest, as well as during physical activity such as when lifting up the paretic arm and structural biomechanical changes within the muscles of the hand. To reduce the involuntary muscle activity, especially in the flexor muscles of the upper extremity, botulinum neurotoxin (BoNT) is the preferred method of treatment; however BoNT may cause long term increases in passive muscle stiffness. At present, it is not known what effect these long-term increases in passive muscles stiffness may have on the patients' ability to open their hands and the recovery of hand function post stroke and how these increases in passive muscle stiffness may further impair hand function in addition to the impacts from flexor hypertonicity. We, therefore, developed computational biomechanical musculoskeletal models to explore the impact of increased muscle stiffness of the flexor muscles after BoNT injection as well as the impact of an increased involuntary muscle activity of the flexor muscles and decreased voluntary activation of the finger extensors on the ability to open the hand in the chronic hemiparetic stroke population. We found that increased muscle stiffness following BoNT limits the ability to extend the fingers in the severely and moderately impaired populations; however, with increased strength these deficits can be overcome. The greatest impairment on the ability to open the hand following

chronic hemiparetic stroke was the result of involuntary muscle activity of the finger flexor muscles that overshadows the non-neural sources of increased flexion torques. These results indicate that physical and pharmaceutical rehabilitation interventions in individuals following a hemiparetic stroke should focus on reducing the involuntary muscle activity of finger flexors to maximize gains in the ability to open and use their paretic hand.

7.1 Introduction

Hand opening required to grasp an object is needed for most activities of daily living. However, for individuals with chronic hemiparetic stroke, finger extension and consequently hand opening is often the most impaired and difficult task to perform (Broeks et al., 1999; Lawrence et al., 2001; Nakayama et al., 1994; Parker et al., 1986). This impairment causes individuals with chronic hemiparetic stroke to rely on their non-paretic hand or caregivers for many activities of daily living, causing a loss of independence and a decreased quality of life.

In individuals with chronic hemiparetic stroke, the main impediment to opening of the hand is the inability to generate sufficient forces required to overcome increased flexion torques about the finger joints (Kamper et al., 2006). This inability to produce sufficient force can be due to muscle weakness stemming from muscle atrophy (Prado-Medeiros et al., 2012; Ryan et al., 2002; Scelsi et al., 1984; Silva-Couto Mde et al., 2014), though minimal atrophy has been demonstrated in the finger muscles (Triandafilou and Kamper, 2012). Therefore, weakness within the fingers is likely due to the inability to effectively activate fingers extensor muscle following a loss in corticospinal projections (Hoffmann et al., 2016; Kamper et al., 2006). The increased flexion torques about fingers have been postulated to be a result of involuntary flexor muscle activity, or hypertonicity, during rest that increases with physical activity, and potential biomechanical changes within the

muscles of the hand. However, as demonstrated in the previous chapters these potential biomechanical changes may not be part of the natural course of recovery for we did not find increases in passive torques in the paretic hand unless the individual has received botulinum neurotoxin (BoNT) injections to treat the involuntary muscle activity. BoNT has the potential to cause long term biomechanical changes within the muscle (Minamoto et al., 2015; Thacker et al., 2012; Ward et al., 2017) that increase the muscle's passive stiffness that are not seen in muscles that have not been injected with BoNT. This increase in muscle stiffness results in increased passive torques about the fingers and decreases of up to 50 degrees in the passive range of motion of the MCP joint (Chapter 6). The remaining source of increased flexion torques originate from involuntary finger flexor activity which seems to be due to a loss of direct corticospinal pathways and an increased reliance on indirect corticoreticulospinal pathways (Baker, 2011; Riddle and Baker, 2010; Riddle et al., 2009). This is manifested as a loss of independent joint control (LIJC) and flexor muscle hyperactivity at rest (Dewald et al., 1995; Dewald et al., 2001; McPherson et al., 2008; Sukal et al., 2007). Loss of independent joint control (LIJC) is often expressed in the form of a flexion synergy in the upper extremity; when an individual attempts to lift their arm they involuntarily flex their elbow, wrist, and fingers (Brunnstrom, 1970; Dewald et al., 1995; Dewald et al., 2001; Miller and Dewald, 2012; Sukal et al., 2007). The flexor muscle hyperactivity at rest is postulated to be related to an increased motoneuron excitability within the spinal cord that results in motor unit firing at rest (McPherson et al., 2008; McPherson et al., 2017) and a hyper-excitable stretch reflex, or spasticity (Kamper and Rymer, 2000; Lance, 1980; O'Dwyer et al., 1996).

It is unknown to what effect the increases in joint torques due to involuntary flexor muscle activity or passive muscle stiffness, due to BoNT, impede the ability to open the hand and recover

hand function post stroke. The resistance from the BoNT, combined with involuntary flexor muscle activity, could have a significant impact on the ability to open the hand and could be a substantial barrier to the recovery of hand function in these individuals. If the long-term consequences of BoNT are detrimental to hand opening, the use of BoNT for the management of muscle hyperactivity following a stroke will need to be reexamined and new rehabilitation and pharmaceutical interventions may need to be developed.

In this study, we will use computational musculoskeletal models to study how increased flexion resistance originating from the biomechanical changes seen in individuals who have received BoNT versus the increased flexion resistance originating from involuntary finger flexor muscle activity impairs the ability to open the hand. These computational models will also be used to determine how the various sources of hand impairments interact with one another and, more specifically, how their compound effects impair the ability to open the hand. This knowledge will lead to greater understanding of the origins of hand impairments following stroke and is essential for the development of new and improved interventions that correctly target the most actual sources of patient impairments. Based on the work in the previous chapter demonstrating substantial long-term decreases in passive range of motion and increases in passive torques about the fingers in individuals who have recieved BoNT injections, we hypothesis that our models will show that the consequences from BoNT will significantly contribute to the observed decreased ability of individuals post stroke to open their hands.

7.2 Methods

Using computational musculoskeletal models, we explored the impact of increased flexion torques due to passive muscle stiffness after BoNT and increased involuntary flexor muscle activity on the ability to open the hand.

7.2.1 Development of the dynamic musculoskeletal models of the hand.

Using the OpenSim platform v3.3 (Delp et al., 2007), a dynamic upper extremity model developed by Saul et al (Saul et al., 2015); which included the kinematic of the shoulder, elbow, and wrist as well as the muscles paths and force generating properties of 32 muscles and muscle compartments crossing the shoulder, elbow, wrist and hand; was used as the basis for building both our non-paretic and BoNT computational musculoskeletal models. The kinematics, masses, and inertias of carpals, metacarpals, and phalanges of the digits were added to the model as described by Binder-Markey & Murray (Binder-Markey and Murray, 2017). The present dynamic model only includes the extrinsic finger muscles for digits two and three, the index and middle fingers respectively. Only hese two fingers were included in the model for they are the primary two fingers required for most activities of daily living involving grasping tasks (Gonzalez et al., 2017; Taylor and Schwarz, 1955) as well as computational limitations that prevented the dynamic simulation of all four fingers (the four finger model can be found in Appendix B). All other muscles were removed from the model. The moment arms for the extrinsic fingers within the hand were updated by matching the muscle paths and wrapping surfaces distal to the wrist as implemented by Lee et al (Lee et al., 2015a, b). The methods described previously by Binder-Markey and Murray were used to incorporate the passive torques about joint each finger (Binder-Markey and Murray, 2017).

7.2.1.1 Experimentally collected passive torque about each finger

The experimental net passive metacarpophalangeal (MCP) torques, the sum of all 4 fingers, was taken from the data collected in the previous two chapters. This torque was then separated into the torque about each finger to be input into the computational model. To separate the total net MCP passive torque into the relative contribution of each finger the following processing was completed. Bending beam strain gauges, connecting the fingers to the modified Wrist Finger Torque Sensor (Stienen et al., 2011), as described in the previous chapter, were used to determine the relative contribution of each finger to the total MCP passive torque. Because strain gauges are sensitive to internal bending and twisting moments that do not contribute to the external torques of the finger, the output moments of the strain gauges were used to determine the relative proportion of torque, P_i, each finger contributed to the total MCP joint torque at each posture of wrist and MCP finger angle and were calculated as:

$$P_i = \frac{M_i^{\varepsilon}}{\sum_{i=2:5} M_i^{\varepsilon}}$$

where M_i^{ε} is the moment estimated by the strain gauge of each finger. The torque about the individual finger, T_i, was found as:

$$T_i = P_i \cdot T_{mcp}$$

where, T_{mcp} is the recorded net MCP joint torque at each wrist and MCP joint posture as described in the previous Chapters 5 & 6. If any anomalous output was found at any finger in any combination of wrist and MCP posture, the output of all the fingers at that combination was discarded and not included in the data set. This procedure was repeated for each of the 35 non-paretic data sets and 8 BoNT data sets collected in the previous two chapters to produce a unique

MCP torque data set for fingers two through five throughout the recorded combinations of wrist and MCP postures.

7.2.1.2 Separation of the structures contributing to the total torque:

Analytical models were fit to each individual finger data set of net MCP joint torques processed above using the same methods described in the previous chapters (Knutson et al., 2000). The total torque, $T_t(\theta, \omega)$, of the analytical model developed for each subject is composed of the sum of two components.

$$T_t(\theta, \omega) = T_{sj}(\theta) + T_e(\theta, \omega) \tag{2}$$

$T_{sj}(\theta)$ consists of the torques contributed by the single-joint structures (intrinsic hand muscles, ligaments, joint capsules, etc.) that are a function of MCP joint posture only and $T_e(\theta, \omega)$ representing the extrinsic finger muscles, which is a function of both wrist and MCP posture (Knutson et al., 2000). These two components then describe the total torque about the MCP joint as a function of wrist and MCP posture and 14 constant parameters. To describe $T_t(\theta, \omega)$, $T_{sj}(\theta)$, and $T_e(\theta, \omega)$ of the non-paretic model and BoNT model the median value of each parameter was found over all the non-paretic data sets and the paretic BoNT data sets, respectively (Table 7.1).

7.2.1.3 Incorporation of the passive single joint torques.

The experimentally collected passive torque contributed by the single joint structures as described by $T_{sj}(\theta)$ found above for the non-paretic MCP joints two and three were added using torsional spring dampers (Binder-Markey and Murray, 2017). Using the same process, the passive single joint torque about the PIP an DIP passive joint torques taken from previous experimental work for the 2nd digit (Kamper et al., 2002) and then scaled for the third digit and incorporated

using torsional spring dampers (Binder-Markey and Murray, 2017). The single joint torques about the MCP, PIP, and DIP were not altered in the BoNT model because there were not substantial differences were found between the paretic and non-paretic hands in individuals who had received the BoNT injections in Chapter 6.

Table 7.1: Median parameters of the analytical fit of the total passive torques about the MCP joints of the index, middle, ring, and little fingers of the non-paretic hands and paretic hands the receive Botulinum Neurontoxin (BoNT). R^2 is the mean R^2 value across all the subjects

	Parameter	A1	k1	theta1	A2	k2	theta 2	A3	k3	B3	phi3	A4	k4	B4	phi4	R^2
Non-Paretic	Index	1.34	5.54E-02	-34.07	1.30	2.96E-01	71.38	1.00	2.94E-02	-1.14	-14.61	0.49	5.94E-02	-0.11	42.93	0.83
	Middle	1.33	6.28E-02	-26.97	1.75	1.26E-01	71.53	1.55	2.96E-02	-1.11	-4.60	0.86	3.77E-02	-0.50	39.83	0.87
	Ring	1.39	6.40E-02	-30.82	1.63	8.75E-02	71.30	1.18	3.00E-02	-1.27	-0.45	1.06	4.55E-02	-0.72	49.29	0.88
	Little	1.22	5.51E-02	-32.30	1.33	1.23E-01	75.18	0.90	3.11E-02	-0.60	-10.18	0.67	3.50E-02	-0.83	53.52	0.82
BoNT Paretic	Index	1.25	7.73E-02	-29.16	3.01	6.52E-02	67.35	2.19	2.77E-02	-1.89	-3.49	1.01	6.62E-02	-0.41	53.01	0.88
	Middle	1.62	6.36E-02	-26.20	3.69	7.44E-01	75.54	1.74	4.06E-02	-1.30	4.46	1.46	4.83E-02	-0.46	35.88	0.85
	Ring	1.24	8.30E-02	-31.53	2.68	8.56E-02	75.14	1.35	3.23E-02	-1.07	11.45	1.31	5.41E-02	-0.80	49.13	0.92
	Little	1.84	6.61E-02	-21.89	2.79	1.52E-01	72.16	0.80	3.22E-02	-1.35	-2.17	1.83	4.18E-02	-2.04	80.06	0.88

$T_t(\theta,\omega) = T_{sj}(\theta) + T_e(\theta,\omega)$ $T_{sj}(\theta) = A_1\left(e^{-k_1(\theta-\theta_1)} - 1\right) - A_2\left(e^{k_2(\theta-\theta_2)} - 1\right)$ $T_e(\theta,\omega) = A_3\left(e^{-k_3(\theta-\theta_3)} - 1\right) - A_4$ $\theta_j = B_j \cdot \omega + \emptyset_j$ $(j = 3,4)$

7.2.1.4 Incorporation of the passive extrinsic finger muscle torques.

The passive torques contributed by the extrinsic finger muscles about each finger were incorporated to complete the non-paretic model by matching the passive torques produced by the extrinsic finger muscles within the model to the experimental extrinsic finger passive torques, $T_e(\theta, \omega)$ (Table 7.1). Torque matching was accomplished by optimizing the tendon slack length of each extrinsic finger muscle within the model as previously described (Binder-Markey and Murray, 2017) (Table 7.2).

Table 7.2: Optimized Tendon Slack Lengths for the Non-paretic Model and Percent Change for all the fingers included in the model

		FDPI	FDSI	EDCI	EIP
Index	Initial tendon slack length	0.3044	0.2772	0.3486	0.1911
	New optimized tendon slack length	0.3097	0.2844	0.3505	0.1981
	Percent change	1.75%	2.58%	0.54%	3.68%
		FDPM	FDSM	EDCM	
Middle	Initial tendon slack length	0.3030	0.2950	0.3650	
	New optimized tendon slack length	0.2978	0.2929	0.3446	
	Percent change	-1.70%	-0.71%	-5.59%	
		FDPR	FDSR	EDCR	
Ring	Initial tendon slack length	0.2915	0.3280	0.3650	
	New optimized tendon slack length	0.2931	0.3072	0.3414	
	Percent change	0.55%	-6.33%	-6.45%	
		FDPL	FDSL	EDCL	EDM
Little	Initial tendon slack length	0.2819	0.3386	0.3350	0.3350
	New optimized tendon slack length	0.2988	0.3436	0.3530	0.3278
	Percent change	6.01%	1.49%	5.37%	-2.16%

The passive torques contributed by extrinsic flexors were modified to develop a model replicating the increased torques and increased muscle stiffness seen in individuals who received BoNT. The finger flexors were modified because only they were injected with BoNT across all subjects and the increases in $T_e(\theta, \omega)$ were only seen as the flexor muscles were stretched (Chapter 6). Using $T_e(\theta, \omega)$ found above for the BoNT data sets (Table 7.1), we employed the same optimization methods to match the passive torques of the extrinsic finger flexor muscles produced within the model to the experimental data; except, rather than the tendon slack length, the passive force length curve of the flexor muscles was optimized at each finger. To standardize the force length curve across the fingers flexors, the median parameters describing the optimized passive force length curve over the fingers was then used to describe the passive force length curve of the all flexor muscles within the BoNT model (Figure 7.1). The passive force length curve was chosen as the parameter to be optimized because current evidence indicates that increased muscle stiffness and force occurring after BoNT is the result of increased collagen in the extracellular matrix (ECM) (Minamoto et al., 2015; Thacker et al., 2012; Ward et al., 2017). Changes to the ECM would only affect the passive force length properties of the muscle and not the length parameters of the muscle or tendon.

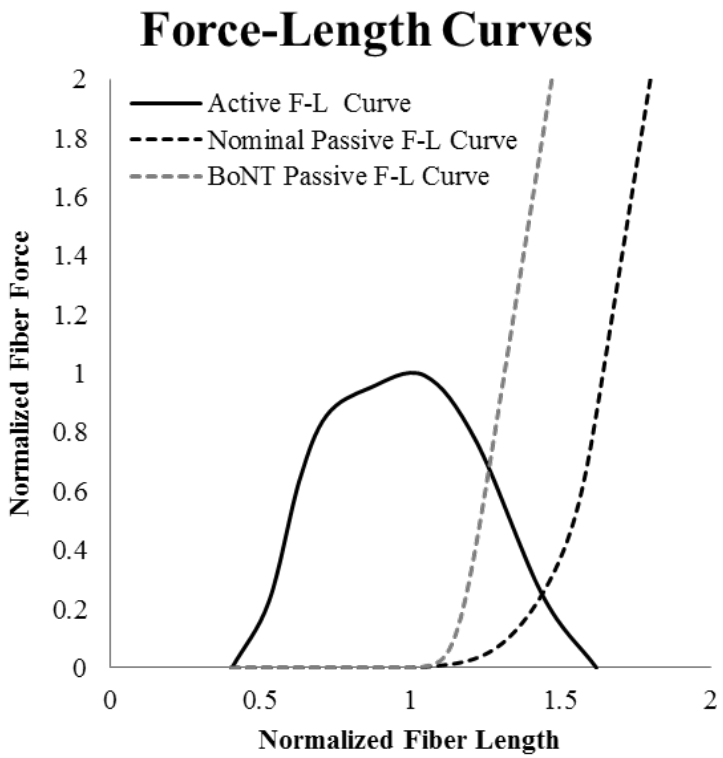

Figure 7.1: Normalized force length (F-L) curves for the active force (solid black line), nominal passive force (dashed black line), and Botulinum Neurotoxin (BoNT) optimized passive force curve (dashed grey line)

7.2.2 Dynamic Simulation Protocol

To assess how increases in torques about the fingers due to biomechanical adaptations versus involuntary muscle activity in individuals with chronic hemiparetic stroke would affect the ability to open the hand a simulation protocol was developed. The dynamic forward simulations were run to mimick altered passive states (using the BoNT model) and active states, described in sections 7.2.3 (summarized in Table 7.3). During the simulations the wrist constrained to 30° of extension, reflecting a wrist posture taken during normal daily reaching and grasping activities (de los Reyes-Guzman et al., 2010; Reghem et al., 2014; Ryu et al., 1991). The forward dynamic simulation process involves the input of muscle excitations and the resultant muscle forces that are

transformed into torques about the joints of the system which then drive the motion of those joints through the solving of the differential equations that defining the dynamics of the system. The input muscle excitations for the simulation were defined over a four second interval using a simple step input function, where the extrinsic finger flexors were activated from one to two seconds and the extrinsic finger extensors activated from two to four seconds (Figure 7.2). To simulate varying levels of weakness the input excitations to the flexor and extensor muscles were set to 10%, 25%, 50%, 75% and 100% of the maximum excitations corresponding to varying levels of impairment from severe to non-paretic (Kamper et al., 2006; Kamper et al., 2003; Miller and Dewald, 2012).

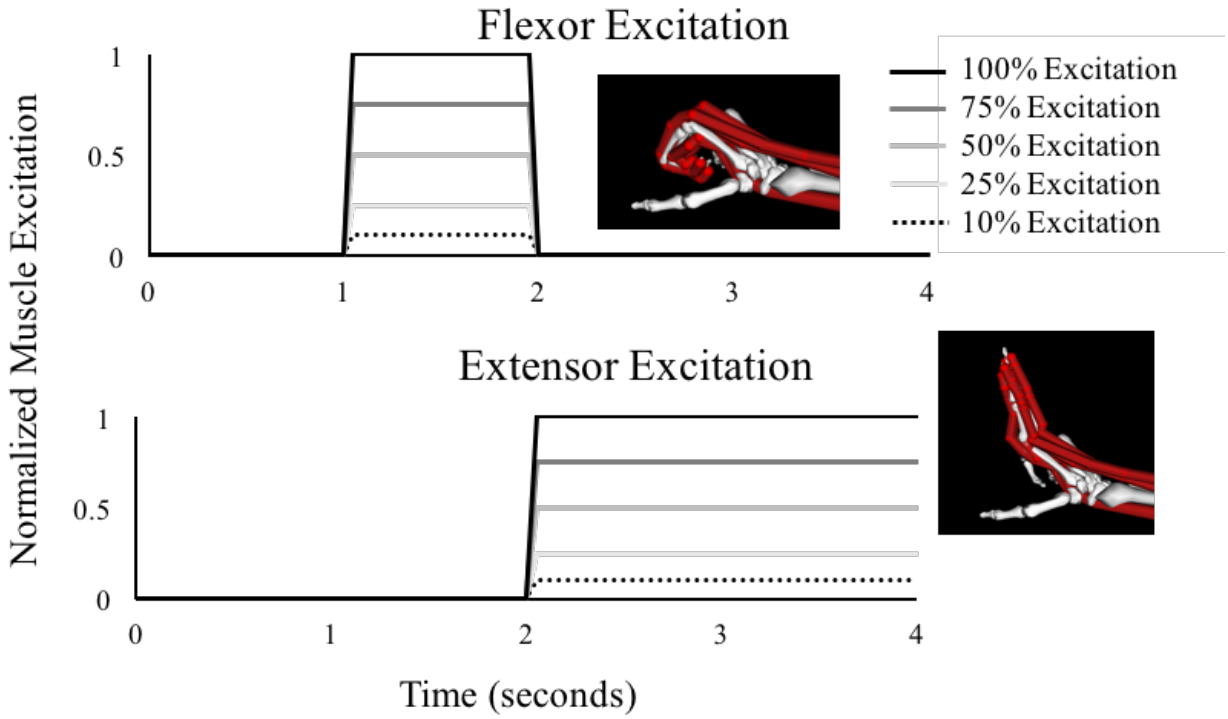

Figure 7.2: Plots of the excitation inputs for the forward dynamic simulations at 10%, 25%, 50%, 75%, and 100% excitations. Image inserts represent the posture at the equilibrium posture after activation of the flexors (top middle) and extensors (bottom right) on the nominal non-paretic model with 100% activation.

7.2.3 Simulations of involuntary muscle activity

7.2.3.1 Muscle hypertonicity at rest

To replicate the increased motoneuron excitability and increased persistent motor unit firing at rest, hypertonicity of the muscles was incorporated into the model by setting the minimum activations for the finger flexors to 0.05 within the non-paretic model (Table 7.3). This approximates the muscle activation of the flexors in moderate to severe chronic stroke survivors as their arm is fully supported (McPherson et al., 2017).

7.2.3.2 Muscle hypertonicity due to a loss of independent joint control

Mimicking the loss of independent joint control and flexion synergy as an individual lifts their arm and the involuntarily flexion at the elbow, wrist, and fingers, the finger flexors were set to be continuously active by setting the minimum activation to 0.35 in the non-paretic model (Table 7.3). 35% was chosen because it has been previously reported that as individuals with severe hand impairments lift their arm, their wrist and finger flexors are activated to 35% of their max activation (Miller and Dewald, 2012).

7.2.3.3 Combining deficits

Involuntary driven muscle activation was combined with the BoNT models to determine the combined effects of these impairments. This was accomplished in the same manner as above except the minimum activations were set in the paretic BoNT model. Simulations including all three of the sources of flexor torque increases was developed by adding the two sources of involuntary activity (rest and loss of independent joint control) and setting the minimum activation of the finger flexors to .40 in the BoNT model (Table 7.3).

Table 7.3: Summary of the Simulations with the model and level of involuntary activation.

Simulations	Model		Minimum activation of finger flexors set to:		
	Non-paretic	BoNT	5%	35%	40%
Non-paretic	X				
BoNT		X			
Hypertonicity	X		X		
LIJC	X			X	
BoNT + Hypertonicity		X	X		
BoNT + LIJC		X		X	
BoNT + LIJC + Hypertonicity		X			X

The equilibrium positions of the MCP, PIP, and DIP joints after the extensor muscles were activated and the extension phase was complete were recorded and compared across the models to analyze to how the various sources of increased flexor torques affect the ability to open the hand. The fingers were determined to be extended if the MCP joint was extended past zero degrees and if the PIP and DIP joints postures were five degrees or less.

7.3 Results

7.3.1 Effects of Increased Torques Following BoNT

The increased torques at the index and middle finger after BoNT injections required high (75% or 100%, respectively) levels of activation to achieve full finger extension (Figure 7.3). At low activations of 10% and 25%, mimicking severe and moderate weakness, there was limited extension of both fingers with the middle finger having greater limitations. With increasing activation, extension was achieved but was still limited as compared to the extension postures of the non-paretic model (Table 7.4).

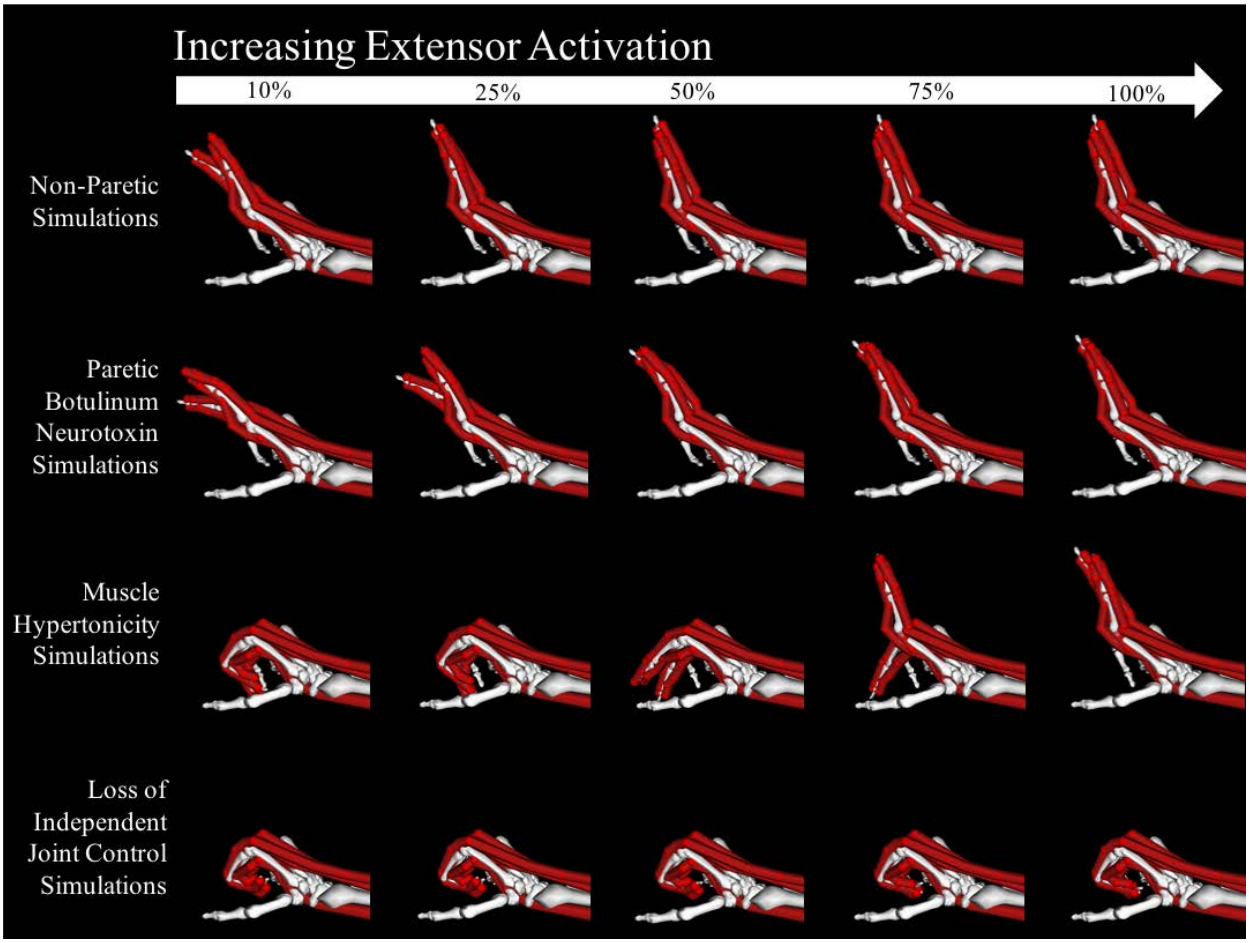

Figure 7.3: Representation of the equilibrium posture at the end of the extension phase of the forward dynamic simulations of the models summarized in Table 7.3 with increasing activation levels (10% to 100% activation) mimicking the weakness in severely impaired to the full strength of non-impaired individuals. Weakness alone does not eliminate the ability to extend the fingers in the non-paretic simulations. Within simulations of increased muscle stiffness following BoNT and muscle hypertonicity decrease the ability to extend the fingers in the weaker simulations however with increased muscle activation, finger extension was achievable. This was not the case when simulating involuntary muscle activity as a result of the loss of independent joint control in which the fingers were unable to extend even with full activation.

7.3.2 Effects of Involuntary Muscle activity

The greatest decreases of finger extension occurred when involuntary drive due to mimicking LIJC and the flexion synergy (35% activation of the extrinsic finger flexors) was incorporated into the models. The activations mimicking the involuntary activity from the LIJC resulted in the

inability to extend either finger even with 100% activation (Figure 7.3). Involuntary activity mimicking muscle hypertonicity at rest (5% activation of the extrinsic flexors) was also a limiting factor in the ability to open the hand though not to the degree of involuntary activity from LIJC (Figure 7.3). The resting hypertonicity limited the extension of the index finger at the 10%, 25%, and 50% activation levels of the extrinsic extensor muscles; the middle finger remained flexed with even 75% activation (Table 7.4). The ability to extend the fingers was only possible at the 75% and 100% activation levels.

7.3.3 Combined effect of Involuntary Activity and Increase Torques Following BoNT

In simulations that combined the increased stiffness following BoNT with involuntary activity from LIJC and both LIJC and hypertonicity, the fingers were unable to extend even with full activation and the extension postures did not vary from the simulations including LIJC alone (Table 7.4). In the simulations combining the increased stiffness following BoNT with hypertonicity, with extensor activations of 10%, 20%, and 50% were the equilibrium postures did not vary from the simulations with hypertonicity alone (Table 7.4). With extensor activations of 100% the extension postures closely matched the postures from the only BoNT model though with a slightly more flexed MCP posture (Table 7.4).

7.3.4 Effects of Weakness Only

At both the index finger and middle fingers decreased activation, mimicking weakness, had minimal impact on the ability to open the fingers. At all activation levels the fingers achieved extension, though with 10% activation the middle finger only extended to neutral (Figure 7.3).

Table 7.4: Summary of extension equilibrium positions of the forward dynamic simulations

		Excitation Input Level														
		10%			25%			50%			75%			100%		
Simulation		MCP	PIP	DIP	MCP	PIP	DIP	MCP	PIP	DIP	MCP	PIP	DIP	MCP	PIP	DIP
Non-Paretic	Index	-37.1	3.5	1.5	-48.6	1.4	1.4	-50.2	1.2	1.2	-50.3	1.1	1.2	-50.3	1.0	1.1
	Middle	-2.5	5.7	1.4	-31.6	1.6	1.3	-39.2	1.3	1.2	-42.0	1.1	1.1	-43.5	1.1	1.1
BoNT	Index	-16.3	22.9	1.5	-38.4	10.2	1.4	-41.3	13.0	1.3	-42.8	1.5	1.2	-45.7	1.3	1.2
	Middle	25.0	3.4	1.4	7.5	5.2	1.3	-26.5	25.6	1.2	-29.8	19.0	1.2	-29.2	8.5	1.1
Hypertonicity	Index	83.3	93.2	1.5	82.2	82.8	1.4	76.3	1.2	1.2	-50.2	1.2	1.2	-50.3	1.1	1.1
	Middle	90.3	68.3	1.5	90.3	55.0	1.4	90.2	1.4	1.2	86.8	1.2	1.1	-28.6	4.7	1.1
LIJC	Index	89.2	105.4	66.7	89.1	105.0	61.7	89.1	104.4	47.8	89.3	103.6	1.3	89.0	102.9	1.2
	Middle	90.5	102.3	69.3	90.5	102.0	67.4	90.5	101.3	63.1	90.5	100.4	56.5	90.5	99.4	39.0
BoNT + Hypertonicity	Index	83.3	93.2	1.5	82.2	82.8	1.4	76.3	1.2	1.2	-40.2	1.8	1.3	-43.8	1.4	1.2
	Middle	90.3	68.3	1.5	90.3	55.0	1.4	90.2	1.4	1.2	86.8	1.2	1.1	-31.4	22.7	1.1
BoNT + LIJC	Index	89.2	105.4	66.7	89.1	105.0	61.7	89.1	104.4	47.8	89.3	103.6	1.3	89.0	102.9	1.2
	Middle	90.5	102.3	69.3	90.5	102.0	67.4	90.5	101.3	63.1	90.5	100.4	56.5	90.5	99.4	39.0
BoNT + LIJC + Hypertonicity	Index	89.6	105.7	68.7	89.5	105.3	64.2	89.5	104.7	52.9	89.9	104.0	1.4	89.6	103.3	1.2
	Middle	90.5	102.6	72.0	90.5	102.3	70.2	90.5	101.8	66.5	90.5	101.1	61.3	90.5	99.9	88.6

7.4 Discussion

In this study, we used computational musculoskeletal models to study how increased flexion torques resulting from either increased muscle stiffness following BoNT injections or involuntary flexor muscle activity impairs the ability to open the hand. Based on the work in the previous chapter demonstrating that individuals who received BoNT injections had increased passive torques at the fingers from increased muscle stiffness, we hypothesized that BoNT would have a significant effect on decreasing the ability to open the hand.

7.4.1 Effect of increased flexion torques on the ability to open the fingers

Our results demonstrated that involuntary flexor muscle activity was a much greater impediment to finger and hand opening than increases in torques due to increased muscle stiffness following BoNT injections. However, the increased muscle stiffness in individuals who received BoNT injections did produce reductions in the range of motion and the ability to extend the fingers throughout all activation levels as compared to the non-paretic model (Figure 7.3). The extension limitations due to the increased muscle stiffness of individuals who received BoNT were particularly pronounced in simulations mimicking individuals with severely and moderately paretic hand function (10% and 25% extensor activity, respectively). Whereas, with involuntary activation from the LIJC, even with full strength (100% extensor activation), finger extension was not possible and the fingers remained fully flexed (Figure 7.3). Additionally, hypertonicity of the muscle with just 5% activation eliminated the ability to extend the fingers in weakened models and required at least 75% strength to extend the index finger and full strength to extend the middle finger.

7.4.2 Sources of the increased flexion torques and clinical implications

Because of the profound effects that the involuntary drive of the flexors has on hand opening, rehabilitation interventions should focus on impacting the underlying physiologic sources of this impairment to have the greatest likelihood of success. Current understanding is that the involuntary drive to the flexor muscles following a stroke is due to a loss of the direct descending corticospinal pathways resulting in an increased reliance on indirect corticoreticulospinal pathways (Baker, 2011; Owen et al., 2017; Riddle and Baker, 2010; Riddle et al., 2009). More specifically, descending portions of the reticulospinal pathways have both motor (ionotropic) and neuromodulatory (metabotropic) components (Kuypers, 1964) that contribute to LIJC and muscle hyperactivity. The loss of independent joint control is the result of an increased reliance on the motor component of the polysynaptic corticoreticulospinal pathway (Baker, 2011; Riddle and Baker, 2010; Riddle et al., 2009). The branching of the ionotropic component of the reticulospinal projections in the spinal cord contributes to the involuntary activation of the flexor muscles of the fingers, wrist, and elbow when the proximal shoulder joint is driven to lift the arm (Brunnstrom, 1970; Dewald et al., 1995; Dewald et al., 2001; Miller and Dewald, 2012; Sukal et al., 2007). In contrast, the resting hypertonicity is likely the result of an upregulation of the neuromodulatory (metabotropic) component of the recticulospinal pathway. This upregulation of the reticular formation increases monoaminergic signaling to the spinal cord, which increases the overall excitability of the spinal motoneurons (Fedirchuk and Dai, 2004; Heckmann et al., 2005; Johnson and Heckman, 2014). This increased excitability results in greater persistent inward currents (PICs) in motor neurons (Heckman et al., 2008; McPherson et al., 2008; McPherson et al., 2017) and hypertonicity and spasticity within the hand muscles.

To improve hand opening and function in the chronic hemipalegic stroke population, rehabilitation and pharmacological interventions should focus on decreasing the reliance on and upregulation of recticulosinal pathways. Rehabilitation training methods that include progressive loading protocols have provided preliminary evidence that even chronic hemiparetic individuals are able to be trained to break out of the flexion synergy and gain greater independent joint control (Ellis et al., 2016; Ellis et al., 2009) of their arm and hands. In addition, a recent study has shown that device-assisted task-specific interventions stimulate cortical reorganization, potentially decreasing the reliance on the cortioreticulospinal pathways (Wilkins et al., 2017).

If these rehabilitation protocols were to progress to a point where independent joint control was regained, the effects of muscle hyperactivity and resting hypertonicity may still prevent these individuals from opening their hand. The current preferred treatment for muscle hyperactivity is BoNT because of its focal application, local effects, and relative long lasting effects (Ozcakir and Sivrioglu, 2007). However, as we have demonstrated, the long-term effects of BoNT may increase muscle stiffness and limit the ability to extend the finger that is most pronounced in those individuals with severe and moderate impairment who would most greatly benefit from any reduction in resistance. BoNT's local and relative long lasting effect stem from its action at the neuromuscular junctions, resulting in paralysis and denervation of the muscle. These actions may also be the cause of the increases in passive muscle stiffness for increased collagen content has been demonstrated in animal models of paralyzed denervated muscles (Faturi et al., 2016; Liu et al., 2016; Nikolaou et al., 2014; Russo et al., 2008) and following BoNT injections (Minamoto et al., 2015; Thacker et al., 2012; Ward et al., 2017).

If we are to effectively treat the muscle hyperactivity, it would be advantageous to target the source of this impairment, the upregulation of the monoaminergic output of the reticular formation to the spinal motoneurons. There are pharmaceutical options currently available that act at the spinal cord (baclofen, diazepam) or brainstem (tizanidine) to reduce motoneuron hyperactivity (Barnes and Johnson, 2008; Gallichio, 2004). However many individuals do not tolerate these drugs well because they act systemically and lead to lethargy and systemic weakness (Barnes and Johnson, 2008; Gallichio, 2004; Ozcakir and Sivrioglu, 2007). If new pharmaceutical treatments can be developed that effectively reduce the involuntary muscle activity without the systemic effects of the current pharmaceuticals, this could eliminate the need for BoNT following a chronic hemiparetic stroke and would have the potential to allow individuals to gain greater hand function.

7.4.3 Limitations

In this study we purposely did not include the hyperactive velocity dependent stretch reflex, spasticity, within our models because our focus was primarily on the overall ability to open the hand and not on the speed of the movement. If speed was an additional factor, then the inclusion of spasticity would be required. However, the hyper-active stretch reflex response that is elicited during reaching tasks has been shown to be overshadowed by the involuntary muscle activity driven by LIJC (Ellis et al., 2017). Thus, adding including spasticity into our models would not have changed the conclusions of this study that involuntary activity from LIJC is the dominating factor preventing the ability to extend the fingers following stroke and that effects of BoNT alone can limit finger extension in weak individuals.

7.5 Conclusion

This study shows that the greatest impediment to opening the hand following chronic hemiparetic stroke is the result of involuntary muscle activity of the finger flexor muscles driven by the LIJC. In addition, we showed that the effects of long-term increased muscle stiffness following BoNT can limit the ability to extend the fingers but the most pronounced effects are in the moderately and severely impaired populations. Our results suggest that rehabilitation and pharmaceutical interventions in individuals following a stroke should focus on the reducing the involuntary flexor muscle activity to regain the ability to open their hands. To further advance arm and hand function following a stroke, more research into developing rehabilitation protocols reducing the expression of the flexion synergy using physical and pharmaceutical means that decrease motoneuron excitability are needed. This should be accomplished without causing long-term increased muscle stiffness or systemic lethargy and weakness.

8 CONCLUSION

The goal of this dissertation was to gain a greater understanding of how hand function is impaired post-stroke by specifically concentrating on the effects of altered passive joint biomechanics separate from the impacts of the neurological impairments. Through both computer simulations and experimental methods this research has given insights into how the different biomechanical changes to the muscles and structures of the hand impact hand opening and how the musculoskeletal system adapts differently after a stroke depending on whether an individual has been treated with BoNT or not. This work has contributed substantially to our understanding of hand impairments following stroke, indicating that to most effectively assist these individuals and gain as much hand function following a stroke, rehabilitation interventions should focus on reducing the neurologic impairments However, biomechanical changes increasing passive muscle stiffness do exist but only following the use of BoNT which can limit the ability to extend the fingers in severely and moderately impaired individuals.

To begin to understand how alterations of the passive biomechanics of the hand impairs function following stroke, we developed a computational musculoskeletal model that accurately incorporates the biomechanical structures of the hand. The complexity of the system required the development of a novel method to incorporate experimentally collected multi-joint dependent passive torques of extrinsic hand muscles into model. This resulted in a dynamic biomechanical model demonstrating coordinated passive movements between the wrist and fingers, mimicking a common phenomenon described as tenodesis. This model then lead to simulations investigating how alterations to the biomechanical structures of the hand are associated with the development and progression of the claw finger deformity often seen in populations with paralyzed or weakened

intrinsic finger muscles, i.e. stroke, spinal cord injury, and ulnar nerve palsy. Through these simulations we found that the deformity and coordinated finger extension was most sensitive to shortening of extrinsic finger flexors as compared to increased joint laxity or decreased mechanical advantage of the extensor mechanism. Indicating that in both the acute and chronic stages of intrinsic finger paralysis maintaining the length of the extrinsic finger flexors should be an area of focus of rehabilitation to prevent or reverse the claw finger deformity.

Equipped with the methods to incorporate and simulate biomechanical changes occurring within the hand following chronic hemiparetic stroke, we needed experimental data to understand how these changes occur within the paretic hand. To collect this data the *in vivo* passive elastic torques in the hand of the chronic hemiparetic stroke population were collected using an innovative experimental protocol that eliminated any muscle activity. Our findings, contrary to previous findings, indicate that after a stroke there are not substantial increases of passive torques about either the wrist or the fingers. Signifying that the increases in stiffness observed clinically and in previous studies are potentially a result of neural hyperactivity related to an increased monoaminergic neuromodulatory drive mediated via the reticulospinal tract (McPherson et al., 2008; McPherson et al., 2017) and not from mechanical changes of the muscles or other soft tissue structures of the hand.

However, the preferred treatment for muscle hyperactivity, the use of BoNT, is problematic for we found increased muscle stiffness in muscles that received BoNT injections resulting in substantially greater torques about the wrist and finger. This long-term consequence that lasts for years and potentially for the life time of these individuals has the opposite effect of the initial desired goal of the BoNT, which is to reduce the passive resistance of the hyperactive muscles.

The origins of these long-term increases are postulated to be due to increased collagen content occurring within the ECM of the muscles following the BoNT injections (Minamoto et al., 2015; Ward et al., 2017) though this has yet to be confirmed in humans.

Using computational biomechanical musculoskeletal models we found that these increases following BoNT can limit the ability to extend the fingers but is most pronounced and detrimental in the severely and moderately impaired populations. However, the greatest impairment to the ability to open the hand following chronic hemiparetic stroke is the result of involuntary muscle activity of the finger flexor muscles driven by the flexion synergy resulting in a loss of independent joint control. The overall results of this work indicate that hand function within post stroke is primarily a result of the neurological deficits of resulting of weakness, a loss of voluntary control of the hand, and muscle hyperactivity but in individuals who have received BoNT the increased muscle stiffness can limit the ability to extend the fingers.

8.1 Contributions

The main contributions of this work are as follows:

- A novel method to enable the incorporation of experimentally measured, length-dependent passive torques produced by muscles that span multiple joints in a biomechanical model.
- Claw finger deformity development and progression after intrinsic muscle paralysis is most sensitive to shortening of extrinsic finger flexors as compared to other biomechanical changes occurring within the hand.

- In the chronic hemiparetic stroke population who have not received BoNT there are not substantial increases of passive elastic torques about either the wrist or the fingers across impairment levels.
- BoNT likely has long-term consequences that increase muscle stiffness, for individuals with chronic hemiparetic stroke who have received BoNT injections have substantial greater passive torques about their wrist and MCP finger joints.
- The long-term increases in muscle stiffness following BoNT only limits the ability to extend the fingers in the severely and moderately impaired populations, however the greatest impairments to hand opening following chronic hemiparetic stroke is the result of involuntary muscle activity of the finger flexor muscles driven by the flexion synergy resulting in LIJC.

8.2 Future Directions

The findings of this work suggest several lines of future work. These lines can be categorized into model development, mechanistic studies, and interventional studies.

The first line of future work is to further develop and improve hand models. The addition of the intrinsic muscles and the complex extensor mechanism to the models developed here would be important step for the exploration of grip strength and endpoint force production of fingers in both the healthy and impaired populations. Additionally, these models could be developed to assist in the improvement of surgical interventions, design of assistive devices, and rehabilitation interventions protocols for a variety of hand impairments.

The second line of future work warranted is exploring the mechanistic changes that are occurring within the muscles following stroke. Our findings in Chapter 6 that the passive torques about the wrist and fingers only increased substantially in individuals who had received BoNT injections indicates that additional research is needed to further explore the mechanisms by which BoNT produces long-term increased muscle stiffness. With the understanding of the mechanisms improved rehabilitation interventions can be developed to avoid this process. Additionally, we did not find increases of torques in the paretic hand of chronic stroke survivors who did not receive BoNT, but further investigation into the interaction of atrophy and tissue level muscle and tendon changes is warranted to further understand how the neurological deficits affect the muscle tendon unit.

The last line of future work is developing studies to improve current rehabilitation interventions. First and foremost because of the detrimental effects BoNT can have in the impaired population other innovative approaches that avoid the use of BoNT need to be explored. These new approaches should include the development of more selective drugs that reduce or inhibit muscle hyperactivity without the side-effects of long-term increases in passive stiffness or systemic lethargy and weakness that current drugs produce. Additionally, to further advance arm and hand function following a stroke, further rehabilitation techniques focusing on disentangling the flexion synergy should be further explored such as progressive loading or assistive device training protocols, that demonstrate preliminary evidence in enabling individuals to break out of these synergies thus increasing independent joint control (Ellis et al., 2016; Ellis et al., 2009) and re-organizing cortical signaling by using remaining resources from the affected hemisphere (Wilkins et al., 2017).

REFERENCES

Adamczyk, M.M., Crago, P.E., 2000. Simulated feedforward neural network coordination of hand grasp and wrist angle in a neuroprosthesis. Ieee T Rehabil Eng 8, 297-304.

Anderson, G.A., 2006. The surgical management of deformities of the hand in leprosy. J Bone Joint Surg Br 88, 290-294.

Arnold, E.M., Ward, S.R., Lieber, R.L., Delp, S.L., 2010. A model of the lower limb for analysis of human movement. Ann Biomed Eng 38, 269-279.

Babikian, S., Valero-Cuevas, F.J., Kanso, E., 2016. Slow Movements of Bio-Inspired Limbs. J Nonlinear Sci 26, 1293-1309.

Bain, G.I., Polites, N., Higgs, B.G., Heptinstall, R.J., McGrath, A.M., 2015. The functional range of motion of the finger joints. The Journal of hand surgery, European volume 40, 406-411.

Baker, S.N., 2011. The primate reticulospinal tract, hand function and functional recovery. J Physiol 589, 5603-5612.

Barclay-Goddard, R.E., Stevenson, T.J., Poluha, W., Thalman, L., 2011. Mental practice for treating upper extremity deficits in individuals with hemiparesis after stroke. Cochrane Database Syst Rev, CD005950.

Barnes, M.P., Johnson, G.R., 2008. Upper motor neurone syndrome and spasticity : clinical management and neurophysiology, 2nd ed. Cambridge University Press, Cambridge ; New York.

Benjamin, E.J., Blaha, M.J., Chiuve, S.E., Cushman, M., Das, S.R., Deo, R., de Ferranti, S.D., Floyd, J., Fornage, M., Gillespie, C., Isasi, C.R., Jimenez, M.C., Jordan, L.C., Judd, S.E., Lackland, D., Lichtman, J.H., Lisabeth, L., Liu, S., Longenecker, C.T., Mackey, R.H., Matsushita, K., Mozaffarian, D., Mussolino, M.E., Nasir, K., Neumar, R.W., Palaniappan, L., Pandey, D.K., Thiagarajan, R.R., Reeves, M.J., Ritchey, M., Rodriguez, C.J., Roth, G.A., Rosamond, W.D., Sasson, C., Towfighi, A., Tsao, C.W., Turner, M.B., Virani, S.S., Voeks, J.H., Willey, J.Z., Wilkins, J.T., Wu, J.H., Alger, H.M., Wong, S.S., Muntner, P., American Heart Association Statistics, C., Stroke Statistics, S., 2017. Heart Disease and Stroke Statistics-2017 Update: A Report From the American Heart Association. Circulation 135, e146-e603.

Bhadane, M.Y., Gao, F., Francisco, G.E., Zhou, P., Li, S., 2015. Correlation of Resting Elbow Angle with Spasticity in Chronic Stroke Survivors. Frontiers in neurology 6, 183.

Bhardwaj, P., Nayak, S.S., Kiswar, A.M., Sabapathy, S.R., 2011. Effect of static wrist position on grip strength. Indian J Plast Surg 44, 55-58.

Binder-Markey, B.I., Murray, W.M., 2017. Incorporating the length-dependent passive-force generating muscle properties of the extrinsic finger muscles into a wrist and finger biomechanical musculoskeletal model. J Biomech 61, 250-257.

Blana, D., Chadwick, E., van den Bogert, A.J., Murray, W.M., 2016. Real-time simulation of hand motion for prosthesis control. Comput Method Biomec 20, In Press.

Brand, P.W., 1958. Paralytic claw hand; with special reference to paralysis in leprosy and treatment by the sublimis transfer of Stiles and Bunnell. J Bone Joint Surg Br 40-B, 618-632.

Brand, P.W., Hollister, A., 1993. Clinical mechanics of the hand, 2nd ed. Mosby Year Book, St. Louis.

Braun, S., Kleynen, M., van Heel, T., Kruithof, N., Wade, D., Beurskens, A., 2013. The effects of mental practice in neurological rehabilitation; a systematic review and meta-analysis. Front Hum Neurosci 7, 390.

Broeks, J.G., Lankhorst, G.J., Rumping, K., Prevo, A.J., 1999. The long-term outcome of arm function after stroke: results of a follow-up study. Disabil Rehabil 21, 357-364.

Brook, N., Mizrahi, J., Shoham, M., Dayan, J., 1995. A biomechanical model of index finger dynamics. Med Eng Phys 17, 54-63.

Brunnstrom, S., 1970. Movement therapy in hemiplegia: a neurophysiological approach, 1st ed. Medical Dept., New York,.

Buffi, J.H., Werner, K., Kepple, T., Murray, W.M., 2015. Computing Muscle, Ligament, and Osseous Contributions to the Elbow Varus Moment During Baseball Pitching. Annals of biomedical engineering 43, 404-415.

Buford, W.L., Jr., Koh, S., Andersen, C.R., Viegas, S.F., 2005. Analysis of intrinsic-extrinsic muscle function through interactive 3-dimensional kinematic simulation and cadaver studies. J Hand Surg Am 30, 1267-1275.

Bunnell, S., 1942. Surgery of the intrinsic muscles of the hand other than those producing opposition of the thumb. J Bone Joint Surg 24, 1-31.

Chan, R.K., 2002. Splinting for peripheral nerve injury in upper limb. Hand Surg 7, 251-259.

Charles, S.K., Hogan, N., 2012. Stiffness, not inertial coupling, determines path curvature of wrist motions. J Neurophysiol 107, 1230-1240.

Cheng, W., Cornwall, R., Crouch, D.L., Li, Z., Saul, K.R., 2015. Contributions of muscle imbalance and impaired growth to postural and osseous shoulder deformity following brachial plexus birth palsy: a computational simulation analysis. J Hand Surg Am 40, 1170-1176.

Colditz, J., 2002. Splinting the Hand with a Peripheral-Nerve Injury, in: Mackin, Callahan, Osterman, Skirven, Schneider, Hunter (Eds.), Rehabilitation of the Hand and Upper Extremity, 5th ed. Mosby, pp. 622-634.

Corbetta, D., Sirtori, V., Moja, L., Gatti, R., 2010. Constraint-induced movement therapy in stroke patients: systematic review and meta-analysis. Eur J Phys Rehabil Med 46, 537-544.

Crouch, D.L., Li, Z., Barnwell, J.C., Plate, J.F., Daly, M., Saul, K.R., 2011. Computer simulation of nerve transfer strategies for restoring shoulder function after adult C5 and C6 root avulsion injuries. J Hand Surg Am 36, 1644-1651.

Crouch, D.L., Plate, J.F., Li, Z., Saul, K.R., 2013. Biomechanical contributions of posterior deltoid and teres minor in the context of axillary nerve injury: a computational study. J Hand Surg Am 38, 241-249.

Crouch, D.L., Plate, J.F., Li, Z., Saul, K.R., 2014. Computational sensitivity analysis to identify muscles that can mechanically contribute to shoulder deformity following brachial plexus birth palsy. J Hand Surg Am 39, 303-311.

Darling, W.G., Cole, K.J., 1990. Muscle activation patterns and kinetics of human index finger movements. J Neurophysiol 63, 1098-1108.

de Gooijer-van de Groep, K.L., de Vlugt, E., van der Krogt, H.J., Helgadottir, A., Arendzen, J.H., Meskers, C.G., de Groot, J.H., 2016. Estimation of tissue stiffness, reflex activity, optimal muscle length and slack length in stroke patients using an electromyography driven antagonistic wrist model. Clin Biomech (Bristol, Avon) 35, 93-101.

de los Reyes-Guzman, A., Gil-Agudo, A., Penasco-Martin, B., Solis-Mozos, M., del Ama-Espinosa, A., Perez-Rizo, E., 2010. Kinematic analysis of the daily activity of drinking from a glass in a population with cervical spinal cord injury. J Neuroeng Rehabil 7, 41.

Delp, S.L., Anderson, F.C., Arnold, A.S., Loan, P., Habib, A., John, C.T., Guendelman, E., Thelen, D.G., 2007. OpenSim: open-source software to create and analyze dynamic simulations of movement. IEEE Trans Biomed Eng 54, 1940-1950.

Delp, S.L., Loan, J.P., Hoy, M.G., Zajac, F.E., Topp, E.L., Rosen, J.M., 1990. An interactive graphics-based model of the lower extremity to study orthopaedic surgical procedures. IEEE Trans Biomed Eng 37, 757-767.

DeMers, M., 2015. OpenSim::FunctionBasedBushingForce Class Reference.

Dewald, J.P., Pope, P.S., Given, J.D., Buchanan, T.S., Rymer, W.Z., 1995. Abnormal muscle coactivation patterns during isometric torque generation at the elbow and shoulder in hemiparetic subjects. Brain 118 (Pt 2), 495-510.

Dewald, J.P., Sheshadri, V., Dawson, M.L., Beer, R.F., 2001. Upper-limb discoordination in hemiparetic stroke: implications for neurorehabilitation. Top Stroke Rehabil 8, 1-12.

Dolly, J.O., Aoki, K.R., 2006. The structure and mode of action of different botulinum toxins. Eur J Neurol 13 Suppl 4, 1-9.

Ebenezer, M., Rao, K., Partheebarajan, S., 2012. Factors affecting functional outcome of surgical correction of claw hand in leprosy. Indian J Lepr 84, 259-264.

Eby, S., Zhao, H., Song, P., Vareberg, B.J., Kinnick, R., Greenleaf, J.F., An, K.N., Chen, S., Brown, A.W., 2016. Quantitative Evaluation of Passive Muscle Stiffness in Chronic Stroke. Am J Phys Med Rehabil 95, 899-910.

Ellis, M.D., Carmona, C., Drogos, J., Traxel, S., Dewald, J.P., 2016. Progressive abduction loading therapy targeting flexion synergy to regain reaching function in chronic stroke: Preliminary results from an RCT. Conf Proc IEEE Eng Med Biol Soc 2016, 5837-5840.

Ellis, M.D., Schut, I., Dewald, J.P.A., 2017. Flexion synergy overshadows flexor spasticity during reaching in chronic moderate to severe hemiparetic stroke. Clin Neurophysiol 128, 1308-1314.

Ellis, M.D., Sukal-Moulton, T., Dewald, J.P., 2009. Progressive shoulder abduction loading is a crucial element of arm rehabilitation in chronic stroke. Neurorehabil Neural Repair 23, 862-869.

Esteki, A., Mansour, J.M., 1997. A dynamic model of the hand with application in functional neuromuscular stimulation. Ann Biomed Eng 25, 440-451.

Faturi, F.M., Franco, R.C., Gigo-Benato, D., Turi, A.C., Silva-Couto, M.A., Messa, S.P., Russo, T.L., 2016. Intermittent stretching induces fibrosis in denervated rat muscle. Muscle Nerve 53, 118-126.

Fedirchuk, B., Dai, Y., 2004. Monoamines increase the excitability of spinal neurones in the neonatal rat by hyperpolarizing the threshold for action potential production. J Physiol 557, 355-361.

Fowler, N.K., Nicol, A.C., Condon, B., Hadley, D., 2001. Method of determination of three dimensional index finger moment arms and tendon lines of action using high resolution MRI scans. J Biomech 34, 791-797.

Fraigne, J.J., Torontali, Z.A., Snow, M.B., Peever, J.H., 2015. REM Sleep at its Core - Circuits, Neurotransmitters, and Pathophysiology. Frontiers in neurology 6, 123.

Freire, B., Dias, C.P., Goulart, N.B., de Castro, C.D., Becker, J., Gomes, I., Vaz, M.A., 2017. Achilles tendon morphology, plantar flexors torque and passive ankle stiffness in spastic hemiparetic stroke survivors. Clin Biomech (Bristol, Avon) 41, 72-76.

French, B., Leathley, M., Sutton, C., McAdam, J., Thomas, L., Forster, A., Langhorne, P., Price, C., Walker, A., Watkins, C., 2008. A systematic review of repetitive functional task practice with modelling of resource use, costs and effectiveness. Health Technol Assess 12, iii, ix-x, 1-117.

French, B., Thomas, L., Leathley, M., Sutton, C., McAdam, J., Forster, A., Langhorne, P., Price, C., Walker, A., Watkins, C., 2010. Does repetitive task training improve functional activity after stroke? A Cochrane systematic review and meta-analysis. J Rehabil Med 42, 9-14.

French, B., Thomas, L.H., Leathley, M.J., Sutton, C.J., McAdam, J., Forster, A., Langhorne, P., Price, C.I., Walker, A., Watkins, C.L., 2007. Repetitive task training for improving functional ability after stroke. Cochrane Database Syst Rev, CD006073.

Friden, J., Lieber, R.L., 2003. Spastic muscle cells are shorter and stiffer than normal cells. Muscle Nerve 27, 157-164.

Gallichio, J.E., 2004. Pharmacologic management of spasticity following stroke. Phys Ther 84, 973-981.

Gao, F., Grant, T.H., Roth, E.J., Zhang, L.Q., 2009. Changes in passive mechanical properties of the gastrocnemius muscle at the muscle fascicle and joint levels in stroke survivors. Arch Phys Med Rehabil 90, 819-826.

Gao, F., Zhang, L.Q., 2008. Altered contractile properties of the gastrocnemius muscle poststroke. Journal of Applied Physiology 105, 1802-1808.

Given, J.D., Dewald, J.P., Rymer, W.Z., 1995. Joint dependent passive stiffness in paretic and contralateral limbs of spastic patients with hemiparetic stroke. J Neurol Neurosurg Psychiatry 59, 271-279.

Goislard de Monsabert, B., Rossi, J., Berton, E., Vigouroux, L., 2012. Quantification of hand and forearm muscle forces during a maximal power grip task. Med Sci Sports Exerc 44, 1906-1916.

Gonzalez, V., Rowson, J., Yoxall, A., 2017. Analyzing finger interdependencies during the Purdue Pegboard Test and comparative activities of daily living. J Hand Ther 30, 80-88.

Gowland, C., Stratford, P., Ward, M., Moreland, J., Torresin, W., Vanhullenaar, S., Sanford, J., Barreca, S., Vanspall, B., Plews, N., 1993. Measuring Physical Impairment and Disability with the Chedoke-Mcmaster Stroke Assessment. Stroke 24, 58-63.

Heckman, C.J., Johnson, M., Mottram, C., Schuster, J., 2008. Persistent inward currents in spinal motoneurons and their influence on human motoneuron firing patterns. Neuroscientist 14, 264-275.

Heckmann, C.J., Gorassini, M.A., Bennett, D.J., 2005. Persistent inward currents in motoneuron dendrites: implications for motor output. Muscle Nerve 31, 135-156.

Hodes, R., Dement, W.C., 1964. Depression of Electrically Induced Reflexes ("H-Reflexes") in Man during Low Voltage Eeg "Sleep". Electroencephalogr Clin Neurophysiol 17, 617-629.

Hoffmann, G., Conrad, M.O., Qiu, D., Kamper, D.G., 2016. Contributions of voluntary activation deficits to hand weakness after stroke. Top Stroke Rehabil 23, 384-392.

Hogg, R.V., Ledolter, J., 1987. Engineering statistics. Macmillan ;
Collier Macmillan, New York

London.
Holzbaur, K.R., Delp, S.L., Gold, G.E., Murray, W.M., 2007a. Moment-generating capacity of upper limb muscles in healthy adults. J Biomech 40, 2442-2449.
Holzbaur, K.R., Murray, W.M., Delp, S.L., 2005. A model of the upper extremity for simulating musculoskeletal surgery and analyzing neuromuscular control. Ann Biomed Eng 33, 829-840.
Holzbaur, K.R., Murray, W.M., Gold, G.E., Delp, S.L., 2007b. Upper limb muscle volumes in adult subjects. J Biomech 40, 742-749.
Hooper, S.L., Guschlbauer, C., Blumel, M., Rosenbaum, P., Gruhn, M., Akay, T., Buschges, A., 2009. Neural control of unloaded leg posture and of leg swing in stick insect, cockroach, and mouse differs from that in larger animals. The Journal of neuroscience : the official journal of the Society for Neuroscience 29, 4109-4119.
Hu, X., Tong, K., Tsang, V.S., Song, R., 2006. Joint-angle-dependent neuromuscular dysfunctions at the wrist in persons after stroke. Arch Phys Med Rehabil 87, 671-679.
Hume, M.C., Gellman, H., McKellop, H., Brumfield, R.H., Jr., 1990. Functional range of motion of the joints of the hand. J Hand Surg Am 15, 240-243.
Johanson, M.E., Murray, W.M., 2002. The unoperated hand: the role of passive forces in hand function after tetraplegia. Hand Clin 18, 391-398.
Johnson, M.D., Heckman, C.J., 2014. Gain control mechanisms in spinal motoneurons. Front Neural Circuits 8, 81.
Kaku, M., Simpson, D.M., 2016. Spotlight on botulinum toxin and its potential in the treatment of stroke-related spasticity. Drug Des Devel Ther 10, 1085-1099.
Kamper, D.G., Fischer, H.C., Cruz, E.G., Rymer, W.Z., 2006. Weakness is the primary contributor to finger impairment in chronic stroke. Arch Phys Med Rehabil 87, 1262-1269.
Kamper, D.G., Harvey, R.L., Suresh, S., Rymer, W.Z., 2003. Relative contributions of neural mechanisms versus muscle mechanics in promoting finger extension deficits following stroke. Muscle Nerve 28, 309-318.
Kamper, D.G., Hornby, G.T., Rymer, W.Z., 2002. Extrinsic flexor muscles generate concurrent flexion of all three finger joints. J Biomech 35, 1581-1589.
Kamper, D.G., Rymer, W.Z., 2000. Quantitative features of the stretch response of extrinsic finger muscles in hemiparetic stroke. Muscle Nerve 23, 954-961.
Kim, H.S., Hwang, J.H., Jeong, S.T., Lee, Y.T., Lee, P.K., Suh, Y.L., Shim, J.S., 2003. Effect of muscle activity and botulinum toxin dilution volume on muscle paralysis. Dev Med Child Neurol 45, 200-206.
Klein, C.S., Brooks, D., Richardson, D., McIlroy, W.E., Bayley, M.T., 2010. Voluntary activation failure contributes more to plantar flexor weakness than antagonist coactivation and muscle atrophy in chronic stroke survivors. J Appl Physiol (1985) 109, 1337-1346.
Knarr, B.A., Ramsay, J.W., Buchanan, T.S., Higginson, J.S., Binder-Macleod, S.A., 2013. Muscle volume as a predictor of maximum force generating ability in the plantar flexors post-stroke. Muscle Nerve 48, 971-976.
Knutson, J.S., Kilgore, K.L., Mansour, J.M., Crago, P.E., 2000. Intrinsic and extrinsic contributions to the passive moment at the metacarpophalangeal joint. J Biomech 33, 1675-1681.
Kozin, S.H., Porter, S., Clark, P., Thoder, J.J., 1999. The contribution of the intrinsic muscles to grip and pinch strength. J Hand Surg Am 24, 64-72.

Krenzer, M., Anaclet, C., Vetrivelan, R., Wang, N., Vong, L., Lowell, B.B., Fuller, P.M., Lu, J., 2011. Brainstem and spinal cord circuitry regulating REM sleep and muscle atonia. PLoS One 6, e24998.

Kuo, P.H., Deshpande, A.D., 2012. Muscle-tendon units provide limited contributions to the passive stiffness of the index finger metacarpophalangeal joint. J Biomech 45, 2531-2538.

Kuypers, H.G., 1964. The Descending Pathways to the Spinal Cord, Their Anatomy and Function. Prog Brain Res 11, 178-202.

Kwah, L.K., Herbert, R.D., Harvey, L.A., Diong, J., Clarke, J.L., Martin, J.H., Clarke, E.C., Hoang, P.D., Bilston, L.E., Gandevia, S.C., 2012. Passive mechanical properties of gastrocnemius muscles of people with ankle contracture after stroke. Arch Phys Med Rehabil 93, 1185-1190.

Lance, J.W., 1980. The control of muscle tone, reflexes, and movement: Robert Wartenberg Lecture. Neurology 30, 1303-1313.

Lawrence, D.G., Kuypers, H.G., 1968. The functional organization of the motor system in the monkey. I. The effects of bilateral pyramidal lesions. Brain 91, 1-14.

Lawrence, E.S., Coshall, C., Dundas, R., Stewart, J., Rudd, A.G., Howard, R., Wolfe, C.D., 2001. Estimates of the prevalence of acute stroke impairments and disability in a multiethnic population. Stroke 32, 1279-1284.

Le Minor, J.M., Rapp, E., 2001. Relative weights of the human carpal bones: biological and functional interests. Ann Anat 183, 537-543.

Lee, J.H., Asakawa, D.S., Dennerlein, J.T., Jindrich, D.L., 2015a. Extrinsic and intrinsic index finger muscle attachments in an OpenSim upper-extremity model. Ann Biomed Eng 43, 937-948.

Lee, J.H., Asakawa, D.S., Dennerlein, J.T., Jindrich, D.L., 2015b. Finger muscle attachments for an OpenSim upper-extremity model. PLoS One 10, e0121712.

Li, K., Zhang, X., 2009. A novel two-stage framework for musculoskeletal dynamic modeling: an application to multifingered hand movement. IEEE Trans Biomed Eng 56, 1949-1957.

Li, L., Tong, K.Y., Hu, X., 2007. The effect of poststroke impairments on brachialis muscle architecture as measured by ultrasound. Arch Phys Med Rehabil 88, 243-250.

Li, Z.M., Zatsiorsky, V.M., Latash, M.L., 2000. Contribution of the extrinsic and intrinsic hand muscles to the moments in finger joints. Clin Biomech (Bristol, Avon) 15, 203-211.

Lieber, R.L., Friden, J., 1998. Musculoskeletal balance of the human wrist elucidated using intraoperative laser diffraction. J Electromyogr Kinesiol 8, 93-100.

Lieber, R.L., Friden, J., 2002. Spasticity causes a fundamental rearrangement of muscle-joint interaction. Muscle Nerve 25, 265-270.

Lieber, R.L., Steinman, S., Barash, I.A., Chambers, H., 2004. Structural and functional changes in spastic skeletal muscle. Muscle Nerve 29, 615-627.

Littler, J.W., 1949. Tendon transfers and arthrodeses in combined median and ulnar nerve paralysis. J Bone Joint Surg Am 31A, 225-234.

Liu, F., Tang, W., Chen, D., Li, M., Gao, Y., Zheng, H., Chen, S., 2016. Expression of TGF-beta1 and CTGF Is Associated with Fibrosis of Denervated Sternocleidomastoid Muscles in Mice. Tohoku J Exp Med 238, 49-56.

Malhotra, S., Pandyan, A.D., Rosewilliam, S., Roffe, C., Hermens, H., 2010. Spasticity and contractures at the wrist after stroke: time course of development and their association with functional recovery of the upper limb. Clin Rehabil 25, 184-191.

McConville, J.T., Churchill, T.D., Kaleps, I., Clauser, C.E., Cuzzi, J., 1980. Anthropometric Relationships of Body and Body Segment Moments of Inertia. Anthropology Research Project AFAMRL-TR-80-119.

McFadden, D., Bracht, M.S., 2003. The relative lengths and weights of metacarpals and metatarsals in baboons (papio hamadryas). Horm Behav 43, 347-355.

McPherson, J.G., Ellis, M.D., Heckman, C.J., Dewald, J.P., 2008. Evidence for increased activation of persistent inward currents in individuals with chronic hemiparetic stroke. J Neurophysiol 100, 3236-3243.

McPherson, J.G., Stienen, A.H., Drogos, J.M., Dewald, J.P., 2017. Modification of Spastic Stretch Reflexes at the Elbow by Flexion Synergy Expression in Individuals With Chronic Hemiparetic Stroke. Arch Phys Med Rehabil.

Mikhail, I.K., 1964. Bone Block Operation for Clawhand. Surg Gynecol Obstet 118, 1077-1079.

Millard, M., Uchida, T., Seth, A., Delp, S.L., 2013. Flexing computational muscle: modeling and simulation of musculotendon dynamics. Journal of biomechanical engineering 135, 021005.

Miller, L.C., Dewald, J.P., 2012. Involuntary paretic wrist/finger flexion forces and EMG increase with shoulder abduction load in individuals with chronic stroke. Clin Neurophysiol 123, 1216-1225.

Minamoto, V.B., Hulst, J.B., Lim, M., Peace, W.J., Bremner, S.N., Ward, S.R., Lieber, R.L., 2007. Increased efficacy and decreased systemic-effects of botulinum toxin A injection after active or passive muscle manipulation. Dev Med Child Neurol 49, 907-914.

Minamoto, V.B., Suzuki, K.P., Bremner, S.N., Lieber, R.L., Ward, S.R., 2015. Dramatic changes in muscle contractile and structural properties after 2 botulinum toxin injections. Muscle Nerve 52, 649-657.

Mirakhorlo, M., Visser, J.M.A., Goislard de Monsabert, B.A.A.X., van der Helm, F.C.T., Maas, H., Veeger, H.E.J., 2016. Anatomical parameters for musculoskeletal modeling of the hand and wrist. International Biomechanics 3, 40-49.

Mirbagheri, M.M., Alibiglou, L., Thajchayapong, M., Rymer, W.Z., 2008. Muscle and reflex changes with varying joint angle in hemiparetic stroke. J Neuroeng Rehabil 5, 6.

Mogk, J.P., Johanson, M.E., Hentz, V.R., Saul, K.R., Murray, W.M., 2011a. A simulation analysis of the combined effects of muscle strength and surgical tensioning on lateral pinch force following brachioradialis to flexor pollicis longus transfer Journal of Biomechanics 44, 669-675.

Mogk, J.P., Johanson, M.E., Hentz, V.R., Saul, K.R., Murray, W.M., 2011b. A simulation analysis of the combined effects of muscle strength and surgical tensioning on lateral pinch force following brachioradialis to flexor pollicis longus transfer J. Biomech. 44, 669-675.

Mozaffarian D, B.E., Go AS, Arnett DK, Blaha MJ, Cushman M, de Ferranti S, Després J-P, Fullerton HJ, Howard VJ, Huffman MD, Judd SE, Kissela BM, Lackland DT, Lichtman JH, Lisabeth LD, Liu S, Mackey RH, Matchar DB, McGuire DK, Mohler ER 3rd, Moy CS, Muntner P, Mussolino ME, Nasir K, Neumar RW, Nichol G, Palaniappan L, Pandey DK, Reeves MJ, Rodriguez CJ, Sorlie PD, Stein J, Towfighi A, Turan TN, Virani SS, Willey JZ, Woo D, Yeh RW, Turner MB; on behalf of the American Heart Association Statistics

Committee and Stroke Statistics Subcommittee, 2015. Heart disease and stroke statistics—2015 update: A Report From The American Heart Association., Circulation, pp. 131:eXX–eXXX.

Murray, W.M., Buchanan, T.S., Delp, S.L., 2000. The isometric functional capacity of muscles that cross the elbow. J Biomech 33, 943-952.

Murray, W.M., Delp, S.L., Buchanan, T.S., 1995. Variation of muscle moment arms with elbow and forearm position. J Biomech 28, 513-525.

Murray, W.M., Hentz, V.R., Friden, J., Lieber, R.L., 2006. Variability in surgical technique for brachioradialis tendon transfer. Evidence and implications. J Bone Joint Surg Am 88, 2009-2016.

Murray, W.M., Kilgore, K.L., Keith, M.W., 2002. Brachioradialis tendon transfers that restore wrist extension: Evaluating outcome in different joint postures. , Second Joint EMBS-BMES Conference. , Houston, TX.

Nakayama, H., Jorgensen, H.S., Raaschou, H.O., Olsen, T.S., 1994. Recovery of upper extremity function in stroke patients: the Copenhagen Stroke Study. Arch Phys Med Rehabil 75, 394-398.

Nelson, C.M., Dewald, J.P.A., Murray, W.M., Year Musculoskeletal Adaption after Hemiparetic Stroke: In Vivo Measurements of Shortened Biceps Brachii Fascicle Lengths and Increased Passive Elbow Stiffness. In Combined Sections Meeting of the American Physical Therapy Association. Indianapolis, IN.

Neumann, D.A., Kelly, E.R., Kiefer, C.L., Martens, K., Grosz, C.M., 2017. Kinesiology of the musculoskeletal system : foundations for rehabilitation, Third edition. ed. Elsevier, St. Louis, Missouri.

Nichols, J.A., Bednar, M.S., Murray, W.M., 2013. Orientations of wrist axes of rotation influence torque required to hold the hand against gravity: a simulation study of the nonimpaired and surgically salvaged wrist. J Biomech 46, 192-196.

Nichols, J.A., Bednar, M.S., Murray, W.M., 2016. Surgical Simulations Based on Limited Quantitative Data: Understanding How Musculoskeletal Models Can Be Used to Predict Moment Arms and Guide Experimental Design. PLoS One 11, e0157346.

Nichols, J.A., Bednar, M.S., Wohlman, S.J., Murray, W.M., 2017. Connecting the wrist to the hand: A simulation study exploring changes in thumb-tip endpoint force following wrist surgery. J Biomech 58, 97-104.

Nikolaou, S., Liangjun, H., Tuttle, L.J., Weekley, H., Christopher, W., Lieber, R.L., Cornwall, R., 2014. Contribution of denervated muscle to contractures after neonatal brachial plexus injury: not just muscle fibrosis. Muscle Nerve 49, 398-404.

O'Driscoll, S.W., Horii, E., Ness, R., Cahalan, T.D., Richards, R.R., An, K.N., 1992. The relationship between wrist position, grasp size, and grip strength. J Hand Surg Am 17, 169-177.

O'Dwyer, N.J., Ada, L., Neilson, P.D., 1996. Spasticity and muscle contracture following stroke. Brain 119 (Pt 5), 1737-1749.

Owen, M., Ingo, C., Dewald, J.P.A., 2017. Upper Extremity Motor Impairments and Microstructural Changes in Bulbospinal Pathways in Chronic Hemiparetic Stroke. Frontiers in neurology 8, 257.

Ozcakir, S., Sivrioglu, K., 2007. Botulinum toxin in poststroke spasticity. Clin Med Res 5, 132-138.

Palti, R., Vigler, M., 2012. Anatomy and function of lumbrical muscles. Hand Clin 28, 13-17.

Parker, V.M., Wade, D.T., Langton Hewer, R., 1986. Loss of arm function after stroke: measurement, frequency, and recovery. Int Rehabil Med 8, 69-73.

Pollock, A., Farmer, S.E., Brady, M.C., Langhorne, P., Mead, G.E., Mehrholz, J., van Wijck, F., 2014. Interventions for improving upper limb function after stroke. Cochrane Database Syst Rev 11, CD010820.

Prado-Medeiros, C.L., Silva, M.P., Lessi, G.C., Alves, M.Z., Tannus, A., Lindquist, A.R., Salvini, T.F., 2012. Muscle atrophy and functional deficits of knee extensors and flexors in people with chronic stroke. Phys Ther 92, 429-439.

Reghem, E., Cheze, L., Coppens, Y., Pouydebat, E., 2014. The influence of body posture on the kinematics of prehension in humans and gorillas (Gorilla gorilla). Exp Brain Res 232, 1047-1056.

Richards, L.G., Olson, B., Palmiter-Thomas, P., 1996. How forearm position affects grip strength. Am J Occup Ther 50, 133-138.

Riddle, C.N., Baker, S.N., 2010. Convergence of pyramidal and medial brain stem descending pathways onto macaque cervical spinal interneurons. J Neurophysiol 103, 2821-2832.

Riddle, C.N., Edgley, S.A., Baker, S.N., 2009. Direct and indirect connections with upper limb motoneurons from the primate reticulospinal tract. The Journal of neuroscience : the official journal of the Society for Neuroscience 29, 4993-4999.

Riordan, D.C., 1953. Tendon transplantations in median-nerve and ulnar-nerve paralysis. J Bone Joint Surg Am 35-A, 312-320; passim.

Russo, T.L., Peviani, S.M., Durigan, J.L., Salvini, T.F., 2008. Electrical stimulation increases matrix metalloproteinase-2 gene expression but does not change its activity in denervated rat muscle. Muscle Nerve 37, 593-600.

Ryan, A.S., Dobrovolny, C.L., Smith, G.V., Silver, K.H., Macko, R.F., 2002. Hemiparetic muscle atrophy and increased intramuscular fat in stroke patients. Arch Phys Med Rehabil 83, 1703-1707.

Ryu, J.Y., Cooney, W.P., 3rd, Askew, L.J., An, K.N., Chao, E.Y., 1991. Functional ranges of motion of the wrist joint. J Hand Surg Am 16, 409-419.

Sancho-Bru, J.L., Perez-Gonzalez, A., Vergara, M., Giurintano, D.J., 2003. A 3D biomechanical model of the hand for power grip. Journal of biomechanical engineering 125, 78-83.

Sancho-Bru, J.L., Perez-Gonzalez, A., Vergara-Monedero, M., Giurintano, D., 2001. A 3-D dynamic model of human finger for studying free movements. J Biomech 34, 1491-1500.

Sapienza, A., Green, S., 2012. Correction of the claw hand. Hand Clin 28, 53-66.

Saul, K.R., Hu, X., Goehler, C.M., Vidt, M.E., Daly, M., Velisar, A., Murray, W.M., 2015. Benchmarking of dynamic simulation predictions in two software platforms using an upper limb musculoskeletal model. Comput Methods Biomech Biomed Engin 18, 1445-1458.

Saul, K.R., Murray, W.M., Hentz, V.R., Delp, S.L., 2003. Biomechanics of the Steindler flexorplasty surgery: a computer simulation study. J Hand Surg Am 28, 979-986.

Scelsi, R., Lotta, S., Lommi, G., Poggi, P., Marchetti, C., 1984. Hemiplegic atrophy. Morphological findings in the anterior tibial muscle of patients with cerebral vascular accidents. Acta Neuropathol 62, 324-331.

Schmit, B.D., Dewald, J.P., Rymer, W.Z., 2000. Stretch reflex adaptation in elbow flexors during repeated passive movements in unilateral brain-injured patients. Arch Phys Med Rehabil 81, 269-278.

Schreuders, T.A.R., Brandsma, J.W., Stam, H.J., 2007. The intrinsic muscles of the hand - Function, assessment and principles for therapeutic intervention. Phys Med Rehab Kuror 17, 20-27.

Schutte, L.M., 1992. Using Musculoskeletal Models to Explore Strategies for Improving Performance in Electrical Stimulation-Induced Leg Cycle Ergometry. Stanford Univeristy, Palo Alto.

Shatz, P., Anatomy & Physiology, http://philschatz.com/anatomy-book/contents/m46495.html.

Shaw, L.C., Price, C.I., van Wijck, F.M., Shackley, P., Steen, N., Barnes, M.P., Ford, G.A., Graham, L.A., Rodgers, H., Bo, T.I., 2011. Botulinum Toxin for the Upper Limb after Stroke (BoTULS) Trial: effect on impairment, activity limitation, and pain. Stroke 42, 1371-1379.

Silva-Couto Mde, A., Prado-Medeiros, C.L., Oliveira, A.B., Alcantara, C.C., Guimaraes, A.T., Salvini Tde, F., Mattioli, R., de Russo, T.L., 2014. Muscle atrophy, voluntary activation disturbances, and low serum concentrations of IGF-1 and IGFBP-3 are associated with weakness in people with chronic stroke. Phys Ther 94, 957-967.

Sirtori, V., Corbetta, D., Moja, L., Gatti, R., 2009. Constraint-induced movement therapy for upper extremities in stroke patients. Cochrane Database Syst Rev, CD004433.

Slowik, J.S., McNitt-Gray, J.L., Requejo, P.S., Mulroy, S.J., Neptune, R.R., 2016. Compensatory strategies during manual wheelchair propulsion in response to weakness in individual muscle groups: A simulation study. Clin Biomech (Bristol, Avon) 33, 34-41.

Smith, L.R., Lee, K.S., Ward, S.R., Chambers, H.G., Lieber, R.L., 2011. Hamstring contractures in children with spastic cerebral palsy result from a stiffer extracellular matrix and increased in vivo sarcomere length. J Physiol 589, 2625-2639.

Smith, R.J., 1984. Metacarpal ligament sling tenodesis. Bull Hosp Jt Dis Orthop Inst 44, 466-469.

Sousa, G.G.Q., de Macedo, M.P., 2015. Effects of a dynamic orthosis in an individual with claw deformity. J Hand Ther 28, 425-428.

Souza, T.R., Fonseca, S.T., Goncalves, G.G., Ocarino, J.M., Mancini, M.C., 2009. Prestress revealed by passive co-tension at the ankle joint. J Biomech 42, 2374-2380.

Srinivasan, H., 1973. The extensor diversion graft operation for correction of intrinsic minus fingers in leprosy. J Bone Joint Surg Br 55, 58-65.

Srinivasan, H., 1976. Patterns of movement of totally intrinsic-minus fingers based on a study of one hundred and forty-one fingers. J Bone Joint Surg Am 58, 777-785.

Standring, S., 2016. Gray's anatomy : the anatomical basis of clinical practice, Forty-first edition. ed. Elsevier Limited, New York.

Stienen, A., Moulton, T.S., Miller, L.C., Dewald, J.P.A., Year Wrist and Finger Torque Sensor for the Quantification of Upper Limb Motor Impairments Following Brain Injury. In 2011 IEEE International Conference on Rehabilitation Robotics. Zurich , Switzerland.

Su, F.C., Chou, Y.L., Yang, C.S., Lin, G.T., An, K.N., 2005. Movement of finger joints induced by synergistic wrist motion. Clin Biomech (Bristol, Avon) 20, 491-497.

Sukal, T.M., Ellis, M.D., Dewald, J.P., 2007. Shoulder abduction-induced reductions in reaching work area following hemiparetic stroke: neuroscientific implications. Exp Brain Res 183, 215-223.

Tabary, J.C., Tabary, C., Tardieu, C., Tardieu, G., Goldspink, G., 1972. Physiological and structural changes in the cat's soleus muscle due to immobilization at different lengths by plaster casts. J Physiol 224, 231-244.

Taylor, C.L., Schwarz, R.J., 1955. The anatomy and mechanics of the human hand. Artif Limbs 2, 22-35.

Taylor, N.L., Raj, A.D., Dick, H.M., Solomon, S., 2004. The correction of ulnar claw fingers: A follow-up study comparing the extensor-to-flexor with the palmaris longus 4-tailed tendon transfer in patients with leprosy. J Hand Surg-Am 29a, 595-604.

Thacker, B.E., Tomiya, A., Hulst, J.B., Suzuki, K.P., Bremner, S.N., Gastwirt, R.F., Greaser, M.L., Lieber, R.L., Ward, S.R., 2012. Passive mechanical properties and related proteins change with botulinum neurotoxin A injection of normal skeletal muscle. J Orthop Res 30, 497-502.

Thelen, D.G., 2003. Adjustment of muscle mechanics model parameters to simulate dynamic contractions in older adults. Journal of biomechanical engineering 125, 70-77.

Thieme, H., Bayn, M., Wurg, M., Zange, C., Pohl, M., Behrens, J., 2013. Mirror therapy for patients with severe arm paresis after stroke--a randomized controlled trial. Clin Rehabil 27, 314-324.

Thieme, H., Mehrholz, J., Pohl, M., Behrens, J., Dohle, C., 2012. Mirror therapy for improving motor function after stroke. Cochrane Database Syst Rev 3, CD008449.

Triandafilou, K.M., Kamper, D.G., 2012. Investigation of hand muscle atrophy in stroke survivors. Clin Biomech (Bristol, Avon) 27, 268-272.

Ward, S.R., Minamoto, V.B., Suzuki, K.P., Hulst, J.B., Bremner, S.N., Lieber, R.L., 2017. Recovery of rat muscle size but not function more than 1 year after a single botulinum toxin injection. Muscle Nerve.

Web_Of_Science, 2017. Times Cited, www.webofknowledge.com.

Wilkins, K.B., Owen, M., Ingo, C., Carmona, C., Dewald, J.P.A., Yao, J., 2017. Neural Plasticity in Moderate to Severe Chronic Stroke Following a Device-Assisted Task-Specific Arm/Hand Intervention. Frontiers in neurology 8, 284.

Williams, P.E., Goldspink, G., 1978. Changes in sarcomere length and physiological properties in immobilized muscle. J Anat 127, 459-468.

Wu, M.M., Pai, D.K., Tresch, M.C., Sandercock, T.G., 2012. Passive elastic properties of the rat ankle. J Biomech 45, 1728-1732.

Zajac, F.E., 1989. Muscle and tendon: properties, models, scaling, and application to biomechanics and motor control. Crit Rev Biomed Eng 17, 359-411.

Zancolli, E.A., 1957. Claw-hand caused by paralysis of the intrinsic muscles: a simple surgical procedure for its correction. J Bone Joint Surg Am 39-A, 1076-1080.

APPENDICES

A Appendix A. Muscle Model Validation

The current muscle model recommended for general use within the OpenSim v3.0+ software system is the "Millard2012EquilibriumMuscle" tool (Millard et al., 2013). However to improve numerical stability and computational efficiency the default settings of the "Millard2012EquilibriumMuscle" tool in OpenSim yield small active forces at fiber lengths where no active force can be generated. Specifically, normalized fiber lengths of less than 0.5 or greater than 1.5 on the normalized force-length curve produce forces of 10% of maximum isometric force. Physiologically, those normalized lengths should not produce any active force. In addition, the default minimum muscle activation is defined as 0.01 (1% of full activation). Therefore, with the default parameters specified in the "Millard2012EquilibriumMuscle" tool, the model does not simulate 0% muscle activation and the resulting force output includes a force that does not arise from the passive muscle force-length curve.

The purpose of the short communication, that this appendix complements, is to both incorporate the length-dependent passive forces of the extrinsic index finger muscles into a biomechanical model of the upper limb and to demonstrate their influence on combined passive movements of the wrist and hand. In order to generate simulations involving 0% muscle activation and muscle force outputs that only arise from the passive muscle force-length curve we edited the default parameters set in the "Millard2012EquilibriumMuscle" tool in OpenSim v3.2. The parameters were edited to replicate the force generating curves that have been implemented in previous kinematic and dynamic models (Holzbaur et al., 2005; Saul et al., 2015). The previously developed Holzbaur 2005 and Saul 2015 dynamic upper extremity models have been used

extensively within and outside of our lab with at least 320 citations between the two models (Web_Of_Science, 2017).

Our edited version of the “Millard2012Equilibrium” muscle model was benchmarked relative to “Muscle Model 4”, implemented in the SIMM and Dynamics Pipeline frameworks. Within the Dynamics Pipeline platform, “Muscle Model 4” is an algorithm based on the well-known muscle modeling work described in Lisa Schutte’s PhD dissertation (Schutte, 1992).

In order to avoid complications associated with computational challenges that arise when simulating the dynamics of the small masses and inertias of the hand, we evaluated the performance of our edited version of the “Millard2012EquilibriumMuscle” tool in OpenSim by performing the simulations with a musculoskeletal model of the upper extremity isolated to the elbow joint. Identical, simplified musculoskeletal elbow models were implemented within both the SIMM and OpenSim platforms. The models included only 4 muscles; the Triceps Long head, Triceps Lateral head, Biceps Long head, and Biceps Short head. The muscle paths, muscle-tendon geometry, and force generating properties were replicated in both models as described previously (Saul et al., 2015).

A gravity-driven, forward dynamic simulation was performed in each platform to compare the passive behavior of each muscle tool during the simulations. The elbow was initially set to 40 degrees of flexion and then allowed to fall with gravity towards an equilibrium posture. The simulation was run for five seconds. The passive muscle dynamics of the modified “Millard2012EquilibriumMuscle” tool within the OpenSim v3.2 platform were then compared to the passive muscle dynamics of the “Muscle Model 4” tool within the Dynamics Pipeline platform during the gravity driven simulations.

Within both models the long head of the bicep brachii's muscle-tendon unit remains lengthened beyond its slack length throughout the simulation. The muscle-tendon slack length is the length at which the muscle-tendon unit begins to produce passive forces (Figure 8.1, see also Eq 8 from manuscript). The short head of the biceps brachii oscillates about its muscle-tendon slack length. The muscle-tendon lengths of both heads of the triceps remain below the muscle-tendon slack length (Figure 8.1). When the muscle-tendon unit is shorter than the slack length the muscle does not produce passive muscle forces (Eq 8 from manuscript). Therefore only the heads of the biceps produce passive forces during this simulation.

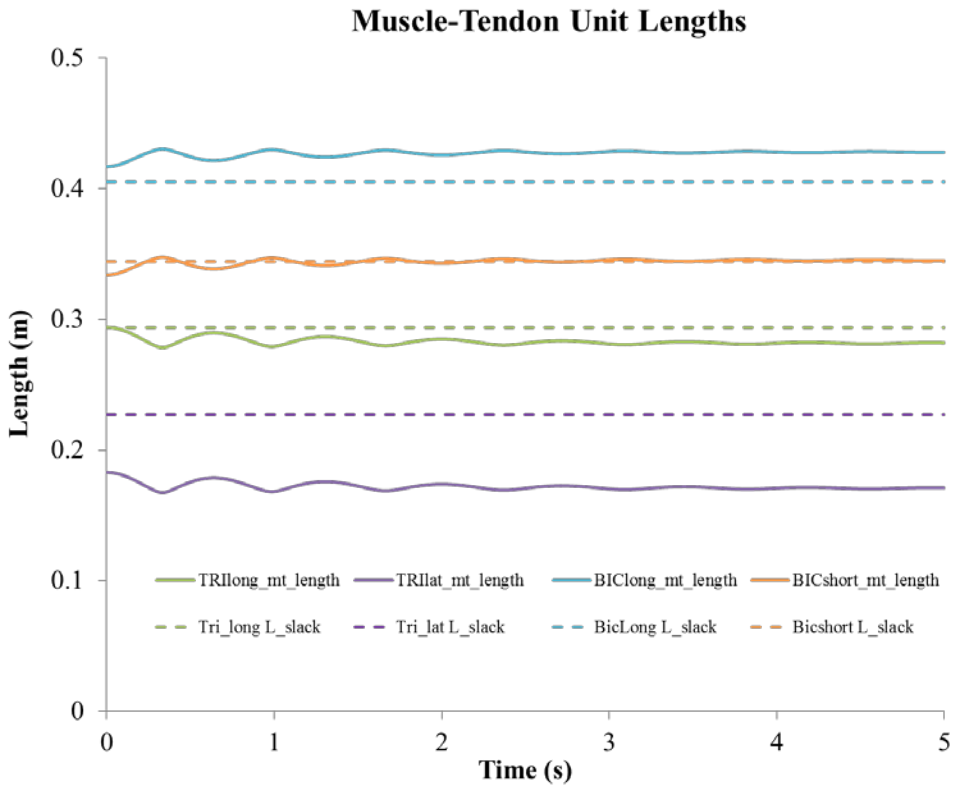

Figure 8.1: Muscle-tendon unit lengths (solid) over time of the triceps long head (green), triceps lateral head (purple), biceps long head (blue), and biceps short head (orange) during the passive forward simulation using the modified "Millard2012EquilbiumMuscle" tool in OpenSim v3.2. The slack length, the length at which passive forces begin, of each muscle is plotted in the dashed lines.

The passive dynamic performance of our edited version of the "Millard2012EquilbriumMuscle" tool implemented in OpenSim v3.2 behaves in the same manner as the "Muscle Model 4" implemented in the Dynamics Pipeline. Of interest is the dynamic performance of the muscles producing force, therefore we are only presenting the performance of the biceps and are not presenting the performance of the triceps. In particular, after a brief initialization, the distribution of muscle-tendon length changes between the muscle fiber and the tendon for the biceps is replicated in both tools (Figure 8.2). The length changes of the biceps long head occur primarily in the muscle fiber (Figure 8.2). The length changes of the biceps short muscle depends on whether the muscle-tendon length is longer or shorter than the slack length (Figure 8.2). When the muscle-tendon unit is longer than the slack length the change occurs in muscle fiber. When the unit is shorter than the slack length the change occurs in the tendon and the fiber length remains at the length in which passive forces begin (Figure 8.2).

Given the assumption of no muscle activation or muscle active force for this analysis, the distinct muscle models in the two different software environments default to models of two passive elastic elements, connected in series, in which the tendon is at approximately 20 times stiffer than the muscle fibers. By definition, when the muscle-tendon unit is longer than its slack length the fiber and tendon are also lengthened beyond their slack lengths. Due to the relatively high tendon stiffness, passive length changes occur in the muscle fibers with relatively little concomitant change in tendon length. This expected behavior is observed in both biceps muscles during the simulations, in both platforms (Figure 8.2).

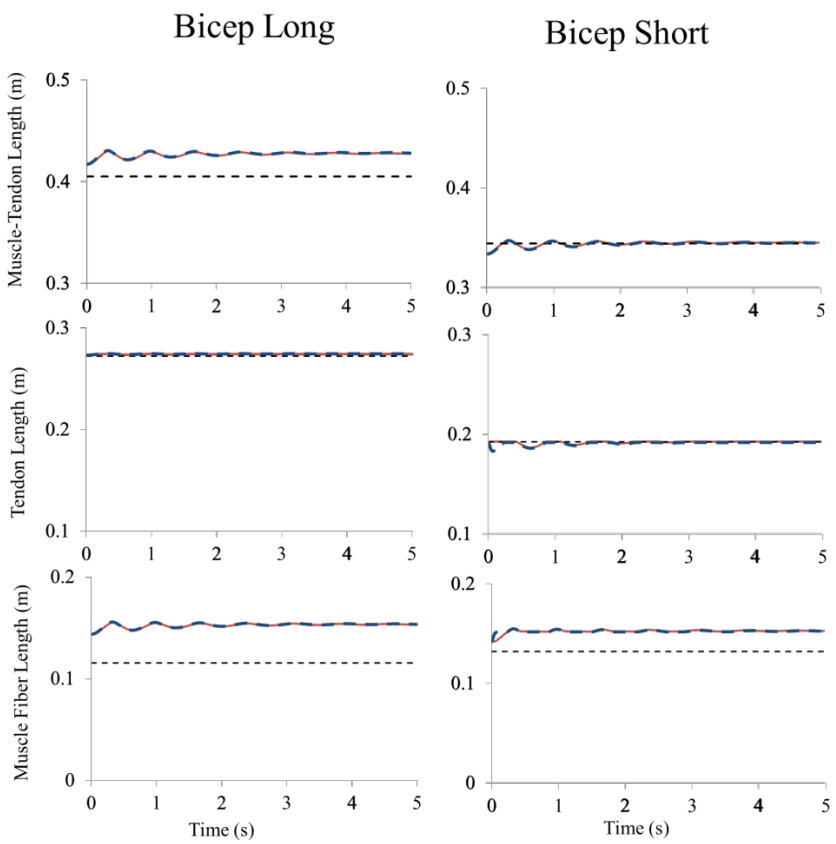

Figure 8.2: The muscle-tendon unit (top), tendon (middle) and muscle fiber (bottom) lengths of the biceps long head (left column) and short head (right column) of the Millard2012Equilibrium tool (red solid) and Muscle Model 4 tool (blue dashed). The slack lengths of the muscle-tendon units, tendons, and muscle fibers (black dashed) are displayed in each graph.

The resultant system dynamics of the musculoskeletal model show that the elbow angle over time using each muscle tool match well (R^2=0.989, RMSE=0.711 over the whole time period) (Figure 8.3). The simulations are nearly identical for the first 2.5 seconds (R^2=0.997, RMSE=0.506 for seconds 0 to 2.5). After 2.5 seconds the joint posture between the models deviate (R^2=0.794, RMSE=0.870 for seconds 2.5 to 5). These differences likely occur due to numerical differences during the calculation of muscle force between the two tools and platforms. As the simulations continue these differences propagate and lead to the increasingly different joint angles.

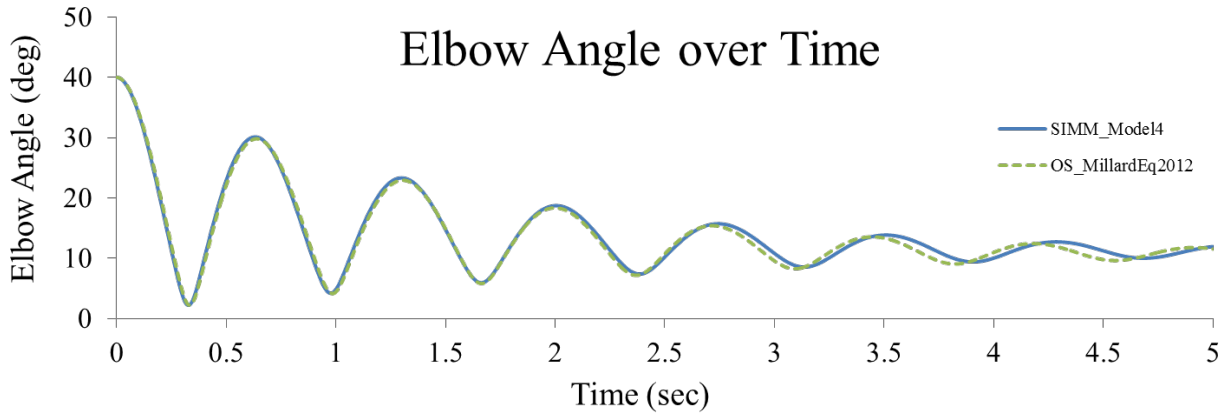

Figure 8.3: Plot of elbow angle over time for a gravity driven simulation within the SIMM and Dynamics Pipline platform using Muscle Model 4 (blue) and the OpenSim platform Millard2012Equilbirum tool (green).

We conclude that the parameter changes we implemented to enable simulations of purely passive muscle forces produce acceptable results, consistent with two elastic elements of varied stiffness connected in series, and replicated when the same parameters are implemented in a different muscle model in a different software platform. Minimal differences in the outputs of the muscle model are observed over a 5 second simulation, as evidenced in Figures 8.2 and 8.3. The main caveats to our implementation are associated with computational robustness: using the default parameters of the “Millard2012EquilbirumMuscle” tool yields faster computation times, and increases computational stability. Our modifications increase the computation time of the simulations and introduce the potential that the muscle tool may become unstable and crash during dynamic simulations; however we did not experience any crashes during the dynamic simulations at the hand or elbow. These trade-offs were necessary for the purposes of this paper.

B Appendix B: Four finger model development

This appendix presents an expanded description of the development of the non-paretic and the BoNT hand models that include digits four and five that could not be run for the full analysis due to computational limitations. The development and model is presented for use in the future once computational capabilities and methods are developed to better handle the very low mass and inertias of digits four and five. The model development will be described in full, as it is the main chapter, as to not leave out relevant details.

B.1 Development of the four finger dynamic musculoskeletal models of the hand.

Using the OpenSim platform v3.3 (Delp et al., 2007), a dynamic upper extremity model developed by Saul et al (Saul et al., 2015), which included the muscles paths and force generating properties of 32 muscles and muscle compartments crossing the shoulder, elbow, wrist and fingers; was used as the basis for building both our non-paretic and BoNT computational musculoskeletal models. Only the extrinsic finger muscles for digits 2-5 were included in the model. All other muscles were removed from the model. The kinematics, masses, and inertias of carpals, metacarpals, and phalanges of digits 2-5 were added as described by Binder-Markey & Murray (Binder-Markey and Murray, 2017). The moment arms for the extrinsic fingers within the hand were updated by matching the muscle paths and wrapping surfaces distal to the wrist as implemented by Lee et al (Lee et al., 2015a, b). The methods described previously by Binder-Markey and Murray were used to incorporate the passive torques about joint each finger (Binder-Markey and Murray, 2017).

B.2 Experimentally collected passive torque about each finger

The experimental net passive metacarpophalangeal (MCP) torques, the sum of all 4 fingers, was taken from the data collected in the previous two chapters. This torque was then separated into

the torque about each finger to be input into the computational model. To separate the total net MCP passive torque into the relative contribution of each finger the following processing was completed. Bending beam strain gauges, connecting the fingers to the modified Wrist Finger Torque Sensor (Stienen et al., 2011), as described in the previous chapter, were used to determine the relative contribution of each finger to the total MCP passive torque. Because strain gauges are sensitive to internal bending and twisting moments that do not contribute to the external torques of the finger, the output moments of the strain gauges were used to determine the relative proportion of torque, P_i, each finger contributed to the total MCP joint torque at each posture of wrist and MCP finger angle and were calculated as:

$$P_i = \frac{M_i^{\varepsilon}}{\sum_{i=2:5} M_i^{\varepsilon}}$$

where M_i^{ε} is the moment estimated by the strain gauge of each finger. The torque about the individual finger, T_i, was found as:

$$T_i = P_i \cdot T_{mcp}$$

where, T_{mcp} is the recorded net MCP joint torque at each wrist and MCP joint posture as described in the previous Chapters 5 & 6. If any anomalous output was found at any finger in any combination of wrist and MCP posture, the output of all the fingers at that combination was discarded and not included in the data set. This procedure was repeated for each of the 35 non-paretic data sets and 8 BoNT data sets collected in the previous two chapters to produce a unique MCP torque data set for fingers two through five throughout the recorded combinations of wrist and MCP postures.

B.3 Separation of the structures contributing to the total torque:

Analytical models were fit to each individual finger data set of net MCP joint torques processed above using the same methods described in the previous chapters (Knutson et al., 2000). The total torque, $T_t(\theta, \omega)$, of the analytical model developed for each subject is composed of the sum of two components.

$$T_t(\theta, \omega) = T_{sj}(\theta) + T_e(\theta, \omega) \tag{2}$$

$T_{sj}(\theta)$ consists of the torques contributed by the single-joint structures (intrinsic hand muscles, ligaments, joint capsules, etc.) that are a function of MCP joint posture only and $T_e(\theta, \omega)$ representing the extrinsic finger muscles, which is a function of both wrist and MCP posture (Knutson et al., 2000). These two components then describe the total torque about the MCP joint as a function of wrist and MCP posture and 14 constant parameters. To describe $T_t(\theta, \omega)$, $T_{sj}(\theta)$, and $T_e(\theta, \omega)$ of the non-paretic model and BoNT model the median value of each parameter was found over all the non-paretic data sets and the paretic BoNT data sets, respectively (Table 8.1).

B.4 Incorporation of the passive single joint torques.

The experimentally collected passive torque contributed by the single joint structures as described by $T_{sj}(\theta)$ found above for the non-paretic MCP joints 2-5 were added using torsional spring dampers (Binder-Markey and Murray, 2017). Using the same process, the passive single joint torque about the PIP an DIP passive joint torques taken from previous experimental work for the 2nd digit (Kamper et al., 2002) and then scaled for digits 3-5 and incorporated using torsional spring dampers (Binder-Markey and Murray, 2017). The single joint torques about the MCP, PIP, and DIP were not altered in the BoNT model because no substantial differences were found

between the paretic and non-paretic hands in individuals who had received the BoNT injections in Chapter 6.

Table 8.1: Parameters of the matched torques.

NON-PARETIC	A1	K1	THETA1	A2	K2	THETA2	A3	K3	B3	PHI3	A4	K4	B4	PHI4	R^2
INDEX	1.34	5.54E-02	-34.07	1.30	2.96E-01	71.38	1.00	2.94E-02	-1.14	-14.61	0.49	5.94E-02	-0.11	42.93	0.83
MIDDLE	1.33	6.28E-02	-26.97	1.75	1.26E-01	71.53	1.55	2.96E-02	-1.11	-4.60	0.86	3.77E-02	-0.50	39.83	0.87
RING	1.39	6.40E-02	-30.82	1.63	8.75E-02	71.30	1.18	3.00E-02	-1.27	-0.45	1.06	4.55E-02	-0.72	49.29	0.88
LITTLE	1.22	5.51E-02	-32.30	1.33	1.23E-01	75.18	0.90	3.11E-02	-0.60	-10.18	0.67	3.50E-02	-0.83	53.52	0.82

BTX PARETIC	A1	k1	theta1	A2	k2	theta2	A3	k3	B3	phi3	A4	k4	B4	phi4	R^2
INDEX	1.25	7.73E-02	-29.16	3.01	6.52E-02	67.35	2.19	2.77E-02	-1.89	-3.49	1.01	6.62E-02	-0.41	53.01	0.88
MIDDLE	1.62	6.36E-02	-26.20	3.69	7.44E-01	75.54	1.74	4.06E-02	-1.30	4.46	1.46	4.83E-02	-0.46	35.88	0.85
RING	1.24	8.30E-02	-31.53	2.68	8.56E-02	75.14	1.35	3.23E-02	-1.07	11.45	1.31	5.41E-02	-0.80	49.13	0.92
LITTLE	1.84	6.61E-02	-21.89	2.79	1.52E-01	72.16	0.80	3.22E-02	-1.35	-2.17	1.83	4.18E-02	-2.04	80.06	0.88

B.5 Incorporation of the passive extrinsic finger muscle torques.

The passive torques contributed by the extrinsic finger muscles about each finger were incorporated to complete the non-paretic model by matching the passive torques produced by the extrinsic finger muscles within the model to the experimental extrinsic finger passive torques, $T_e(\theta, \omega)$ (Table 8.1). Torque matching was accomplished by optimizing the tendon slack length of each extrinsic finger muscle within the model as previously described (Binder-Markey and Murray, 2017) (Table 8.2). Following the optimization, the FDSM muscle was found to be operating at fiber lengths longer than all the other flexors therefore, the tendon slack length of the FDSM was modified to place the FDSM fibers in the same operational range as the other flexors.

Table 8.2: Optimized Tendon Slack Lengths for the Non-paretic Model and Percent Change for all the fingers included in the model

		FDPI	FDSI	EDCI	EIP
Index	Initial tendon slack length	0.3044	0.2772	0.3486	0.1911
	New optimized tendon slack length	0.3097	0.2844	0.3505	0.1981
	Percent change	1.75%	2.58%	0.54%	3.68%
		FDPM	FDSM	EDCM	
Middle	Initial tendon slack length	0.3030	0.2950	0.3650	
	New optimized tendon slack length	0.2978	0.2929	0.3446	
	Percent change	-1.70%	-0.71%	-5.59%	
		FDPR	FDSR	EDCR	
Ring	Initial tendon slack length	0.2915	0.3280	0.3650	
	New optimized tendon slack length	0.2931	0.3172	0.3414	
	Percent change	0.55%	-3.29%	-6.45%	
		FDPL	FDSL	EDCL	EDM
Little	Initial tendon slack length	0.2819	0.3386	0.3350	0.3350
	New optimized tendon slack length	0.2988	0.3436	0.3530	0.3278
	Percent change	6.01%	1.49%	5.37%	-2.16%

The passive torques contributed by extrinsic flexors were modified to develop a model replicating the increased torques and increased muscle stiffness seen in individuals who received BoNT. The finger flexors were modified because only they were injected with BoNT across all subjects and the increases in $T_e(\theta, \omega)$ were only seen as the flexor muscles were stretched (Chapter 6). Using $T_e(\theta, \omega)$ found above for the BoNT data sets (Table 8.1), we employed the same optimization methods to match the passive torques of the extrinsic finger flexor muscles produced within the model to the experimental data; except, rather than the tendon slack length, the passive force length curve of the flexor muscles was optimized at each finger. To standardize the force length curve across the fingers flexors, the median parameters describing the optimized passive force length curve over the four fingers was then used to describe the passive force length curve of the all flexor muscles within the BoNT model (Table 8.3).

Table 8.3 Table of the unimpaired and BoNT parameters defining the passive force length curve within the Millardequlibrium2012 muscle model within the OpenSim platform.

Passive Muscle Model Parameters	Unimpaired	BoNT
Strain at Zero Force	0	0
Strain at One Norm Force	0.6405	0.3120
Stiffness at Low Force	0.0751	0.1022
Stiffness at One Norm Force	6.3163	6.3268
Curviness	0.6658	0.8612